Control of an Axial Flux Permanent Magnet Machine for very wide Constant Power Speed Range

By

Jonida CEKANI

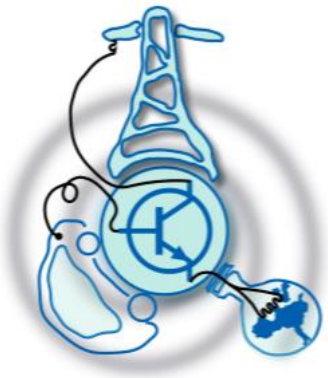

Submitted to the Department of Electrical Engineering, Electronics, Computers and Systems
In partial fulfillment of the requirements for the degree of
Erasmus Mundus Joint Master in

Sustainable Transportation and Electrical Power Systems

at the
UNIVERSITY OF OVIEDO
August 2019

Author…….

CEKANI Jonida

Certified by……...……

GIULII CAPPONI, Fabio

Associate Professor

Thesis Supervisor

Control of an Axial Flux Permanent Magnet Machine for very wide Constant Power Speed Range

By

Jonida CEKANI

Submitted to the Department of Electrical Engineering, Electronics, Computers and Systems
On August 2019, in partial fulfillment of the requirements for the degree of
Erasmus Mundus Joint Master in

Sustainable Transportation and Electrical Power Systems

Abstract

Nowadays, there is an increase in electric power consumption within the vehicles, which is predicted to soon exceed the generation capabilities of the traditional Lundell (claw-pole) alternator. Therefore, Research is focusing on other electric machines topologies, able to provide constant power over a wide range of engine speed, work both as a starter and an alternator and maintain a high efficiency, while not exceeding space limitations. The present thesis reports on the Axial Flux Permanent Magnet Machine with a Novel Mechanical Flux Weakening technique. The principle of operation is explained and a closed loop control for the flux weakening regulation is proposed. As a result, it is demonstrated through simulations that 10:1 constant power speed range can be attained, and possibly extended.

Thesis Supervisor: GIULII CAPPONI, Fabio
Title: Associate Professor at DIAEE, La Sapienza

Keywords: Axial flux permanent magnet machine, Alternator, Mechanical flux weakening, Constant power, Field weakening

TABLE OF CONTENTS

LIST OF FIGURES

LIST OF TABLES

ABBREVIATIONS

AFPM	-	Axial Flux Permanent Magnet
PM	-	Permanent Magnet
CTSR	-	Constant Torque Speed Region
CPSR	-	Constant Power Speed Region
FW	-	Field Weakening
BEMF	-	Back Electro Motive Force
OP	-	Operating Point

Chapter 1

AFPM Machine with Novel Mechanical Flux Weakening

1.1 Introduction

In present day vehicles, there is an increasing request for extra comfort, safety and entertainment features. These added loads call for higher power generation from alternators. In modern high-end cars, the alternator provides current up to 300 Amps, connected to the 12 Volts bus. The main demerit of the traditional Lundell (claw-pole) alternator are the rather large losses (low efficiency), around 50% at full power and high speed [1]. Lundell's theoretical limits of 4kW are therefore likely to be exceeded soon, as producing electricity on board with such high losses is not acceptable, at the increasing electric power levels.

With this increase, the generator rated torque becomes comparable with the torque required to start the engine (150-250Nm) [2]. Up until now, the starter was a separate electric machine. However, the new topologies under investigation should provide both the functions of a starter and an alternator (S/A), as a compromise between space limitations and increasing size of electric machines, coming with higher power rating. That said, the prospective S/A should provide maximum constant torque for engine speed typically up to 250 rev/min, and should work as an alternator, producing constant electrical power, throughout a wide range of engine speed (typically from 600 rev/min up to 6000 rev/min).

The ongoing Research is only focusing on AC machines, to avoid the maintenance required for the brushes. Particularly, the induction machine (IM), switched reluctance (SR), and permanent magnet machines of both surface (SPM) and interior (IPM) magnets, are being investigated for the S/A application. IM is compact and cost-effective, but it is not good in terms of starting torque. SR machine, on the other hand, has a torque vs speed characteristic well suited for the S/A function, but it is prone to torque ripple and acoustic noise. PM machines provide high torque density and high efficiency. In the SPM configuration, magnets benefit from the ventilation at the airgap. Yet, SPM machines cannot achieve a wide constant power speed range (CPSR), since the phase inductance is typically too low to control the voltage, using the armature reaction flux

(Traditional Field Weakening). IPMs can attain a wider CPSR, but its buried magnets are prone to demagnetization because of the high temperatures.

The Axial Flux Permanent Magnet (AFPM) machine of double rotor-single stator configuration, investigated in the present thesis, benefits from the features of a typical SPM and employs mechanical flux weakening. This method decreases the magnitude of flux linkage by manipulating the position of field producing components, rather than by using the armature reaction flux. Thus, armature inductance doesn't play any role in field weakening (FW). Furthermore, this method can serve as a safety measure, since a sudden loss of control in traditional field weakening, during high speed operation, would increase the terminals voltage to unacceptable values.

In the case of an AFPM machine, one option for performing mechanical flux weakening is by increasing the axial distance of the magnet-carrying rotors relative to the stator. This way, the magnitude of airgap flux density and therefore, the flux linked with the windings, can be decreased. Even though this option seems theoretically feasible, in practice a high amount of energy would be required to deal with the attractive force between the iron stator and the PM rotor discs.

Another option is investigated on this thesis. By increasing the angular displacement between the rotors, the flux linked with the stator windings decreases and the induced voltage can be kept at a constant value. Furthermore, the airgap flux density doesn't change in this process, such that ideally, no energy is required for the displacement. These lead to the prospect of achieving a very wide CPSR, while maintaining a high efficiency.

In other papers, it was explained how this angular displacement can be performed mechanically, using a cam/spring configuration to create a speed dependent device [3], and a torque dependent device [2]. As a result, it was demonstrated that the induced back electro-motive force (BEMF) remains almost constant. However, open loop control made the angular displacement regulation susceptible to disturbances and parameter uncertainties. Furthermore, mechanical devices used to control the shifting process aren't easy to configure.

This thesis introduces a novel technique, where the angular displacing of the rotors is performed using the direct axis current i_d, to produce a shifting torque. In the following chapters, the topology of the AFPM machine, and the proposed field weakening method

are described in detail, based on a prototype currently under construction at the Electrical Machines Lab, DIAEE, La Sapienza. Closed loop control, for the angular phase displacement regulation, was designed on MATLAB/SIMULINK. The effectiveness in keeping the power constant above base speed is illustrated through simulation results. In the end, a comparison between the proposed electro-mechanical field weakening and the traditional field weakening, is included.

1.2 AFPM Machine Topology

The analyzed AFPM machine prototype, consists of two iron rotor-discs with surface mounted PMs, and a slotted iron-core stator in the middle. A simple illustration is presented in Figure 1 [3], not including the stator slots. The three-phase winding is wound around the stator in a toroidal way, where the number of coils for one phase is the same as the number of poles (i.e. one coil per pole per phase). The winding has rectangular shape, according to the core cross section.

The PMs on the two rotor discs are mounted in such a way, that magnets of the same polarity face each other. Each north pole magnet drives flux axially across its adjacent

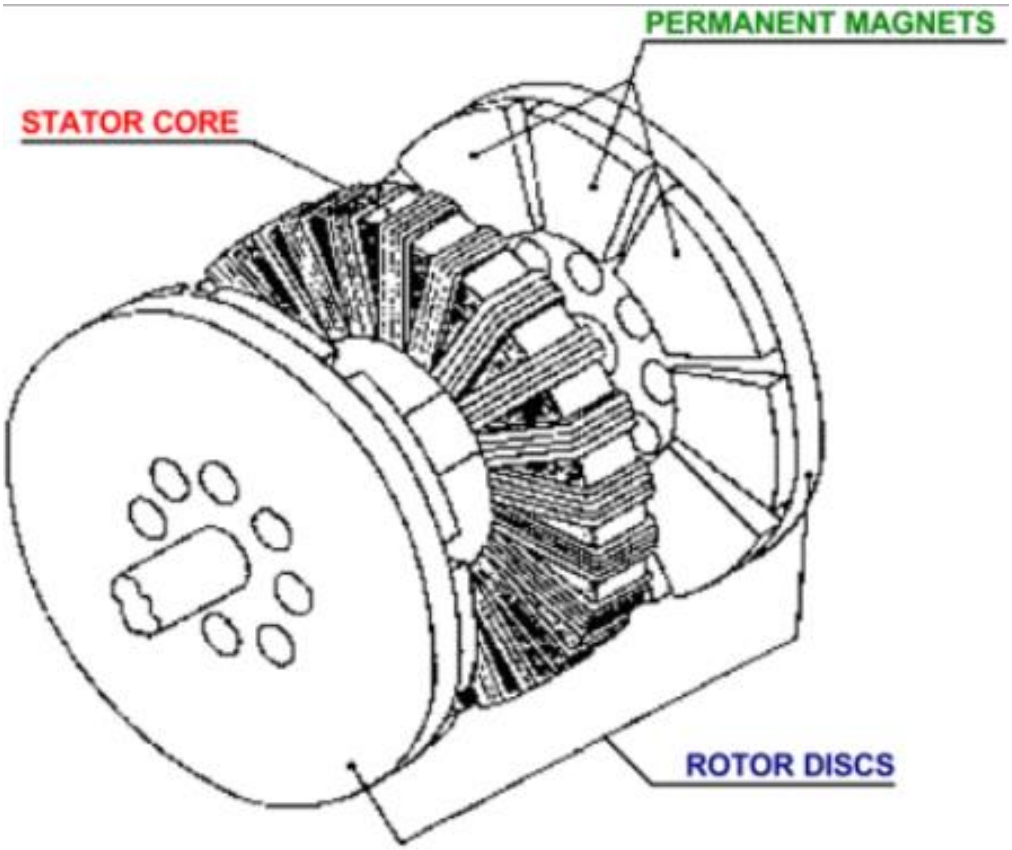

Figure 1: Schematic of an AFPM machine

annular airgap and into the stator iron. The flux then travels circumferentially through the stator iron for one pole pair length, back across the airgap into the adjacent south pole, and through the back iron of the rotor discs. The total PM flux linked with the stator winding is the result of equal flux contributions from both rotor discs. This is illustrated in Figure 2 [3], where just one coil is shown for ease of visualization.

The active portion of the coil is only the radially directed one, facing the magnets. Axially directed end windings do not contribute to rotational torque and neither to BEMF production, since they are parallel to the magnetic field. Therefore, their length should be minimized to reduce losses. The total rotational torque is the sum of all the tangential forces acting on the active portions of all the coils, whenever current flows through them. Polarities of the facing magnets are such that additive BEMF-s are induced on each side of a coil's active part, whenever this rotates in the field.

1.2.1 AFPM Machine with weakened flux linkage

Alternator operation at high engine rev/min (such as above 1000 rpm) would increase the induced voltage at the terminals to unacceptable values. To maintain a constant voltage even at high speeds, the flux linked with the stator winding must be decreased accordingly.

As was previously mentioned, the total PM flux linked with the stator winding is the sum of equal flux contributions from both rotor discs. When they are perfectly aligned (zero angular displacement between the facing magnetic poles), maximum flux is linked (i.e. rated flux linkage), like it is portrayed in Figure 2 [3]. The machine would operate this way for speed lower than a base value that corresponds to base voltage induced.

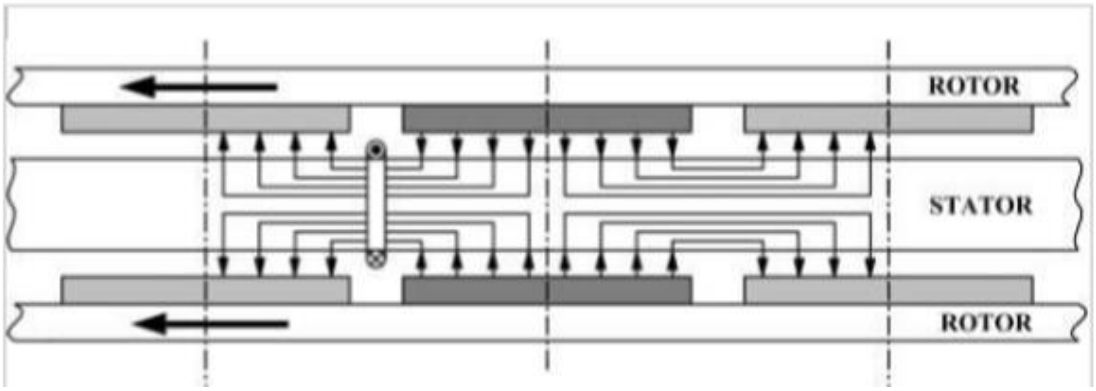

Figure 2: Schematic of the flux linkage paths in an AFPM machine

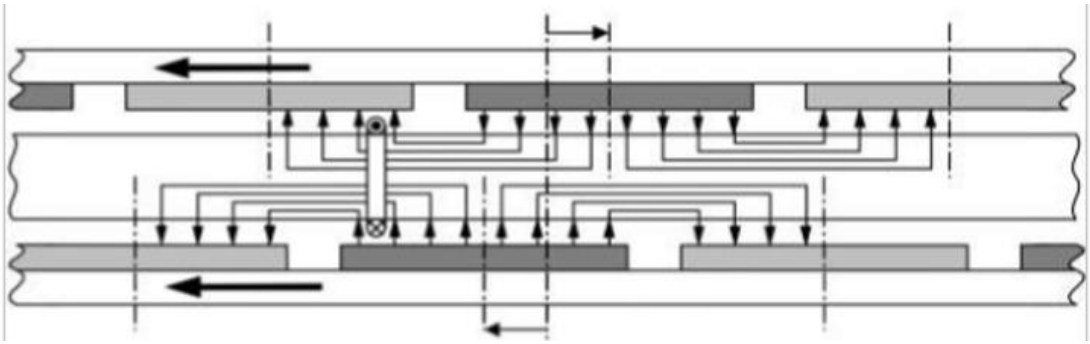

Figure 3: Mechanical weakening of the flux linkage via the regulation of the angular phase displacement between the two PM rotor discs

If the two rotors were to be positioned in such a way that a south pole of one would be facing a north pole of the other, the flux contributions from each of them would cancel each other at the stator core, ideally leading to zero flux linkage. This condition corresponds to 180 electrical degrees of angular displacement between the rotors, and zero induced voltage. Any amount of electrical angular displacement between 0 and 180 degrees will lead to a lower than rated (maximal) flux linkage, depicted in Figure 3 [3].

The variation of the angular phase displacement between the rotor discs will only affect the flux density at the stator core, while the airgap flux density remains unchanged. Therefore, no energy is ideally required in mechanical flux weakening. In the next section, it will be described, among other things, how to maintain a constant induced voltage, by varying the angular phase displacement accordingly with speed.

1.2.2 Comments regarding the AFPM Machine Topology

a) Machine is symmetric, consisting of two identical active halves
b) Machine is isotropic, therefore stator phase inductances are constant and equal. The same is valid for mutual inductances
3) A hub is mounted on the shaft, which connects with the rotor discs through bearings, thus allowing them to synchronously rotate with the shaft, and also have an angular phase displacement with respect to it.
4) The respective angular displacements of the two rotor discs, from the aligned position, are in any case equal in magnitude and in opposite directions. To ensure this, a shifting synchronizer is included in the lab prototype.

1.3 AFPM machine mathematical model

1.3.1 Simplifications in the model

To facilitate the analysis, the no load magnetic field distribution is considered purely sinusoidal (no higher order harmonics). In practice this might not stand true, especially for a slotted stator machine. Therefore, the induced BEMF waveform at no load (zero current) is also sinusoidal. The three-phase stator winding is fed with voltages and currents that are assumed perfectly sinusoidal and balanced (phase a, phase b, and phase c quantities have the same amplitude and are displaced by 120 degrees). Hence, all the relevant quantities governing the machine (i.e. currents, voltages, magnetic fluxes) are of sinusoidal waveform.

Summary of simplifications:

1. Sinusoidal flux distribution along the airgap
2. Phase voltages and currents are sinusoidal and balanced (no harmonics, neither homopolar components are present)
3. No iron losses (i.e. hysteresis and eddy currents losses are neglected)
4. No saturation effects, neither temperature effects (i.e. inductance and resistance are considered constant)
5. No friction losses in the mechanical parts (i.e. hub, bearings)

1.3.2 Convention of the model

A three-phase symmetric quantity (i.e. current, voltage, linked flux) can be represented by a vector in the complex plane, that rotates with electrical frequency ω_e. The components of this vector along two orthogonal axes (direct “d” and quadrature “q” axes), that rotate with the same electrical frequency, are DC quantities. Furthermore, in a synchronous reference frame, the direct axis (d-axis) is always aligned with the PM flux rotating vector (referred to as $\boldsymbol{\lambda_{PM}}$ in Figure 4).

The selection of this convention is justified as follows:

1. Reduced number of equations (only 2 coordinates, instead of 3)
2. Reduced number of terms, as there are no mutual inductance terms present on the equations

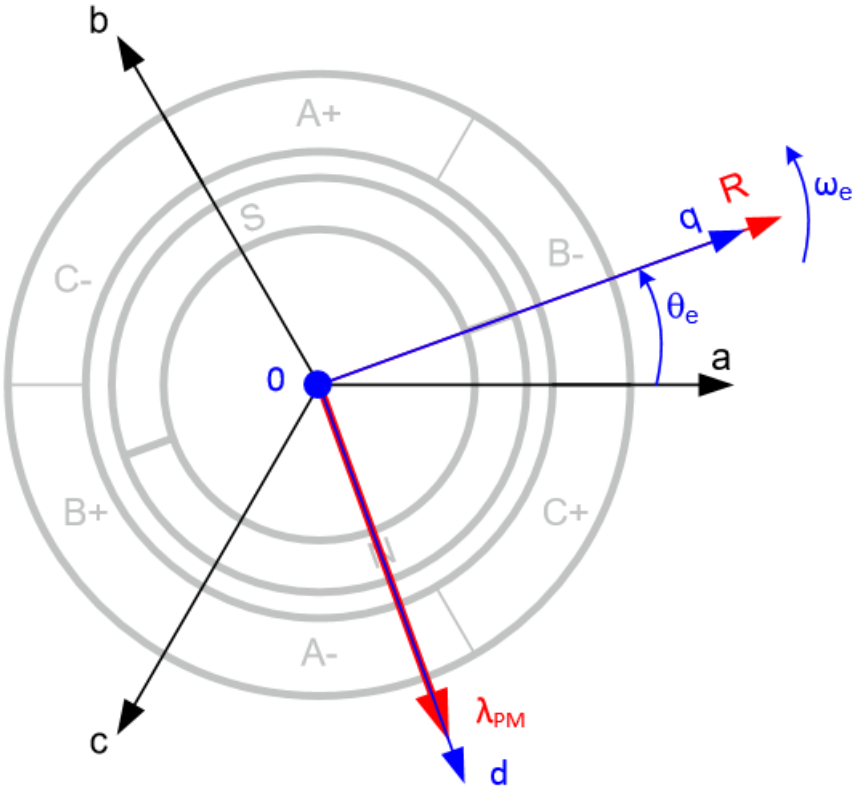

Figure 4: Synchronous reference frame

3. The analysis is more intuitive since, like in a DC machine, there is one field producing current and one torque producing current
4. The design of controllers is usually done in the synchronous reference frame, because it is simpler to control DC signals than sinusoidal signals

1.3.3 AFPM mathematical model in the (dq) synchronous reference frame

The total PM flux linked with the stator windings is the vector sum of equal flux contributions by each of the two PM rotor disc. When the rotors are perfectly aligned, the vector sum becomes a simple algebraic sum. This corresponds to the condition of maximum (i.e. rated) total PM flux linkage Λ_{PM}. Introducing an angular displacement between the two rotors yields weakened flux linkage, a condition which is depicted in the dq-plane diagram of Figure 5. Since the angular phase displacement of one rotor disc, with respect to the aligned position, is always equal to that of the second rotor disc, $\lambda_{PM_{1q}}$ and $\lambda_{PM_{2q}}$ cancel each other, so that there is no residual linked PM flux in the q-axis: $\lambda_{PM_q} = 0$

Stator voltage equations in (dq)-coordinates are of similar form with equations in three-phase (abc)-coordinates, with the addition of the terms in bold, which arise to maintain equivalency between the transformations:

$$v_q = Ri_q + \frac{d\lambda_q}{dt} + \boldsymbol{\omega_e \lambda_d}$$

$$v_d = Ri_d + \frac{d\lambda_d}{dt} - \boldsymbol{\omega_e \lambda_q}$$

Torque equation in (dq)-coordinates is:

$$T = \frac{3}{2} P\left(\lambda_d i_q - \lambda_q i_d\right)$$

There are two PM rotor discs, therefore, one torque equation can be written for each of them:

$$T_1 = \frac{3}{2} P(\lambda_{1d} i_q - \lambda_{1q} i_d)$$

$$T_2 = \frac{3}{2} P(\lambda_{2d} i_q - \lambda_{2q} i_d)$$

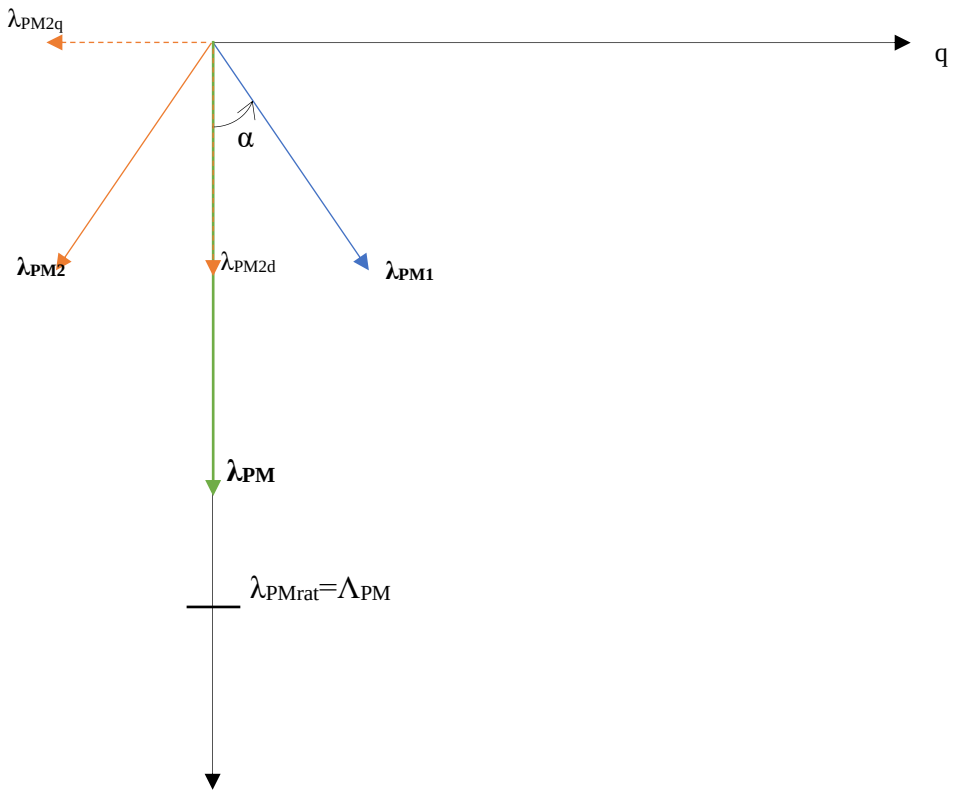

Figure 5: Diagram of PM flux linkage vectors and their projections, for displaced rotor discs

The general form of flux linkage equations in (dq)-coordinates is:

$$\lambda_q = L_q i_q$$

$$\lambda_d = L_d i_d + \lambda_{PM}$$

Looking at Figure 5 above, we can write the flux linkage equations as:

$$\lambda_{1q} = \frac{L_q i_q}{2} + \Lambda_{PM1} \sin(\alpha) = \frac{L_q i_q}{2} + \frac{\Lambda_{PM}}{2} \sin(\alpha)$$

$$\lambda_{1d} = \frac{L_d i_d}{2} + \Lambda_{PM1} \cos(\alpha) = \frac{L_d i_d}{2} + \frac{\Lambda_{PM}}{2} \cos(\alpha)$$

$$\lambda_{2q} = \frac{L_q i_q}{2} - \Lambda_{PM2} \sin(\alpha) = \frac{L_q i_q}{2} - \frac{\Lambda_{PM}}{2} \sin(\alpha)$$

$$\lambda_{2d} = \frac{L_d i_d}{2} + \Lambda_{PM2} \cos(\alpha) = \frac{L_d i_d}{2} + \frac{\Lambda_{PM}}{2} \cos(\alpha)$$

$$\lambda_q = \lambda_{1q} + \lambda_{2q} = L_q i_q$$

$$\lambda_d = \lambda_{1d} + \lambda_{2d} = L_d i_d + \Lambda_{PM} \cos(\alpha)$$

Substituting the final flux linkage equations, in the voltage and torque equations, while considering that $L_q = L_d$, we get:

$$v_q = R i_q + L_q \frac{di_q}{dt} + \omega_e L_d i_d + \omega_e \Lambda_{PM} \cos(\alpha) \quad (1)$$

$$v_d = R i_d + L_d \frac{di_d}{dt} - \Lambda_{PM} \sin(\alpha) \frac{d\alpha}{dt} - \omega_e L_q i_q \quad (2)$$

$$T_1 = \frac{3}{2} P \frac{\Lambda_{PM}}{2} (\cos(\alpha)\, i_q - \sin(\alpha) i_d)$$

$$T_2 = \frac{3}{2} P \frac{\Lambda_{PM}}{2} (\cos(\alpha)\, i_q + \sin(\alpha) i_d)$$

Total motoring torque is the sum of torque contributions from both rotor discs:

$$T_{mot} = T_1 + T_2 = \frac{3}{2} P \Lambda_{PM} \cos(\alpha)\, i_q \quad (3)$$

The interesting part is that a shifting torque can be produced using the d-axis current, mathematically expressed as:

$$T_{shift} = T_1 - T_2 = -\frac{3}{2} P \Lambda_{PM} \sin(\alpha)\, i_d \quad (4)$$

A negative i_d increases the angular displacement between the rotor discs, while a positive i_d would tend to bring them into alignment.

Equations (1)-(4) above model the electromagnetic behavior of the AFPM machine. The mechanical behavior can be described by two separate equations, one for the motoring torque, and the other for the shifting torque.

$$T_{mot} - T_{load} = J_{mot}\frac{d\omega_{mot}}{dt} + B_{mot}\omega_{mot} = J_{mot}\frac{d^2\vartheta_{mot}}{dt^2} + B_{mot}\frac{d\,\vartheta_{mot}}{dt} \qquad (5)$$

$$T_{shift} = J_{shift}\frac{d\omega_{shift}}{dt} + B_{shift}\omega_{shift} = J_{shift}\frac{d^2(2\alpha_{shift})}{dt^2} + B_{shift}\frac{d\,(2\alpha_{shift})}{dt} \qquad (6)$$

It should be noted that equations (1)-(4) use the electrical frame, therefore ω_e is expressed in units of electrical rad/sec, and α is in electrical radians. Meanwhile, in equations (5) and (6), ω_{mot} and ω_{shift} are in mechanical rad/sec and α_{shift} is in mechanical radians. Electrical and mechanical quantities are related by the number of pole pairs P, as:

$$\omega_{mot} = \frac{\omega_e}{P}$$

$$\alpha_{shift} = \frac{\alpha}{P}$$

T_{shift} models the combined effect of respective shifting torques in each of the rotors, therefore ω_{shift} is the relative shifting speed of rotor 1 from rotor 2. This is double the shifting speed of one rotor from the shaft.

Looking at equation (4), if $\alpha = 0$ then $\sin(\alpha) = 0$ and $T_{shift} = 0$, therefore, regardless how big the negative d-axis current is, the rotors cannot get past the state of alignment. As a conclusion, in order to modify the angular phase displacement and perform FW, the initial angle α_{min} must be different from zero. In the AFPM prototype, mechanical stops are used to prevent the rotors from going under a certain angular phase displacement α_{min}. Another mechanical stop at $\alpha = \alpha_{max} = 90^o$ electrical (i.e. 90°/P in mechanical degrees), will not allow the rotors inertia to send them again towards alignment (@ 360° electrical angular displacement between the rotors), thus preventing the compromising of flux regulation.

Having an initial angular phase displacement different from zero, means that the PM total flux linkage across the Constant Torque Speed Range, is lower than rated and equal to:

$$\Lambda_{PM}\cos\left(\alpha_{\min}\right)$$

This condition is illustrated in the PM flux linkage vector diagram of Figure 6. Looking at equation (3) for the motoring torque, $\cos(\alpha) < 1$, therefore Motoring Torque Capability will be lower than 100%. With greater initial angular displacement, comes lower Motoring Torque Capability. The selection of the minimum angular position for the mechanical stops is discussed in detail in the 4th Chapter.

Induced voltage on q-axis, assuming steady state (SS) $i_d = 0$, is calculated as:

$$E_q = \omega_e \Lambda_{PM} \cos(\alpha)$$

Based on Figure 6, the induced voltage at rated speed is equal to:

$$E_{base} = \omega_{base} \Lambda_{PM} \cos(\alpha_{min})$$

For frequency higher than base frequency, PM flux linkage needs to decrease, in order to maintain a constant induced voltage. In mechanical flux weakening, this is performed by increasing the angular phase displacement α with frequency, according to the following relation:

$$\omega_e \Lambda_{PM} \cos(\alpha) = E_{base} = \omega_{base} \Lambda_{PM} \cos(\alpha_{min})$$

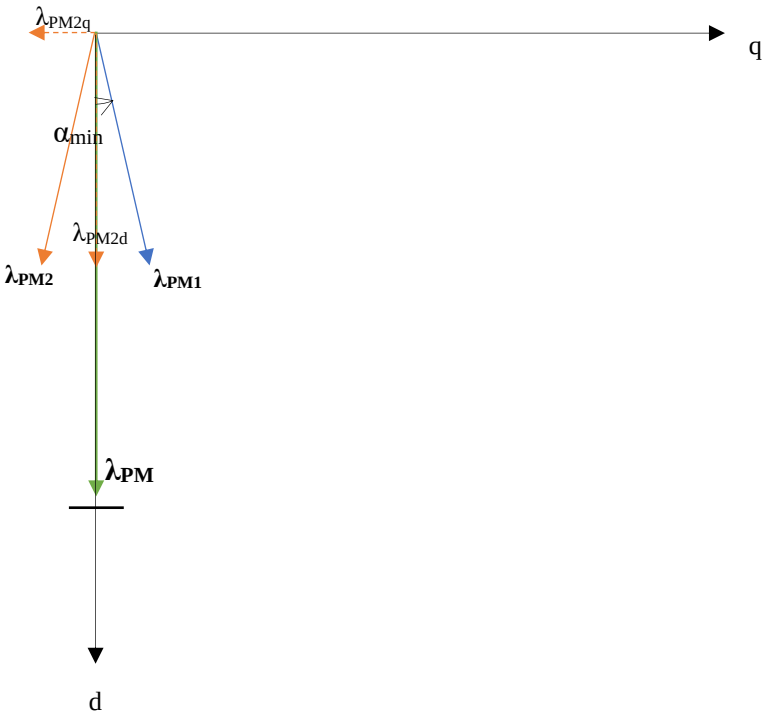

Figure 6: Vector diagram of PM flux linkage, during operation in Constant Torque Region

$$\cos(\alpha) = \frac{E_{base}}{\Lambda_{PM}} \frac{1}{\omega_e}$$

$$\alpha = arcos\left(\frac{\cos(\alpha_{min})}{n_{pu}}\right) \quad (7)$$

The relation expressed by equation (7), is plotted in Figure 7, for a random choice of $\alpha_{min} = 10^o$.

It is important to emphasize that, based on equation (7), a theoretical infinite speed can be attained while maintaining constant induced voltage, corresponding to an electrical angular phase displacement of 90 degrees. Therefore, CPSR can be theoretically increased to infinity.

Equation (7) is used later in the field weakening control logic, to generate the reference for the angular phase displacement α, depending on speed of rotation.

The set of equations [(1)-(6)] model the fundamental electromagnetic and mechanical behavior of the AFPM machine, representing therefore its mathematical model:

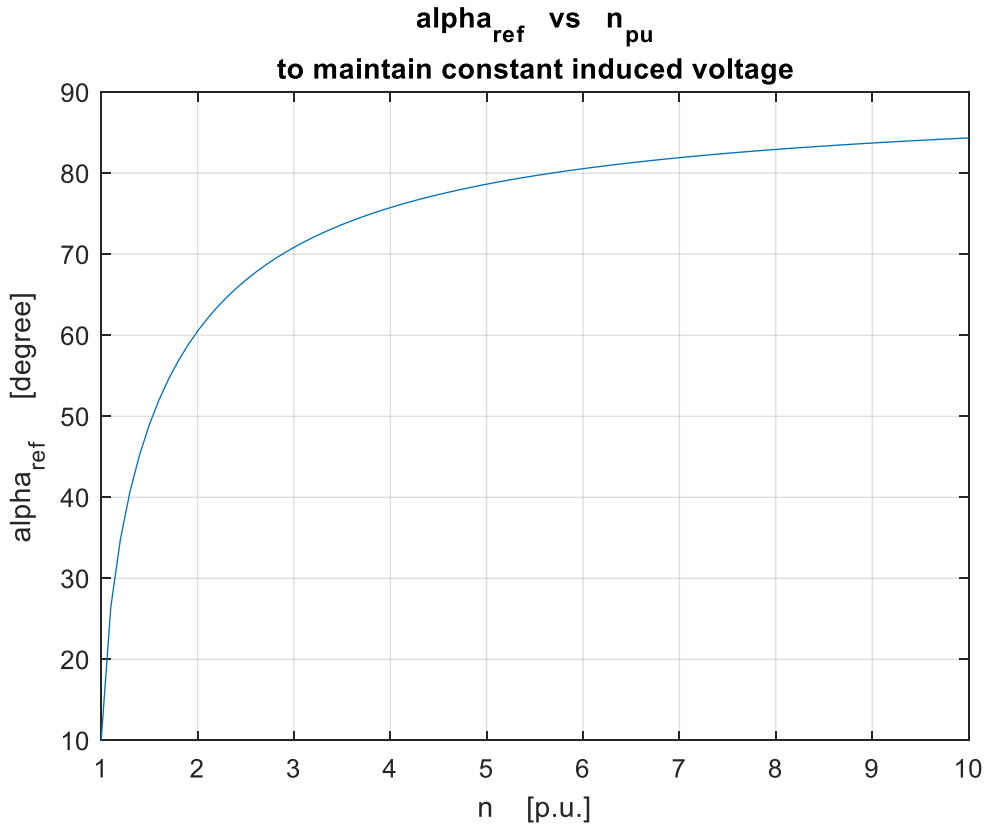

Figure 7: Required angular phase displacement to maintain constant induced voltage with Mechanical Flux Weakening

$$v_q = Ri_q + L_q \frac{di_q}{dt} + \omega_e L_d i_d + \omega_e \Lambda_{PM} \cos(\alpha) \quad (1)$$

$$v_d = Ri_d + L_d \frac{di_d}{dt} - \Lambda_{PM} \sin(\alpha) \frac{d\alpha}{dt} - \omega_e L_q i_q \quad (2)$$

$$T_{mot} = \frac{3}{2} P \Lambda_{PM} \cos(\alpha)\, i_q \quad (3)$$

$$T_{shift} = -\frac{3}{2} P \Lambda_{PM}\, sin(\alpha)\, i_d \quad (4)$$

$$T_{mot} - T_{load} = J_{mot} \frac{d^2 \vartheta_{mot}}{dt^2} + B_{mot} \frac{d\, \vartheta_{mot}}{dt} \quad (5)$$

$$T_{shift} = J_{shift} \frac{d^2 (2\alpha_{shift})}{dt^2} + B_{shift} \frac{d\, (2\alpha_{shift})}{dt} \quad (6)$$

1.4 Model of the AFPM machine prototype on MATLAB/SIMULINK

To evaluate the effectiveness of the proposed Mechanical Flux Weakening in our AFPM machine prototype, first its model was developed on the MATLAB/SIMULINK environment, based on equations (1)-(6) of the mathematical model.

Libraries of SIMULINK provide the necessary block functions to build a model of the machine, while the parameters are based on the AFPM machine prototype under construction at the lab and were declared in a MATLAB script. The provided parameters are included in the following table:

Table 1: Provided parameters of the AFPM machine prototype

Electro-magnetic parameters:	
Rated torque T_n	50 Nm
Rated speed n_n	3000 RPM
Rated power P_n	15.7 kW
Rated current I_n	50 A
Rated induced phase voltage (@ n_n) E_{phrms}	102 V
Stator resistance R	37 mΩ
Stator inductance L_{pu}	0.57 pu
Pole pairs P	8
Mechanical parameters:	
Rotor disc outer diameter D_e	220 mm
Rotor disc inner diameter D_i	140 mm

Rotor disc thickness th	7 mm
Rotor disc material	iron
Hub diameter D_{hub}	90 mm
Hub length L_{hub}	52 mm
Hub material	Aluminum
PM big base PM_a	35 mm
PM small base PM_b	18 mm
PM height PM_h	40 mm
PM thickness PM_{th}	4 mm
PM material	2x16 Nd-Fe-B

In order to complete the AFPM machine model, some other electro-magnetic and mechanical parameters were calculated and declared in the script, derived from those provided in the prior table. Specifically, the calculated parameters and the formulas used in the script are:

Electro-magnetic parameters:

$$\omega_{mot_n} = n_n 2\frac{\pi}{60}$$

$$\omega_{e_n} = Pn_n 2\frac{\pi}{60}$$

$$\Lambda_{PM} = \sqrt{2}\frac{E_{ph_{rms}}}{\omega_{e_n}}$$

$$i_{dq_{lim}} = \sqrt{2}I_n$$

$$L_d = L_{d_{pu}} L_{base} = L_{d_{pu}} \frac{Z_{base}}{\omega_{e_n}} = L_{d_{pu}} \frac{E_{ph_{rms}}/I_n}{\omega_{e_n}}$$

Mechanical:

(note: moment of inertia with respect to the axis of rotation)

$$J_{mot} = 2J_r + 2 * 16J_{PM} + J_{hub} + J_{shaft} + J_{load}$$

$$J_{shift} = 2J_r + 2 * 16J_{PM}$$

$$J_r = \frac{1}{2} M_r [\left(\frac{D_e}{2}\right)^2 + \left(\frac{D_i}{2}\right)^2]$$

$$M_r = V_r Density_{Fe} = \left\{\pi * th * \left[\left(\frac{D_e}{2}\right)^2 - \left(\frac{D_i}{2}\right)^2\right]\right\} Density_{Fe}$$

$$J_{hub} = \frac{1}{2} M_{hub} [\left(\frac{D_i}{2}\right)^2 + \left(\frac{D_{hub}}{2}\right)^2]$$

$$M_{hub} = V_{hub} * Density_{Al} = \left\{\pi * th * \left[\left(\frac{D_i}{2}\right)^2 - \left(\frac{D_{hub}}{2}\right)^2\right]\right\} Density_{Al}$$

Calculating the inertia of the permanent magnets and that of the shaft, wasn't straightforward, so we had to rely on the technical drawings of the AFPM machine prototype (see Figure 8). Using the dimensional data, the scale of the drawing was determined and used to calculate the shaft length and then its moment of inertia:

$$L_{shaft} = 0.258 * scale$$

$$J_{shaft} = \frac{1}{2} M_{shaft} \left(\frac{D_{shaft}}{2}\right)^2$$

$$M_{shaft} = V_{shaft} * Density_{Fe} = \left[\pi \left(\frac{D_{shaft}}{2}\right)^2 L_{shaft}\right] * Density_{Fe}$$

Permanent magnets of our AFPM machine prototype have a trapezoidal shape, depicted in Figure 8. To calculate their moment of inertia with respect to the axis of rotation, the parallel axis theorem was used, also known as Huygens-Steiner theorem. It states that, if the body is made to rotate about a new axis, which is parallel to the axis going through its center of mass and displaced from it by a distance *d*, then the moment of inertia *I* with respect to the new axis is related to I_{cm} by: $I=I_{cm}+md^2$. Based on this theorem and Figure 8:

$$J_{PM} = J_{PM_{CM}} + M_{PM} \left(\frac{D_i}{2} + h_{CM}\right)^2$$

$$J_{PM_{CM}} = \frac{h}{144(a+b)} (16h^2ab + 4h^2b^2 + 4h^2a^2 + 3a^4 + 6a^2b^2 + 6a^3b + 6a^3 + 3b^4)$$

$$h_{CM} = \frac{h}{3} * \frac{2 * a + b}{a + b}$$

$$M_{PM} = V_{PM} * Density_{NdFeB} = \left(\frac{PM_a + PM_b}{2} * PM_h * PM_{th}\right) * Density_{NdFeB}$$

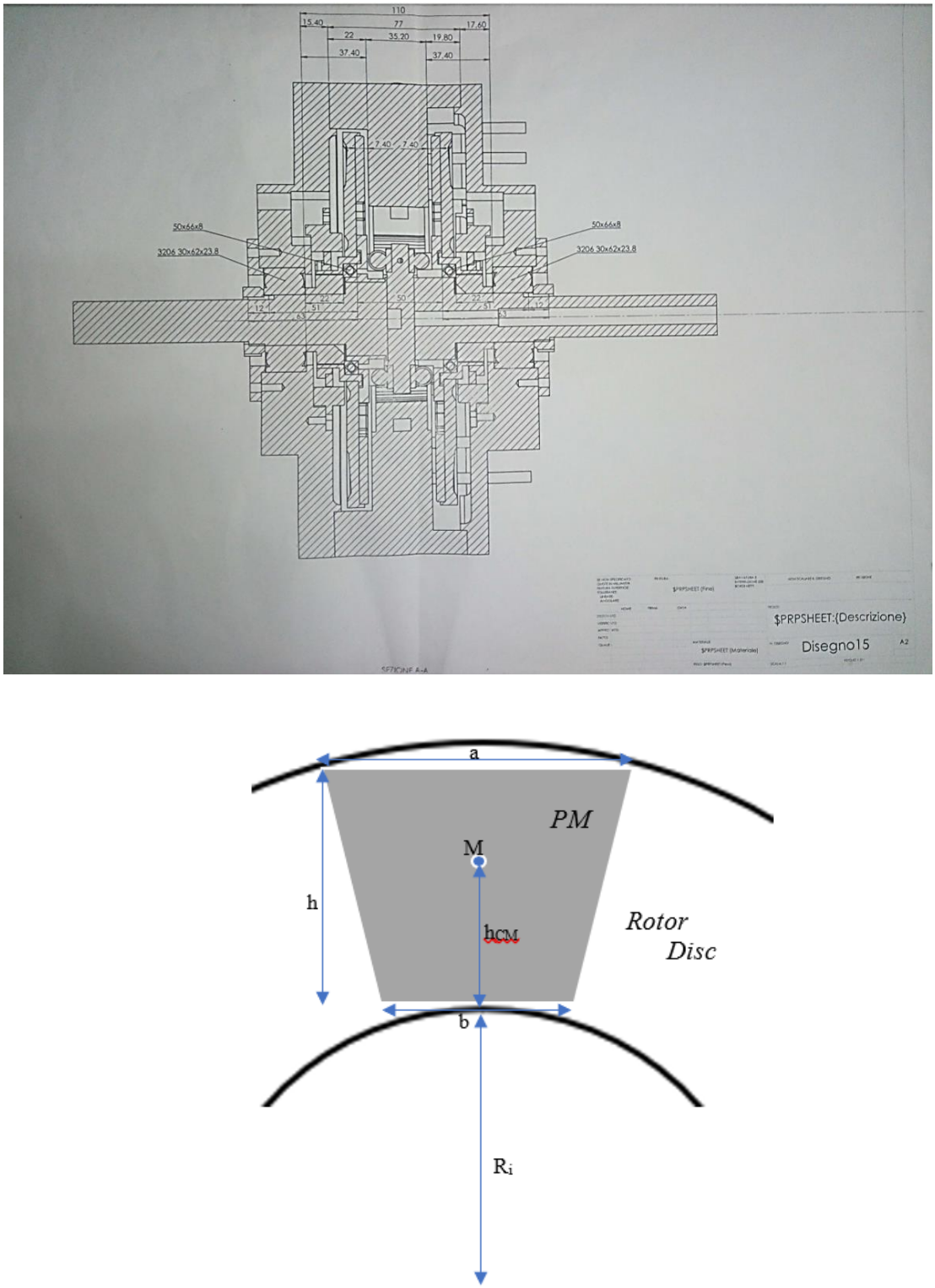

Figure 8: Technical drawing of the AFPM machine prototype (up), PMs shape and dimensions (bottom)

The values for the minimum and maximum angular phase displacement were also declared in the script, as α_{min} and α_{max}, respectively. Initially, the value for α_{min} was chosen randomly.

The complete script for the AFPM machine model is:

```
% Electro-magnetic parameters
Pn=15700;            % W
Tn=50;               % Nm
n_n=3000;            % RPM
P=8;                 % pole pairs
E_ph_rms=102;        % V
In=50;               % A
R=0.037;             % Ohm
Ld_pu=0.57;          % p.u.
omega_mot_n=n_n*2*pi/60;
omega_e_n=P*omega_mot_n;
LambdaPM=sqrt(2)*E_ph_rms/omega_e_n;
i_dq_lim=sqrt(2)*In;
iq_rat=sqrt(2)*In;
Ld=Ld_pu*E_ph_rms/In/omega_e_n;
Lq=Ld;

alpha_min=pi/16;
alpha_max=pi/2;

% Mechanical parameters
% Rotor dimensions
D_e=0.220;                                  % m
D_i=0.140;
th=0.007;
M_r=((pi*th*((D_e/2)^2-(D_i/2)^2))*7874);   % M=V*iron_density
J_r=1/2*M_r*((D_e/2)^2+(D_i/2)^2);

% PM dimensions
PM_a=0.035;                                 % m
PM_b=0.018;
PM_h=0.040;
PM_th=0.004;
M_PM=((PM_a+PM_b)/2*PM_h*PM_th)*7500;                          %
M_PM=V_PM*NdFeB_density
```

```
J_PM=PM_h/(144*(PM_a+PM_b))*(16*PM_h^2*PM_a*PM_b+4*PM_h^2*PM_b^2
+4*PM_h^2*PM_a^2+3*PM_a^4+6*PM_a^2*PM_b^2+6*PM_a^3*PM_b+6*PM_a*P
M_b^3+3*PM_b^4)+M_PM*(D_i/2+0.0221)^2;

% Hub dimensions
D_hub=0.09;                                          % m
L_hub=0.052;
M_hub=(pi*th*((D_i/2)^2-(D_hub/2)^2))*2710;                          %
M_hub=V_hub*aluminium_density
J_hub=1/2*M_hub*((D_i/2)^2+(D_hub/2)^2);

% Shaft dimensions
scale=1.47;
D_shaft=0.09;                                        % m
L_shaft=0.258*scale;
M_shaft=(pi*(D_shaft/2)^2*L_shaft)*7874;                             %
M_shaft=V_shaft*iron_density
J_shaft=1/2*M_shaft*(D_shaft/2)^2;

J_load=0;
T_load=0;
J_mot=2*J_r+2*16*J_PM+J_hub+J_shaft+J_load;
B_mot=0;
J_shift=2*J_r+2*16*J_PM;
B_shift=0;
```

The SIMULINK electromagnetic model of the AFPM machine, was developed based on equations (1)-(4) of the mathematical model. This subsystem has four inputs and four outputs, as it is illustrated in Figure 9. In a real machine, for the purpose of control, inputs are phase voltages and outputs are phase currents. Besides these, two additional inputs and two additional outputs were added in the model, which connect with the mechanical subsystem: ω_e and α, T_{mot} and T_{shift}, respectively.

Another model was created on SIMULINK, for the mechanical subsystem, based on equations (5) and (6), as it is illustrated in Figure 10. The shifting torque subsystem has some additional blocks included, that serve to model the effect of mechanical stops.

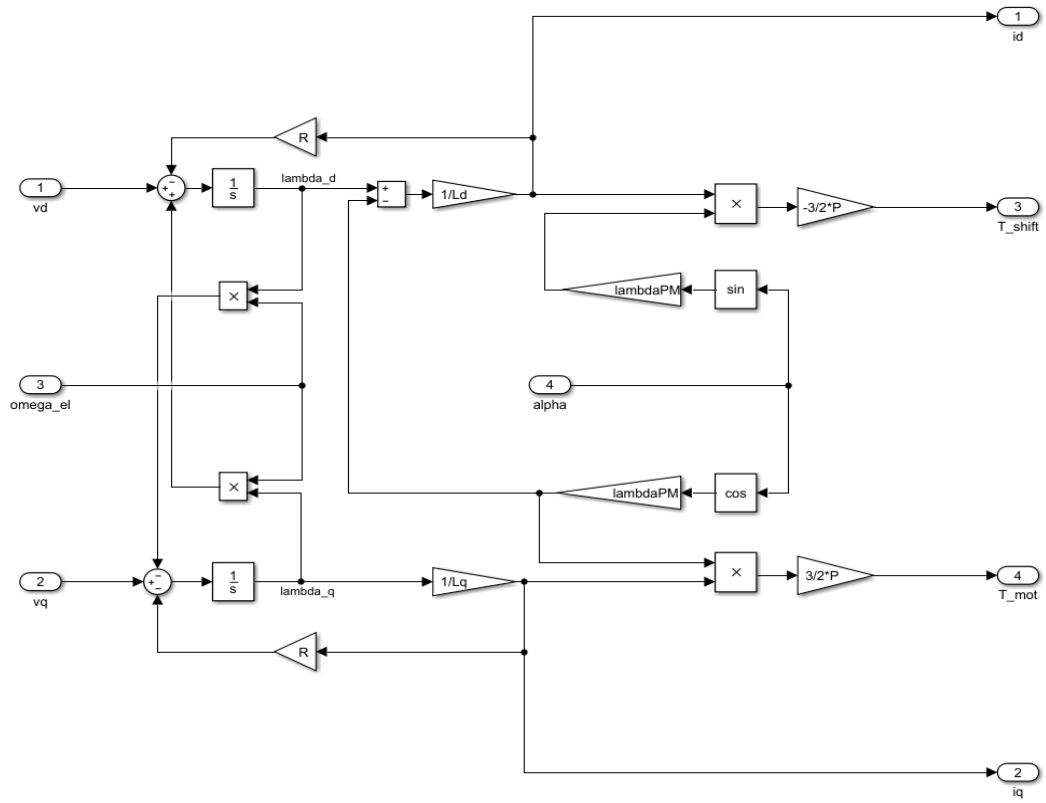

Figure 9: SIMULINK electromagnetic model of the AFPM machine

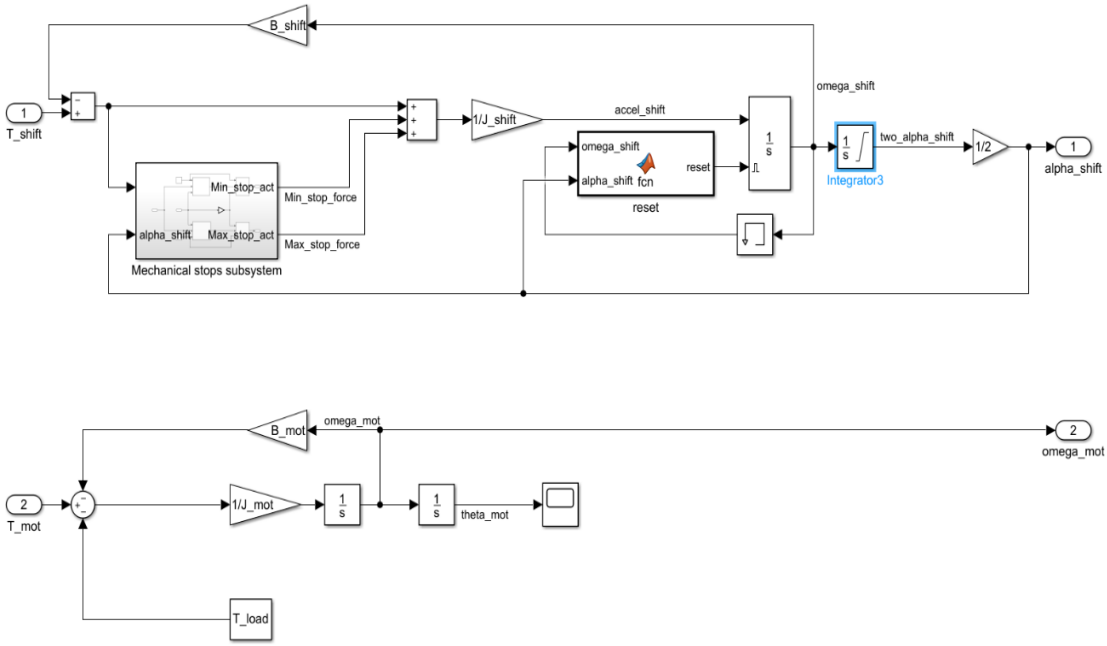

Figure 10: SIMULINK mechanical model of the AFPM machine

Particularly, this effect extends to three variables of the mechanical subsystem, that are:

$\alpha_{shift}, \omega_{shift}$ and $\frac{d\omega_{shift}}{dt} = accel_{shift}$

As first instance, integrator block 3 calculates the mechanical angular phase displacement between the two rotors (i.e. $2\alpha_{shift}$), integrating their relative angular speed of displacement ω_{shift}. The mechanical stops are represented in this integrator, as an upper saturation level for the maximum angular border, and a lower saturation level for the minimum. Since the variables declared on a MATLAB script are for the electrical α_{min} and α_{max}, here they must be divided by no. of pole pairs P to get the mechanical equivalents and multiplied by two to get $2\alpha_{min}$ and $2\alpha_{max}$ (see Figure 11). Having an initial angular phase displacement is also represented in the integrator block parameters.

Secondly, since ω_{shift} is calculated also from an integrator block, it keeps increasing or decreasing incrementally depending in the direction of the shifting acceleration. But, when rotors hit the mechanical stops, their real speed instantly becomes zero, even though the shifting acceleration might still be different from zero. To reflect this, the reset option is activated in the integrator block parameters, and it is driven by a MATLAB function (see "reset" block in Figure 10) written in C code.

```
function reset =fcn(omega_shift,alpha_shift)

pp=8;

alpha_shift_max=pi/2/pp;
 alpha_shift_min=pi/16/pp;


if alpha_shift==alpha_shift_min && omega_shift~=0
    reset=1;
elseif alpha_shift==alpha_shift_max && omega_shift~=0
    reset=1;
else
    reset=0;
end
```

This function has as inputs $\alpha_{shift}, \omega_{shift}$, and as output the reset TRUE or FALSE value. First, the name and structure of the function are declared in the MATLAB script, followed by initialization of needed variables such as pole pairs (P), minimum and maximum angular phase displacement in mechanical degrees $\alpha_{shift_{min}}, \alpha_{shift_{max}}$ respectively. Then, the body of the function contains an "if/else if" condition, for when

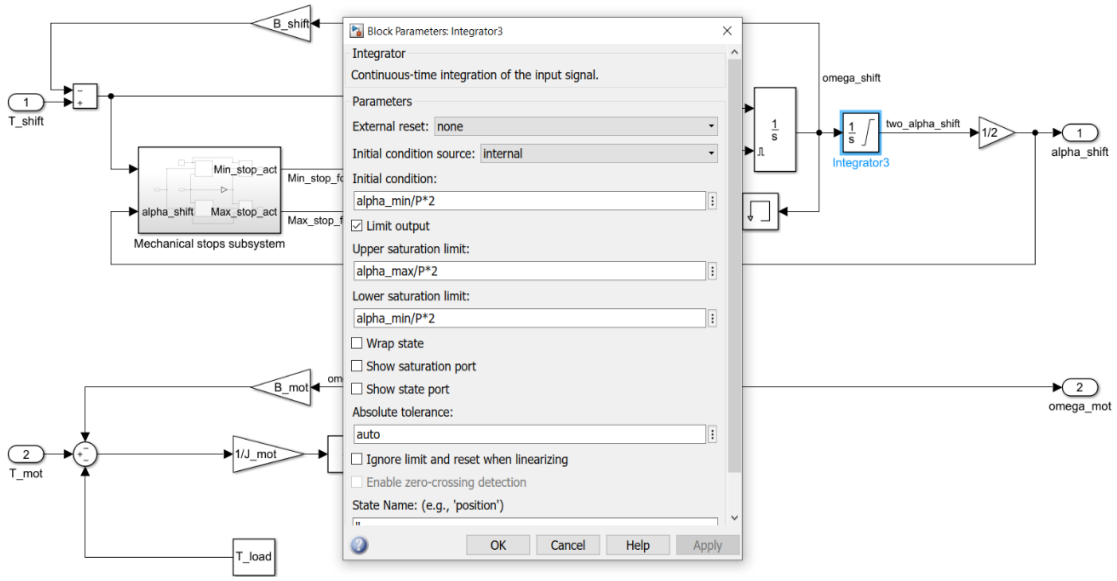

Figure 11: Setting the saturations and initial condition of alpha integrator, based on the mechanical borders

the reset option must be triggered, which is if α_{shift} is equal (= =) to the minimum position ($\alpha_{shift_{min}}$) or else if it is equal to the maximum border ($\alpha_{shift_{max}}$).

The addition of the "and" condition (&&) on the above cases was required, otherwise the reset would be continuously true, not allowing shifting speed to increment from zero. Now, reset is triggered, only if ω_{shift} is different (~=) from zero, at the same time. In all other cases, reset option is equal to zero (i.e. not triggered).

Lastly, another aspect to be modelled is the relation between direction of the shifting acceleration and reaction of the mechanical stops. These last react to the rotors with an equal but opposite torque, preventing the rotors from further moving, only if said rotors are tending to go past the stops. In other words, if the rotors are at the position of the minimum stop and at the same moment, they have a negative shifting acceleration that comes from a negative shifting torque (tending to align), the stops will act with an equal but positive torque. This way the final total torque acting is zero. Same logic for the combination of position at the maximum stop and positive shifting torque. In all other cases, mechanical stops will not affect the mechanical subsystem. To model this, another subsystem is created inside it, named the mechanical stops subsystem (see Figure 13). It has as inputs the resulting shifting torque and the mechanical angular phase displacement a_{shift}. Outputs are reactions of the minimal and maximal mechanical borders. In Figure 12 the mechanical stops subsystem is illustrated with all its components. The switch blocks on the left, output the value of resulting torque coming from input port 1, if the rotors are at one of the border positions, or output zero in all other cases. Following the

same logic, switch blocks on the right, output an equal but opposite torque of that coming from input port 1, if said torque is negative in case of the minimal border, or positive for the maximal border, or output zero (i.e. no reaction from mechanical stops) in other cases. As a final step, the electromagnetic subsystem and the mechanical subsystem are connected, forming the AFPM machine system. The link between them requires a multiplication of the mechanical variables by the number of pole pairs (P), to get the electrical ones, as it is illustrated in Figure 14

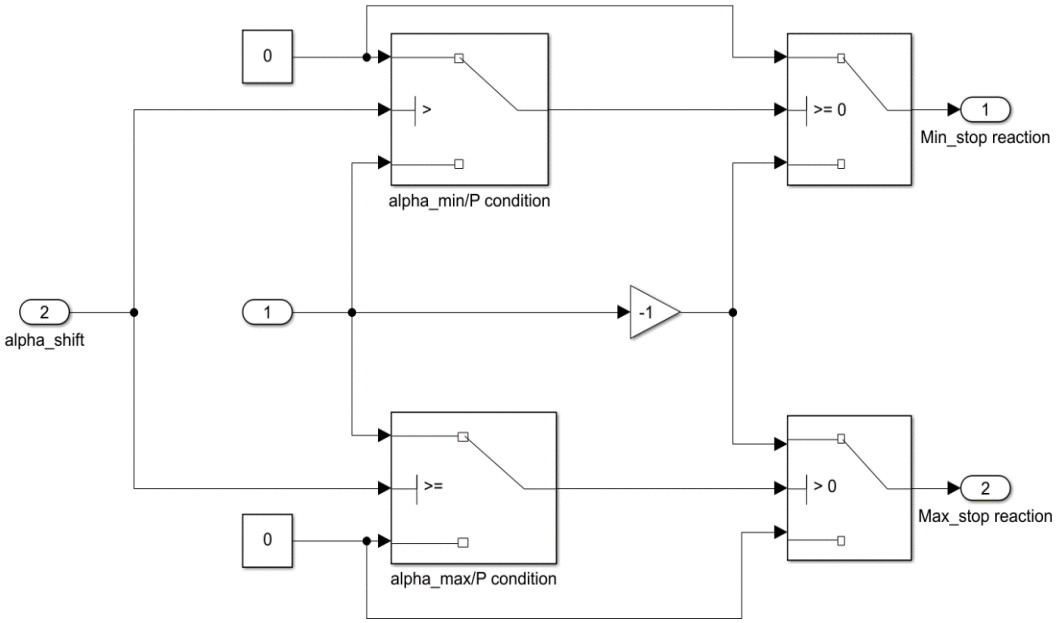

Figure 12: Mechanical stops subsystem

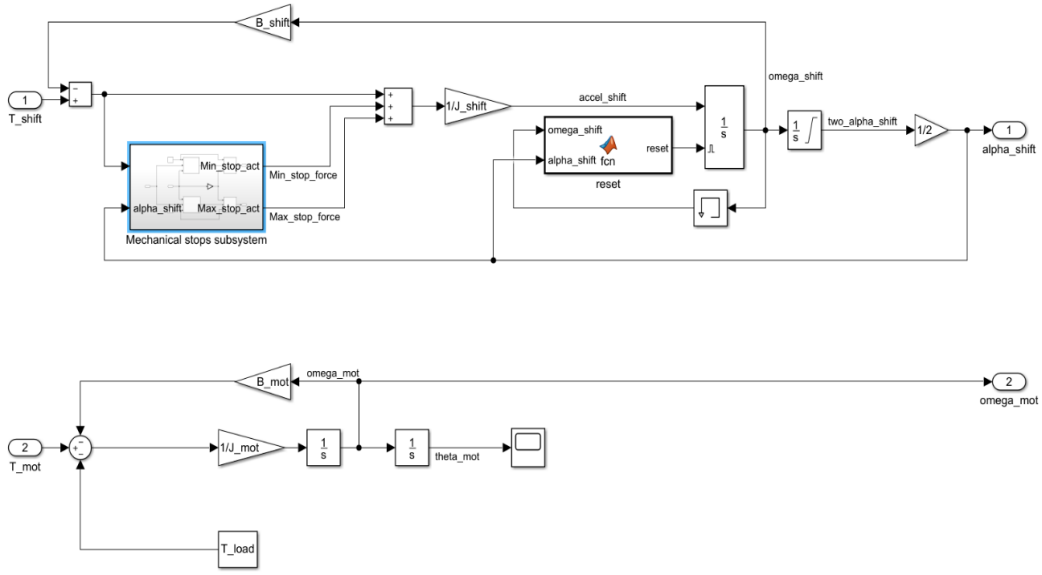

Figure 13: Mechanical stops subsystem inside the mechanical system

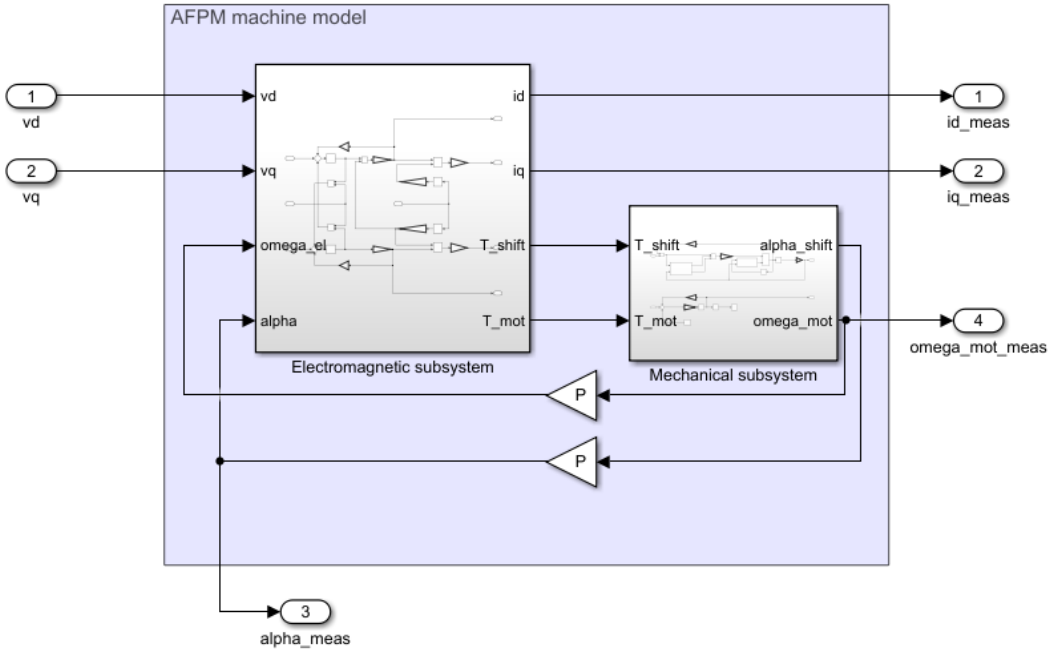

Figure 14: SIMULINK model of the AFPM machine

Chapter 2

Closed Loop Control of the Angular Phase Displacement

2.1 General Outline of Closed Loop Control for the Angular Phase Displacement

Once the AFPM machine model was completed, next step was the design of the closed loop control for the angular phase displacement. Based on equation (4) of the AFPM machine mathematical model, a shifting torque can be produced using the d-axis current, as:

$$T_{shift} = T_1 - T_2 = -\frac{3}{2} P \Lambda_{PM} \, sin(\alpha) \, i_d$$

Therefore, the output of the angular phase displacement (alpha) controller should be, precisely, the d-axis current.

An inner d-axis-current control loop is also necessary, to guarantee a fast buildup of the required current, and in the same time prevent spikes in voltage levels when a current command is executed. This way, the outer alpha control loop employs a "well-behaved" current as a control variable, making the angular phase displacement regulation more robust.

The overall control block diagram is depicted in Figure 15 The design was developed in the Laplace domain, under the simplification of unity feedback transfer function (i.e. measured and actual signals are considered identical)

To make the connection between the control and the AFPM machine model, in the latter, two inputs and four outputs were added (see Figure 14). Inputs are the (dq)-axes voltages, which are outputs for the (dq)-current controllers. Outputs of the AFPM machine

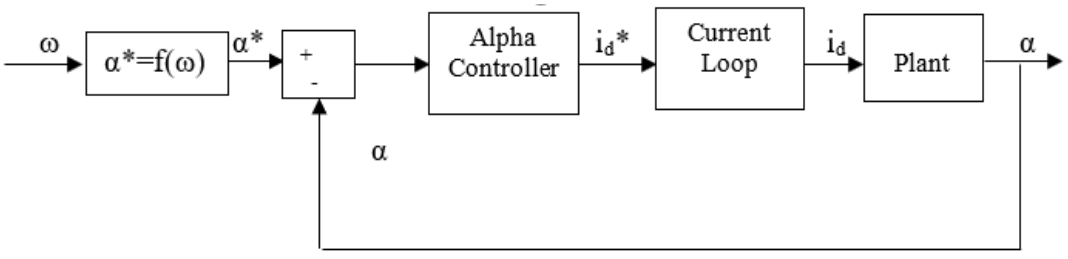

Figure 15: Negative feedback control loop for the regulation of the angular phase displacement

subsystem are measured $i_{d_{meas}}$, $i_{q_{meas}}$, α_{meas} and $\omega_{mot_{meas}}$. The first two are necessary for the (dq) current control loops, and the last two are necessary for the field weakening control. The q-axis current control loop was included in the design, since it follows the same logic as for the d-axis, but it is not required for the field weakening implementation.

2.2 Closed Loop Control of d-axis Current

The closed loop scheme for the control of d-axis current (same for q-axis current) is depicted in the block diagram of Figure 16. The level of d-axis current is changed by the inverter, which feeds the machine with the appropriate voltage. Normally, the response of the inverter is very fast (kHz) when compared to the rate of change of current or alpha. Hence the voltage response was considered that follows the reference instantaneously, and inverter model was ignored in the design of the proportional-integral (PI) current controller.

First, the plant transfer function was calculated. The AFPM machine equations, relating (dq) voltages and (dq) currents, are equations (1) and (2), hereby called again:

$$v_q = Ri_q + L_q \frac{di_q}{dt} + \omega_e L_d i_d + \omega_e \Lambda_{PM} \cos(\alpha)$$

$$v_d = Ri_d + L_d * \frac{di_d}{dt} - \Lambda_{PM} \sin(\alpha) \frac{d\alpha}{dt} - \omega_e L_q i_q$$

These are nonlinear equations, however, only the first two right hand side terms were considered for the transfer function:

$$v_q = Ri_q + L_q \frac{di_q}{dt}$$

$$v_d = Ri_d + L_d \frac{di_d}{dt}$$

Their Laplace equivalents are:

$$v_q(s) = Ri_q(s) + L_q s i_q(s) = i_q(s)(R + sL_q)$$

$$v_d(s) = Ri_d(s) + L_d s i_d(s) = i_d(s)(R + sL_d)$$

Having $L_q = L_d$, one mutual transfer function can be written for both axes:

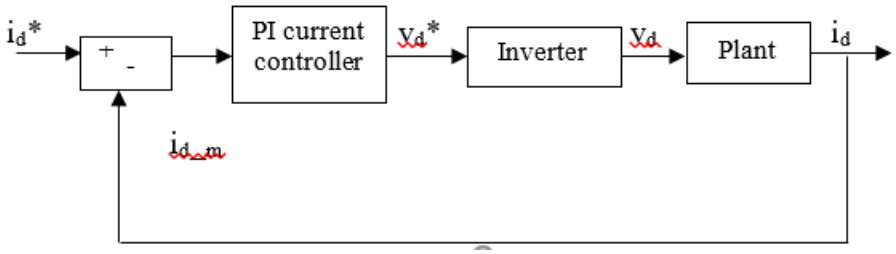

Figure 16: Block diagram for closed loop control of d-axis current

$$\frac{i_d(s)}{v_d(s)} = \frac{1}{L_d s + R} = \frac{1/L_d}{\left(s + \frac{R}{L_d}\right)}$$

The transfer function of the PI current controller is:

$$PI_i(s) = k_p + \frac{k_i}{s} = \frac{k_p\left(s + \frac{k_i}{k_p}\right)}{s}$$

Consequently, open loop transfer function is:

$$OL_i(s) = \frac{k_p\left(s + \frac{k_i}{k_p}\right)}{s} \frac{\frac{1}{L_d}}{\left(s + \frac{R}{L_d}\right)}$$

This would give a second order closed loop transfer function, hence a second order response to a step command in $i_{d_{ref}}$. Zero-pole cancellation method was used instead, to achieve a first order response:

$$\frac{k_i}{k_p} = \frac{R}{L_d}$$

Therefore, open loop transfer function reduces to:

$$OL_{i_{zpc}}(s) = \frac{\frac{k_p}{L_d}}{s}$$

Closed loop transfer function is calculated as:

$$CL_{i_{zpc}}(s) = \frac{i_{d_{meas}}}{i_{d_{ref}}} = \frac{OL_{i_{zpc}}(s)}{1 + OL_{i_{zpc}}(s)} = \frac{\frac{\frac{k_p}{L_d}}{s}}{1 + \frac{\frac{k_p}{L_d}}{s}} = \frac{\frac{k_p}{L_d}}{s + \frac{k_p}{L_d}}$$

A desired bandwidth of 200 Hz was chosen, as a common value for current regulation. The controller parameters, that give the required bandwidth, were finally calculated as:

$$\omega_{BW} = \frac{k_p}{L_d} = 2\pi f_{BW}$$

$$k_p = 2\pi f_{BW} L_d$$

$$k_i = k_p \frac{R}{L_d} = 2\pi f_{BW} R$$

The MATLAB script, for the calculation of PI controller's gains is written as follows:

```
% Control

s=tf('s');

R_e=R;
Ld_e=Ld;
Lq_e=Ld_e;

% Control current:
f_BW_i=200;
kp_i=2*pi*f_BW_i*Ld_e;
ki_i=2*pi*f_BW_i*R_e;
current_loop=2*pi*f_BW_i/(s+2*pi*f_BW_i);
```

The first line of declaration sets the "s" character to be recognized by MATLAB as the Laplace variable. The subscript "e" after the name of machine parameters stands for "estimated". This was done to differentiate between real machine parameters and control parameters, as these two often are not equal. The last line is used to calculate the transfer function of the design current loop with the chosen PI parameters. This allows us, to then plot the predicted step response (see Figure 17) using the following line:

step(current_loop)

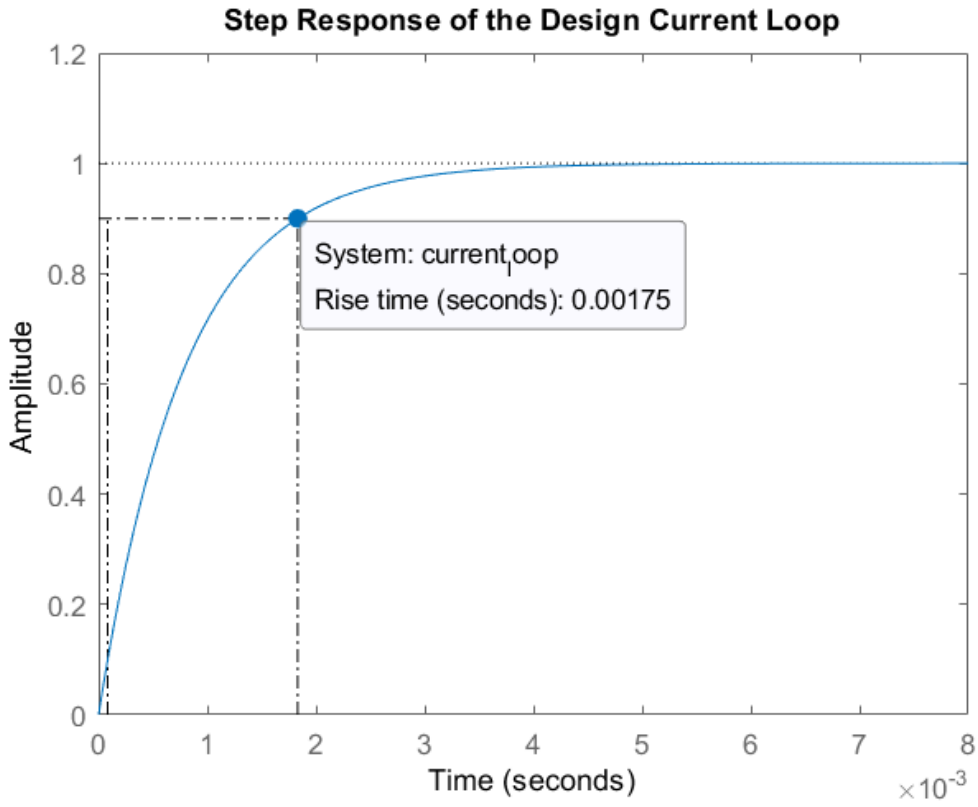

Figure 17: Step response of the design current loop

As expected, our chosen PI parameters produce a first order response, with a rise time (i.e. the time required for a signal to rise from 10 per cent to 90 per cent of its steady value) of $0.35/f_{BW}$=1.75 ms.

After calculating the PI_i controller gains, according to our requirements, the (dq) current control loops were modelled in the SIMULINK environment as well, using the PID controller blocks provided in the SIMULINK libraries (see Figure 18).

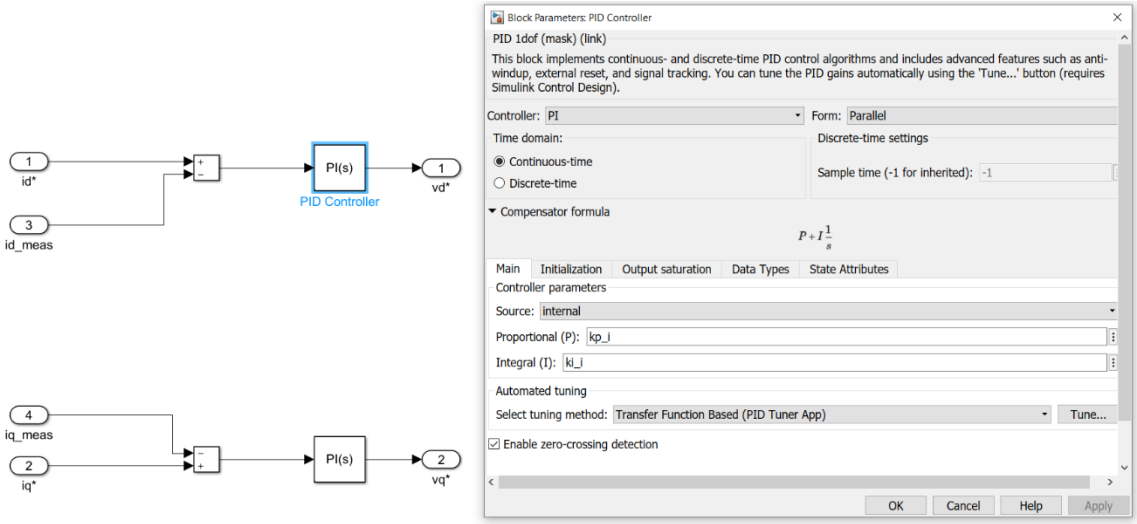

Figure 18: Current PI controllers

PI_i controller gains were calculated without considering half of the terms in equations (1) and (2), recalled below:

$$v_q : \omega_e L_d i_d + \omega_e \Lambda_{PM} \cos(\alpha)$$

$$v_d : -\omega_e L_q i_q - \Lambda_{PM} \sin(\alpha) \frac{d\alpha}{dt}$$

First term in both equations is apparent voltage, coming from the coordinate transformation. Second term of first equation is the induced back emf, while second term of the second equation is voltage required with a change in the rotor angular phase displacement. By omitting these terms during the PI_i design, d-axis and q-axis controllers can be decoupled, making them responsible only for changing the current on their respective axis. However, these terms represent additional voltage requirements. Therefore, they were added to the reference voltage from PI_i controllers, as feedforward compensation for the coupling between axes, the back-emf induced, and the disturbance from alpha variation. The SIMULINK subsystem, that calculates the voltage compensation according to the above equations, is illustrated in Figure 19.

Finally, the current control subsystem and the voltage compensation subsystem were connected to the AFPM machine model, as it is illustrated in Figure 20. A step command was given to the d-axis current reference. In Figure 21, the measured d-axis current

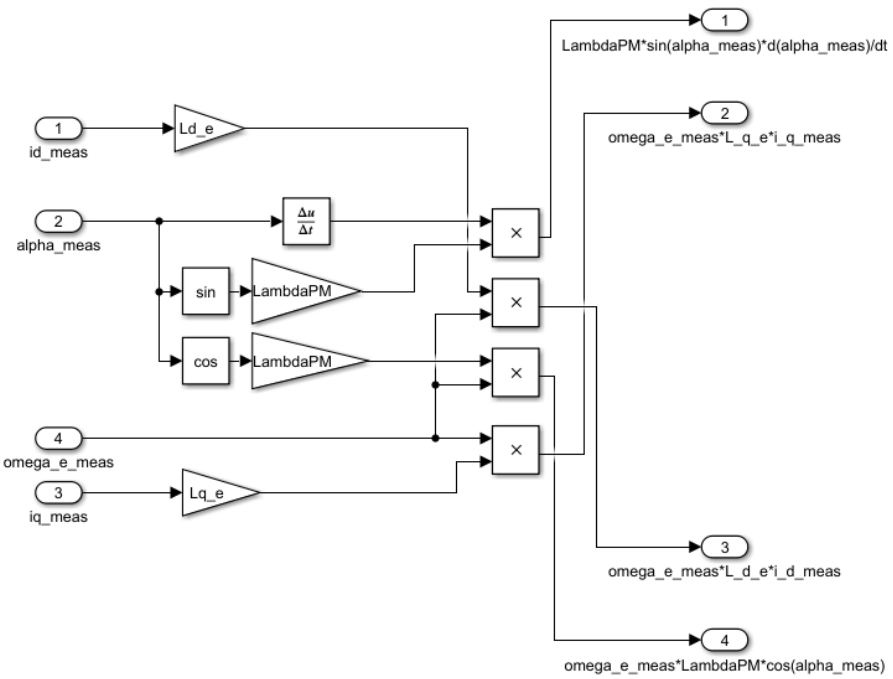

Figure 19: Feedforward voltage compensation subsystem

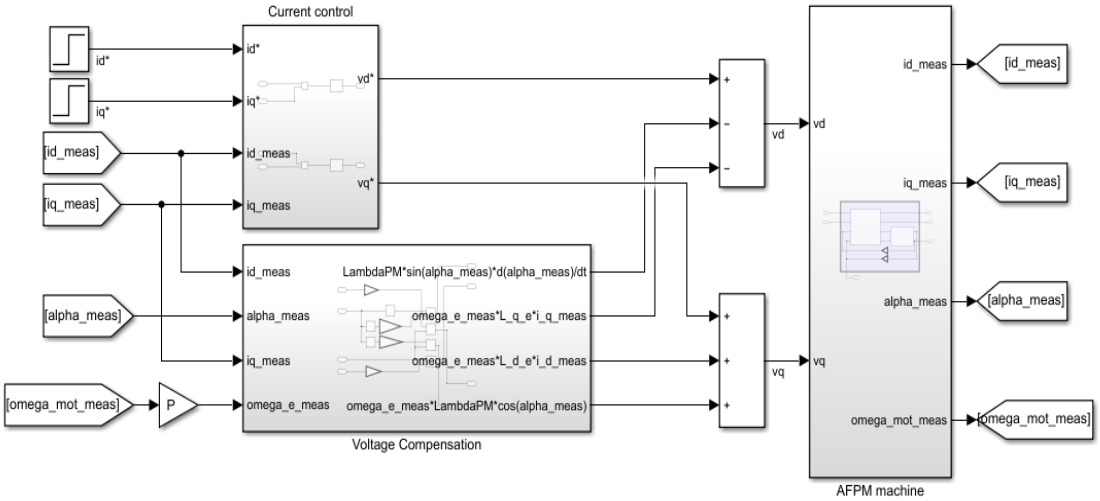

Figure 20: AFPM machine together with current control

response is compared with the predicted response from our design. As expected, the responses are very much alike. The actual rise time is 1.701 msec, with the predicted one being a bit bigger, at 1.75 msec. This is a good approximation, considering that the plant transfer function belonging to the predicted response, does not account for the nonlinearity of the actual system.

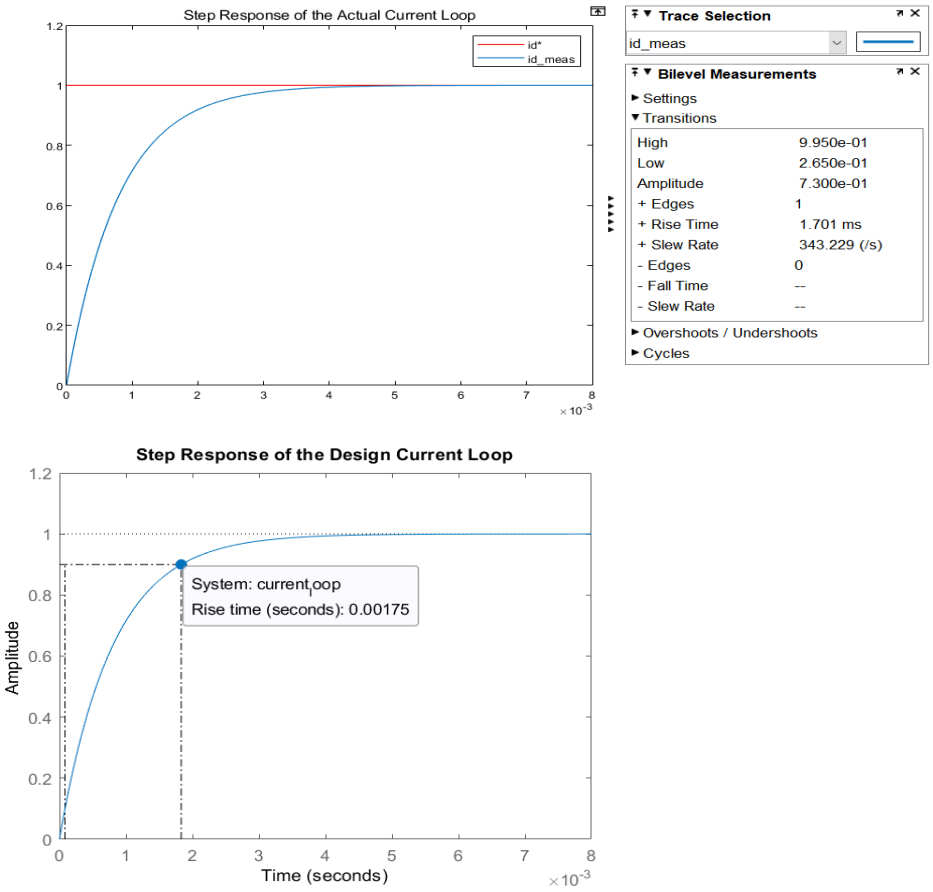

Figure 21: Comparison between the actual current step response and the predicted current step response from design

2.3 Closed Loop Control of the Angular Phase Displacement

Once the current loop was implemented and verified, we could proceed with the design of the angular phase displacement (alpha) control loop. Same as for the current loop, the design followed in the Laplace domain. The schematic of the control block diagram is presented in Figure 22. Current loop was neglected in the design (i.e. its transfer function was considered equal to 1), since its dynamics are at least one order of magnitude faster than those of the angular phase displacement. In particular, the aim was to find the controller type and its gains, but before that, the plant transfer function had to be calculated.

2.3.1 Identification of the plant transfer function $\frac{\alpha(s)}{i_d(s)}$

The equation that relates d-axis current and the angular phase displacement, once again, is:

$$T_{shift} = J_{shift}\frac{d^2(2\alpha_{shift})}{dt^2} + B_{shift}\frac{d\,(2\alpha_{shift})}{dt} = -\frac{3}{2}P\Lambda_{PM}\,sin(\alpha)\,i_d$$

Since working with the electrical units is more intuitive for the angular phase displacement, the above equation is re-written substituting the mechanical α_{shift} with $\frac{\alpha}{P}$ Also, in practice, resistance B_{shift} is very small, therefore it is neglected in the design:

$$B_{shift} = 0$$

$$T_{shift} = J_{shift}\frac{d^2\left(\frac{2\alpha}{P}\right)}{dt^2} = -\frac{3}{2}P\Lambda_{PM}\,sin(\alpha)\,i_d$$

$$J_{shift}\frac{d^2\left(\frac{2\alpha}{P}\right)}{dt^2} + \frac{3}{2}P\Lambda_{PM}\,sin(\alpha)\,i_d = 0 \qquad (8)$$

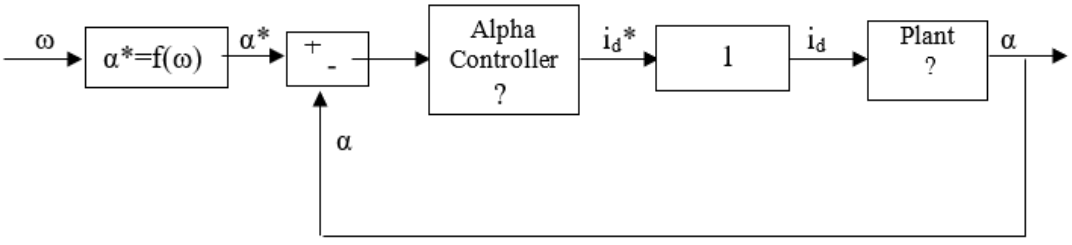

Figure 22: Control block diagram for the regulation of the angular phase displacement (alpha)

This is still a non-linear equation, as for the presence of the sine function, and the multiplication between two variables such as alpha and d-axis current. To find the plant transfer function, we had to linearize this equation around an operating point (OP).

The linear approximation of a function $f(x)$ around a point of interest $(a, f(a))$ is basically the tangent line with this function on that point (see Figure 23). In general, a multivariable function $f(x, y)$ can be linearized around a point $(x, y, f(x, y))$, using the following formula:

$$f(x,y) \approx f(a,b) + \frac{\partial f(x,y)}{\partial x}|_{a,b}\,(x-a) + \frac{\partial f(x,y)}{\partial y}|_{a,b}\,(y-b)$$

Left-hand side of equation (8) is a function of three variables: alpha, second order derivative of alpha, and d-axis current:

$$f(\ddot{\alpha}, \alpha, i_d) = 2\frac{J_{shift}}{P}\,\ddot{\alpha} + \frac{3}{2}P\Lambda_{PM}\,sin(\alpha)\,i_d = 0$$

Therefore, our equation can be linearly approximated in the vicinity of an OP $(\ddot{\alpha_0}, \alpha_0, i_{d_0})$, as:

$$f(\ddot{\alpha}, \alpha, i_d) \approx f\left(\ddot{\alpha_0}, \alpha_0, i_{d_0}\right) + \frac{\partial f(\ddot{\alpha}, \alpha, i_d)}{\partial \ddot{\alpha}}|_{\ddot{\alpha_0},\alpha_0,i_{d_0}}(\ddot{\alpha} - \ddot{\alpha_0})$$
$$+ \frac{\partial f(\ddot{\alpha}, \alpha, i_d)}{\partial \alpha}|_{\ddot{\alpha_0},\alpha_0,i_{d_0}}(\alpha - \alpha_0) + \frac{\partial f(\ddot{\alpha}, \alpha, i_d)}{\partial i_d}|_{\ddot{\alpha_0},\alpha_0,i_{d_0}}\left(i_d - i_{d_0}\right) = 0$$

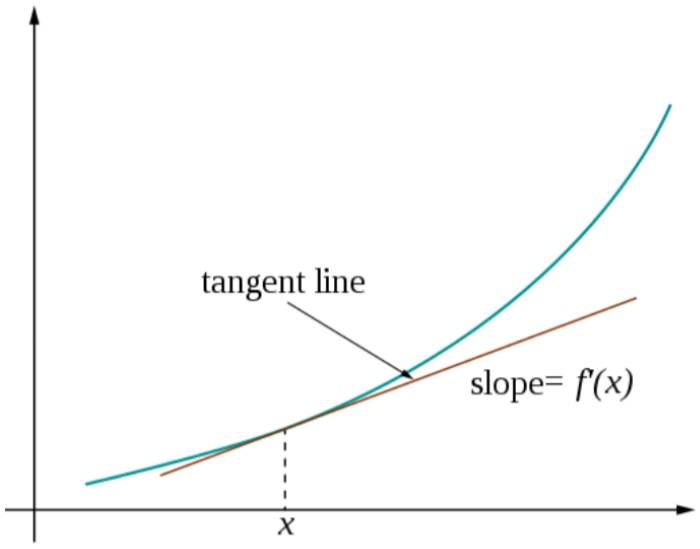

Figure 23: An approximation of f(x)=x^2 at (x,f(x))

Partial derivatives are equal to:

$$\frac{\partial f(\ddot{\alpha}, \alpha, i_d)}{\partial \ddot{\alpha}}|_{\ddot{\alpha_0}, \alpha_0, i_{d_0}} = 2\frac{J_{shift}}{P} + 0$$

$$\frac{\partial f(\ddot{\alpha}, \alpha, i_d)}{\partial \alpha}|_{\ddot{\alpha_0}, \alpha_0, i_{d_0}} = 0 + \frac{3}{2}P\Lambda_{PM}\cos(\alpha_0)i_{d_0}$$

$$\frac{\partial f(\ddot{\alpha}, \alpha, i_d)}{\partial i_d}|_{\ddot{\alpha_0}, \alpha_0, i_{d_0}} = 0 + \frac{3}{2}P\Lambda_{PM}\, sin(\alpha_0)$$

Meanwhile, $f(\ddot{\alpha_0}, \alpha_0, i_{d_0})$ is equal to zero, at any OP. Consequently, our linearized equation is:

$$2\frac{J_{shift}}{P}(\Delta\ddot{\alpha_0}) + \frac{3}{2}P\Lambda_{PM}\cos(\alpha_0)\, i_{d_0}(\Delta\alpha_0) + \frac{3}{2}P\Lambda_{PM}\, sin(\alpha_0)\,(\Delta i_{d_0}) = 0$$

After linearizing, Laplace transformation can be applied, keeping in mind that $\Delta\ddot{\alpha_0}$ is simply the second order derivative of alpha (in the vicinity of OP_0):

$$2\frac{J_{shift}}{P}s^2\Delta\alpha(s)_0 + \frac{3}{2}P\Lambda_{PM}\cos(\alpha_0)\, i_{d_0}\Delta\alpha(s)_0 + \frac{3}{2}P\Lambda_{PM}\, sin(\alpha_0)\,\Delta i_d(s)_0 = 0$$

$$\Delta\alpha(s)_0\left(2\frac{J_{shift}}{P}s^2 + \frac{3}{2}\Lambda_{PM}\cos(\alpha_0)\, i_{d_0}\right) + \Delta i_d(s)_0\frac{3}{2}P\Lambda_{PM}\, sin(\alpha_0) = 0$$

Therefore, the plant transfer function is:

$$\frac{\Delta\alpha(s)}{\Delta i_d(s)}_0 = -\frac{\frac{3}{2}P\Lambda_{PM}\, sin(\alpha_0)}{2\frac{J_{shift}}{P}s^2 + \frac{3}{2}P\Lambda_{PM}\cos(\alpha_0)\, i_{d_0}}$$

It should be noted that this is a variable transfer function (indicated by the subscript "0"), changing with different operating points. *S*ince OPs are considered those of steady state condition, this means that the second order derivative of alpha is equal to zero, at any OP $\ddot{\alpha_0} = 0$. Therefore, for the following equation to stand true:

$$f(\ddot{\alpha_0}, \alpha_0, i_{d_0}) = 2\frac{J_{shift}}{P}\ddot{\alpha_0} + \frac{3}{2}P\Lambda_{PM}\, sin(\alpha_0)\, i_{d_0} = 0$$

the d-axis current, at any OP, must be zero as well $i_{d_0} = 0$. Hence, the plant transfer function is reduced to:

$$\frac{\alpha(s)}{i_d(s)}_0 = -\frac{\frac{3}{2}P\Lambda_{PM}\,sin(\alpha_0)}{2\frac{J_{shift}}{P}s^2}$$

$$= -\frac{\frac{3}{4}\frac{P^2}{J_{shift}}\Lambda_{PM}\,sin(\alpha_0)}{s^2}$$

$$G_{ai_{d_0}}(s) = -\frac{A_0}{s^2}$$

The operating point chosen for the linearization is that where $\alpha_0 = \alpha_{min}$.

Finally, the plant transfer function, at OP ($\alpha_0 = \alpha_{min}$), was calculated to be:

$$\frac{\alpha(s)}{i_d(s)}_{\alpha\_min} = -\frac{\frac{3}{4}\frac{P^2}{J_{shift}}\Lambda_{PM}\,sin(\alpha_{min})}{s^2}$$

$$G_{ai_{d_{\alpha\_min}}}(s) = -\frac{A_{\alpha\_min}}{s^2}$$

This type of transfer function is a double integrator. It can be represented in the complex plane by two poles on the origin. From the control theory point of view, this means that applying a step command on the input (d-axis current) would produce an oscillatory response on the output (angular phase displacement). To verify this, on our SIMULINK model, a negative step command was given to the d-axis current, at t=0 sec. Figure 24 and Figure 25 show the response in the angular phase displacement, with activated saturation limits on the alpha integrator (random α_{min}, α_{max}=90°) representing the mechanical stops, and without these limits (with an initial angular phase displacement), respectively. Figure 25 confirms the oscillatory response we were expecting.

2.3.2 Identification of Alpha Controller type and tuning of the gains

Having a known plant transfer function, a controller for the angular phase displacement was next to be designed. A robust field weakening regulation loop, needs an alpha controller that:

1. Guarantees stability
2. Achieves zero steady state error
3. Produces the desired reasonable dynamics
4. Rejects common disturbances

Different types of controllers were analyzed and compared, starting from the simplest, to find the one that would satisfy the four requirements above.

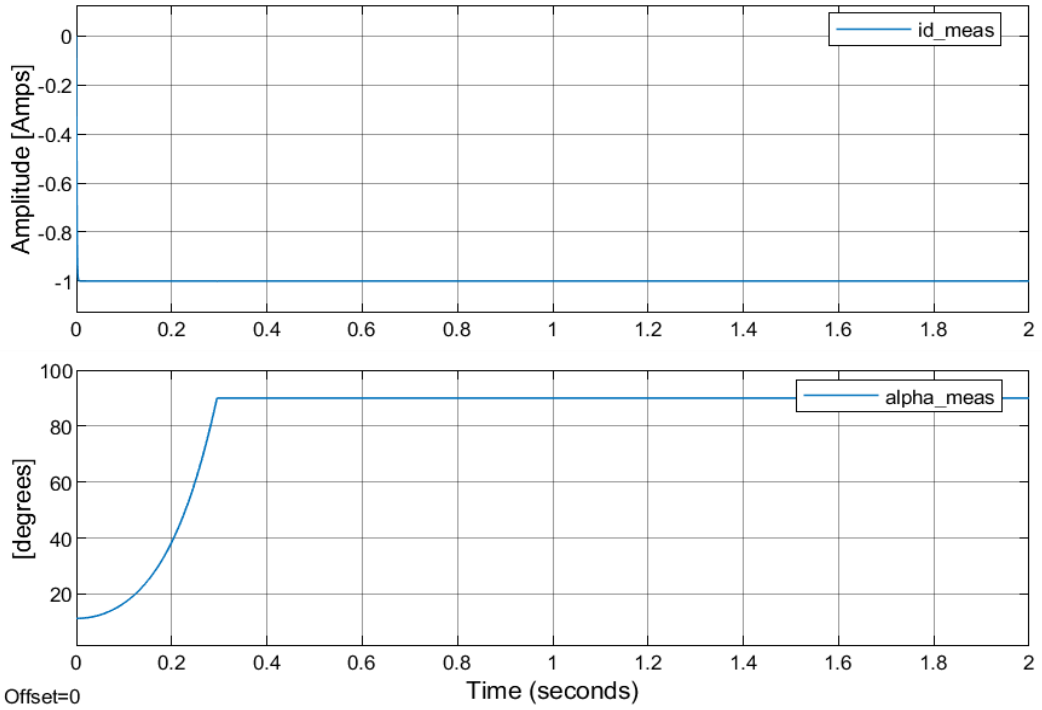

Figure 24: Alpha response to a negative unit step command in d-axis current, with activated saturation limits on the alpha integrator

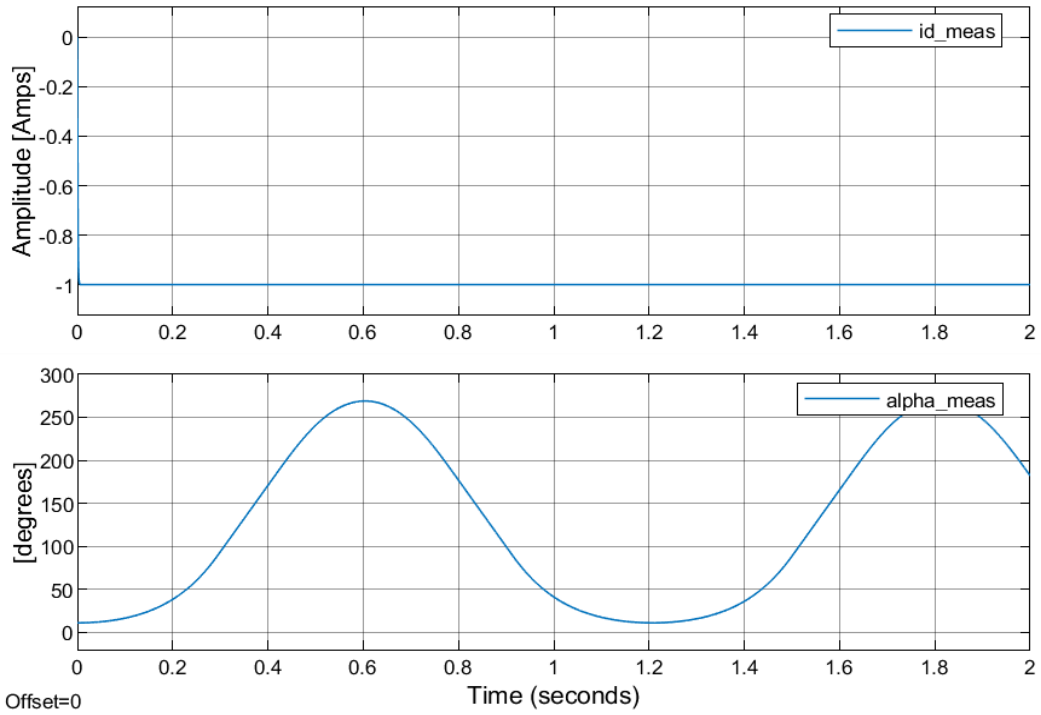

Figure 25: Alpha response to a negative unit step command in d-axis current, with de-activated saturation limits on the alpha integrator

2.3.2.1 Proportional controller (P)

The transfer function of this type of controller is:

$$G_P(s) = k_p$$

If it is connected to our plant, the open loop transfer function would be:

$$G_{OL_P}(s) = G_P(s) * G_{ai_{d_0}}(s) = \frac{\alpha_{meas}}{\varepsilon_\alpha}$$

$$= -k_p * \frac{A_0}{s^2}$$

It should be noted that $G_{OL_P}(s) > 0$ must always stand true, for a positive error $\alpha_{error} = \alpha_{ref} - \alpha_{meas} > 0$ to produce an increase in α_{meas}, reducing the error. If $G_{OL_P}(s) < 0$, the error will only rise, making the system unstable.

Therefore, k_p must be negative.

Closed loop transfer function is calculated as:

$$G_{CL_P}(s) = \frac{\alpha_{meas}}{\alpha_{ref}} = \frac{G_{OL_P}(s)}{1 + G_{OL_P}(s)}$$

$$= \frac{-k_p \frac{A_0}{s^2}}{1 - k_p \frac{A_0}{s^2}} = \frac{-k_p A_0}{s^2 - k_p A_0}$$

$$= \frac{a}{s^2 + a}$$

Depending on the sign of "a", this transfer function has the following location of poles in the complex plane:

If a<0: $+\sqrt{a} + 0i$

$-\sqrt{a} + 0i$

If a>0:

$0 + \sqrt{a}i$

$0 - \sqrt{a}i$

So, for a positive k_p (a<0), one from the two poles is located on the right-hand side of the plane, making the closed loop unstable, as we predicted above.

In comparison, a negative k_p (a>0) produces a pair of imaginary poles with zero real value, which gives an oscillatory response of constant amplitude, in response to a step alpha reference.

In conclusion, a simple P-controller does not satisfy any of the three requirements, therefore it was excluded as an option.

2.3.2.2 Proportional Integral controller (PI)

The transfer function of a PI is:

$$G_{PI}(s) = k_p + \frac{k_i}{s}$$

Then, open loop transfer function is equal to:

$$G_{OL_{PI}}(s) = G_{PI}(s) * G_{ai_d}(s)$$

$$= (k_p + \frac{k_i}{s})\left(-\frac{A_0}{s^2}\right) = -\frac{k_p\left(s + \frac{k_i}{k_p}\right)}{s}\frac{A_0}{s^2}$$

$$= -\frac{k_p A_0\left(s + \frac{k_i}{k_p}\right)}{s^3}$$

The stability of the respective closed loop system is evaluated by analyzing the root-locus of the open loop transfer function $G_{OL_{PI}}(s)$. The root locus of a transfer function illustrates how the respective closed loop poles travel in the complex plane, starting from the poles and the zeros of the open loop, when the gain of the open loop is increased.

In our case $G_{OL_{PI}}(s)$ has n=3 poles on the origin, and m=1 zero on the real axis. If $k_i > 0$, the ratio $\frac{k_i}{k_p}$ is negative (k_p must always be negative, otherwise the system will be unstable, as it was explained in the previous page) therefore the zero will be located on the right-hand side. In contrast, it will be located on the left-hand side, if k_i and k_p are both negative. These two cases are illustrated in Figure 26, where the zero is represented with a circle, and the three overlapped poles are represented with the filled cross.

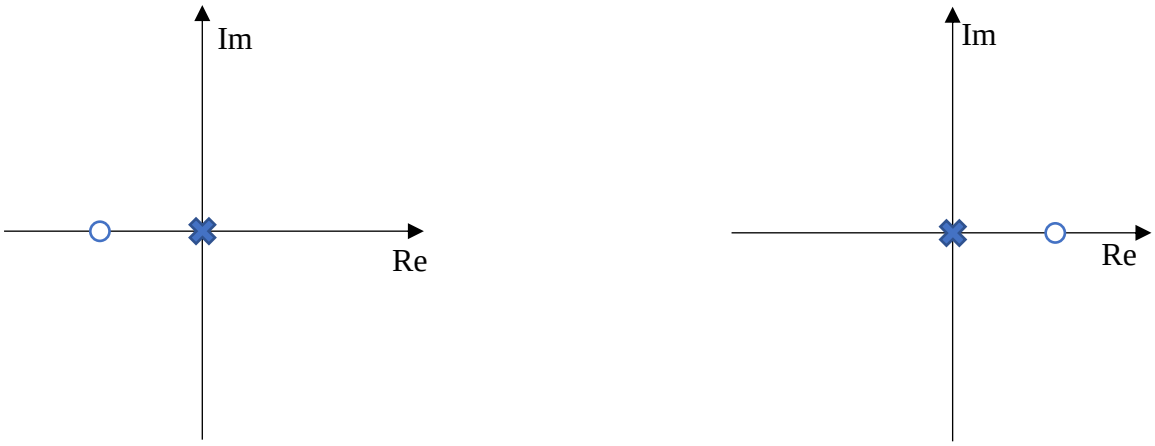

Figure 26: Map of open loop m=3 poles and n=1 zero, if kp<0, ki<0 (left graph) and if kp<0, ki>0 (right graph)

From the control theory, two rules of the root locus are:

1. *Root locus branches (i.e. trajectories of the closed loop poles) start at the open loop [n] poles, and end at open loop [m] zeros, if n=m. If n>m, [n-m] branches end at infinity.*
2. *If a point on the real axis exist on the left of an odd number of open loop poles and zeros, then that point is on a root locus branch*

If the zero is located on the right side, like in the case of the right graph in Figure 26, any point along the real axis interval between origin and the zero, will be on the left of an odd number of open loop poles and zeros (one zero), making this segment a branch of the locus. Therefore, the closed loop system will be unstable, because at least one pole of the closed loop will be always located on the right side, irrespective to the positive value of k_i and the negative value of k_p.

This left us with only the case of the left graph in Figure 26 (k_i and k_p are both negative), to evaluate for stability. Based on the rules above, we know for sure that one of the three closed loop poles will always be located on the left real axis, between the zero and origin (i.e. is a stable pole). To find out what happens with the two other poles, we referred to another rule of the root-locus theory:

3. *Each one of the poles trajectories follows its own asymptote, and the resulting locus is symmetric about the real axis.*

We have three poles, therefore there will be three asymptotes. One of the asymptotes it's along the real negative axis, starting at origin. Symmetry requires that the three

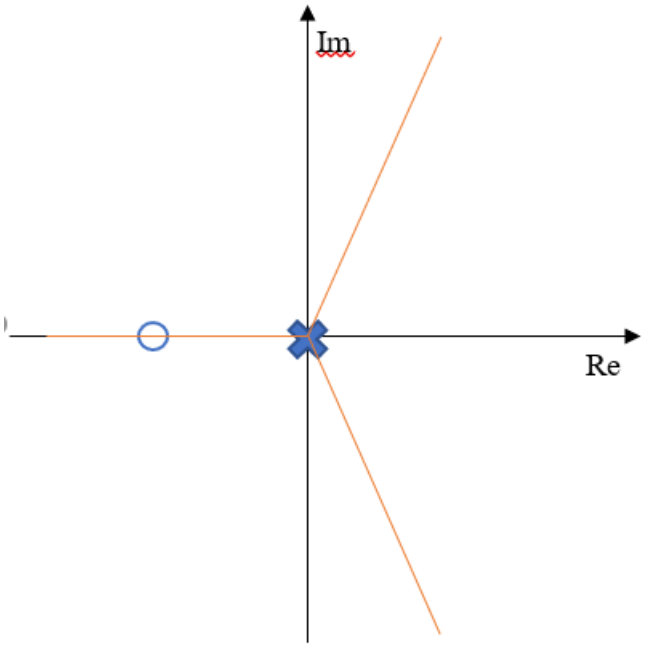

Figure 27: Map of open loop n=3 poles and m=1 zero, together with asymptotes of root locus, for a PI controller

asymptotes are 120° displaced from one-another. This is illustrated in Figure 27. Thus, it was concluded that two from three closed loop poles, would form an imaginary pair with positive real value, making the closed loop system unstable.

Consequently, the PI controller was also excluded from the options.

2.3.2.3 Proportional Derivative controller (PD)

Transfer function of a PD controller is of the following form:

$$G_{PD}(s) = k_p + k_d s$$

Then, open loop transfer function is equal to:

$$G_{OL_{PD}}(s) = G_{PD}(s) * G_{ai_d}(s)$$

$$= (k_p + k_d s)\left(-\frac{A_0}{s^2}\right) = -k_d\left(s + \frac{k_p}{k_d}\right)\frac{A_0}{s^2}$$

$$= -\frac{k_d A_0\left(s + \frac{k_p}{k_d}\right)}{s^2}$$

The stability in closed loop was again analyzed using the root locus of the open loop transfer function. In this case, there are n=2 poles on the origin and m=1 zero. If $k_p > 0$, the ratio $\frac{k_p}{k_d}$ is negative (k_d must always be negative, otherwise the system will be

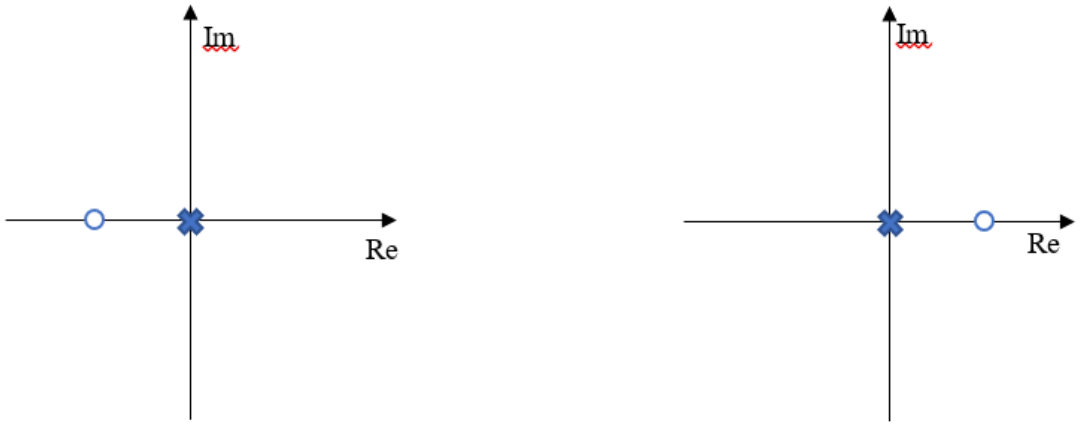

Figure 28: Map of open loop m=2 poles and n=1 zero, if kd<0, kp<0 (left graph) and if kd<0, kp>0 (right graph)

unstable, as it was explained previously), therefore the zero will be located on the right-hand side. In contrast, it will be located on the left-hand side, if k_p and k_d are both negative. These two cases are illustrated in Figure 28, where the zero is represented with a circle, and the two overlapped poles are represented with the filled cross.

If $k_p > 0$ (right graph of Figure 28), a point on the positive real axis interval, between origin and the zero would always be on the left of an odd number of open loop poles and zeros (one zero). Then, based on rule no.2 written above, this branch is part of the root locus. Therefore, based also on rule no.1, one closed loop pole would always be on the positive real axis, between origin and the zero, making the system unstable.

If both k_p and k_d are negative (left graph of Figure 28), the negative real axis interval between -∞ and the zero is on the left of on odd number of open loop poles and zeros. Based on rule no.2, this interval is part of the root locus. However, the trajectories of the closed loop poles, are more involved than in the previous cases.

Therefore, the root locus was plotted using the "rlocus()" function of the MATLAB library:

rlocus(-(s+1)*(-A_zero/s^2))

The transfer function inside "rlocus()" represents our $G_{OL_{PD}}(s)$, in the conditions where $k_p = k_d = -1$, and the command illustrates the trajectories of closed loop poles, when both k_p and k_d are increased negatively from -1, while maintaining a constant ratio $\frac{k_p}{k_d} = 1$. The plotted trajectories are presented in Figure 29. The negative real axis interval on

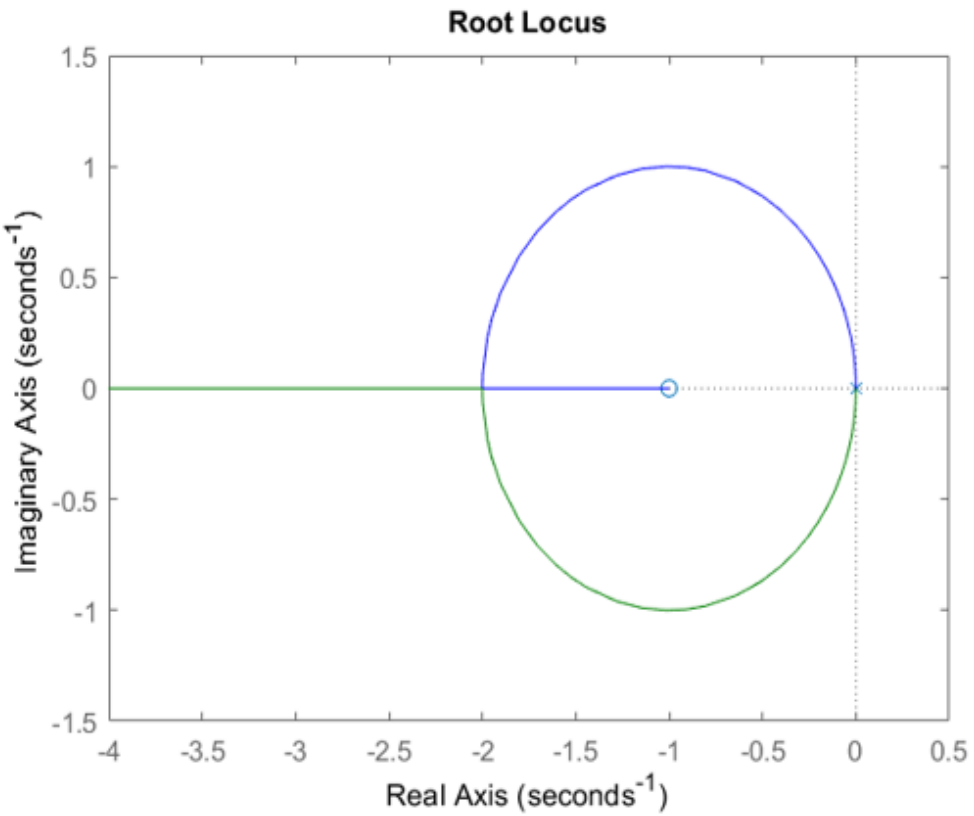

Figure 29: Trajectories of closed loop poles, for negatively increasing kd from -1, while maintaining kp/kd=1

the left of the zero is part of the locus, as expected. Closed loop poles are initially imaginary, becoming real for big enough negative $k_p = k_d$. In any case, they remain on the left-hand side of the plane, therefore the closed loop system is always stable.

The closed loop pole trajectories of Figure 29 are specific to the case of negatively increasing k_p and k_d from -1, while maintaining $\frac{k_p}{k_d} = 1$. Even though the shape of the locus might change for other values of k_p and k_d, the statements regarding stability remain true.

Therefore, we concluded that a PD controller would fulfill at least the first from the four requirements, i.e. guaranteeing stability, if it was connected to our plant:

$$G_{ai_{d_0}}(s) = -\frac{A_0}{s^2}$$

where A is operating point dependent:

$$A_{\alpha_{min}} = \frac{3}{4} * \frac{P^2}{J_{shift}} * \Lambda_{PM} * sin(\alpha_{min})$$

This part was followed by the selection of k_p and k_d, according to our requirements regarding dynamics. For that, the closed loop characteristic denominator is analyzed:

$$G_{CL_{PD}}(s) = \frac{\alpha_{meas}}{\alpha_{ref}} = \frac{G_{OL_{PD}}(s)}{1 + G_{OL_{PD}}(s)}$$

$$= \frac{(k_p + k_d s)\left(-\frac{A_0}{s^2}\right)}{1 + (k_p + k_d s)\left(-\frac{A_0}{s^2}\right)}$$

$$= \frac{-A_0 k_d s - A_0 k_p}{s^2 - A_0 k_d s - A_0 k_p} = \frac{-A_0 k_p \left(\frac{k_d}{k_p} s + 1\right)}{-A_0 k_p \left(\frac{1}{-A_0 k_p} s^2 + \frac{k_d}{k_p} s + 1\right)}$$

$$= \frac{(\tau_{PD} s + 1)}{\left(\frac{1}{-A_0 k_p} s^2 + \tau_{PD} s + 1\right)}$$

Therefore, the closed loop characteristic polynomial is:

$$s^2 - A_0 k_d s - A_0 k_p$$

From control theory, the canonical form for the second order characteristic polynomial, is:

$$s^2 + 2\zeta\omega_n s + \omega_n^2$$

where, ζ (zeta) is the damping of the second order system and ω_n is the natural frequency. This last is very close to ω_{BW} (the frequency where the amplitude drops by 3dB from the maximum amplitude). These values are chosen by the designer of the control loop. By equalizing two last polynomials, we get for k_p and k_d

$$\omega_n^2 = -A_0 k_p$$

$$k_p = -\frac{\omega_n^2}{A_0}$$

$$2 * \zeta * \omega_n = -A_0 k_d$$

$$k_d = -\frac{2\zeta\omega_n}{A_0}$$

Some lines were added to the MATLAB script, to calculate k_{p_α} and k_{d_α} according to our desired $\omega_{BW_\alpha} = 2\pi f_{BW_\alpha}$ and ζ_α:

```
J_shift_est=J_shift;
B_shift_est=B_shift;
% Control alpha:
alpha_zero=alpha_min ;
A_zero=3/4*P^2/J_shift_est*LambdaPM*sin(alpha_zero);
alpha_vs_id=-A_zero/s^2;
f_BW_alpha=5;
zeta_alpha=1;
kp_alpha=-(2*pi*f_BW_alpha)^2/A_zero;
kd_alpha=-2*zeta_alpha*2*pi*f_BW_alpha/A_zero;
alpha_open=alpha_vs_id*(kp_alpha+kd_alpha*s)*current_loop;
alpha_loop=feedback(alpha_open,1);
```

We chose a damping factor $\zeta_\alpha = 1$ because this value implies 0% of peak overshoot on the step response, according to the control theory formula:

$$PO = 100 * e^{\frac{-\zeta\pi}{\sqrt{1-\zeta^2}}}$$

Two last lines of the script calculate the open loop and the closed loop transfer function of our design, respectively. The presence of the current loop was included in the transfer functions as well.

Through the command step(alpha_loop), the step response of the designed closed loop was plotted, illustrated in Figure 30. Even though we expected 0% overshoot, our response had 14% of overshoot, as it can be seen in the upper graph of Figure 30. This happens because our designed closed loop transfer function has also one zero, which influences the response by increasing the overshoot and speeding up the overall response time. The Zero in discussion comes from the bolded numerator in the transfer function below:

$$G_{CL_{PD}}(s) = \frac{(\boldsymbol{\tau_{PD} * s + 1})}{\left(\frac{1}{-A_0 * k_p} * s^2 + \tau_{PD} * s + 1\right)}$$

Another transfer function named "a", with the same characteristic equation but with unity numerator, was declared in MATLAB and its step response was plotted in the same

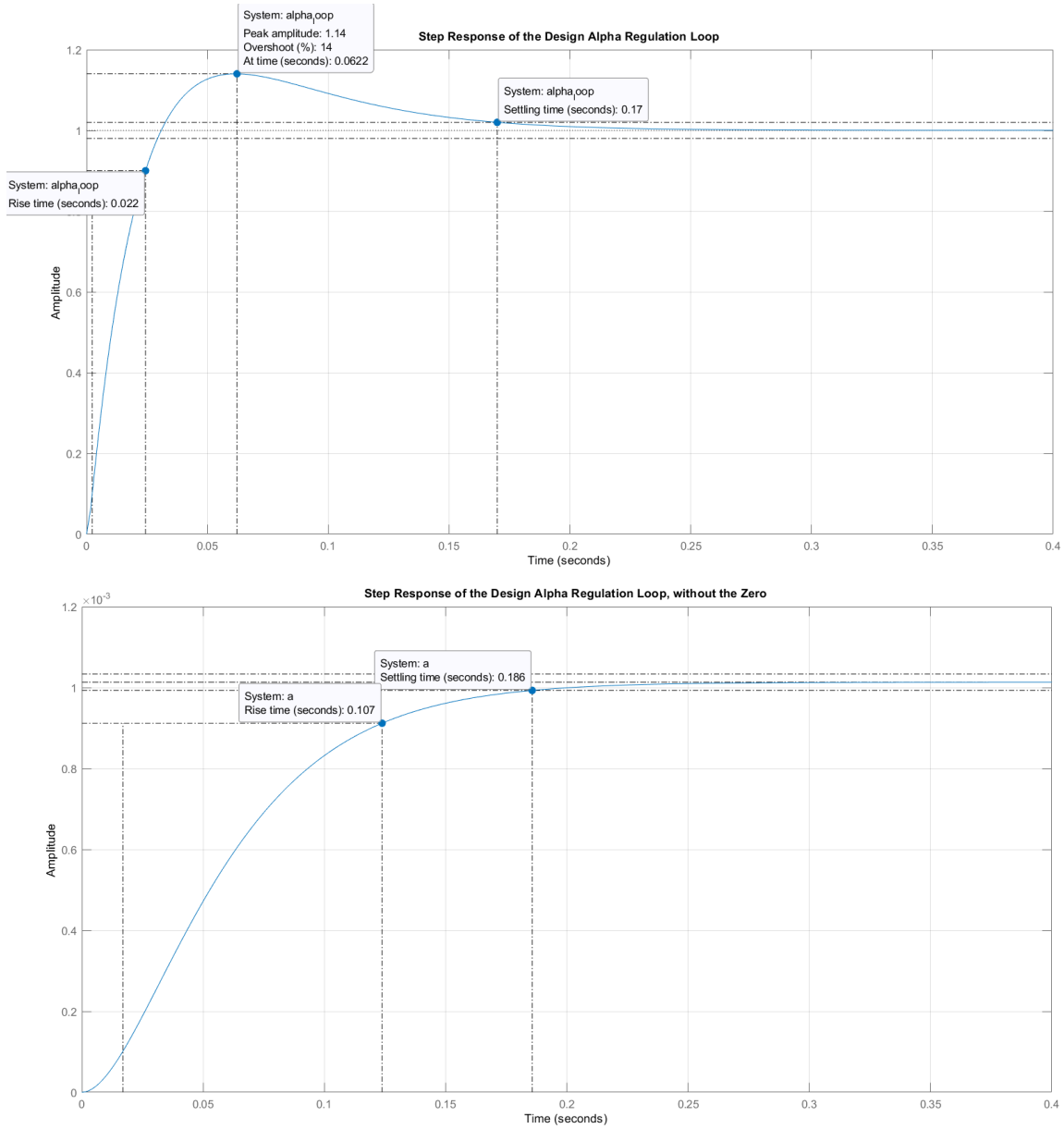

Figure 30: Step response of the design alpha loop, with (upper) and without (lower) the Zero in the transfer function

manner. The resulting response is illustrated in Figure 30, lower graph. As expected from our design, overshoot is equal to 0% and the response is much slower, coming from the lack of the Zero.

The existent AFPM machine model and current control in SIMULINK, were modified to incorporate the angular phase displacement control, with the PD controller parameters we calculated in the MATLAB script previously. This is illustrated in Figure 31.

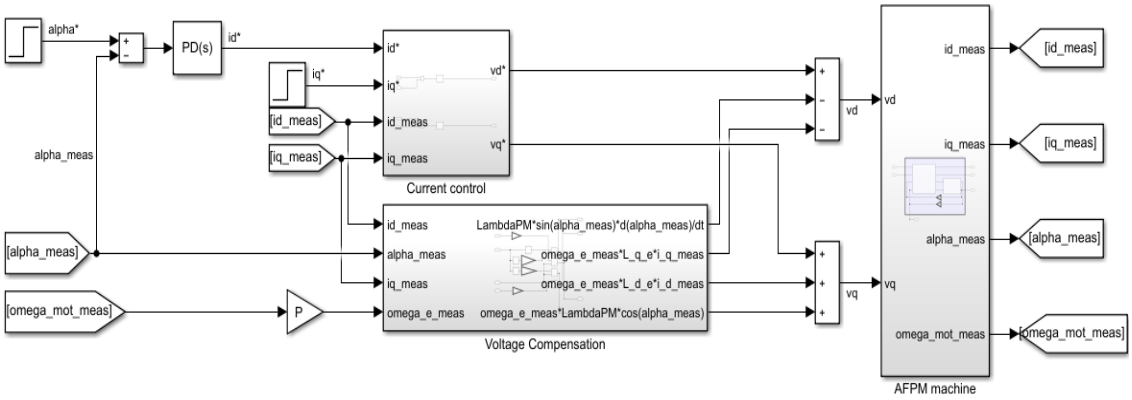

Figure 31: AFPM machine together with alpha control and current control

Numerous step commands of different amplitudes were given to α_{ref}, for analyzing the performance of the designed PD controller, at various operating points. It is important to emphasize that the PD controller was designed for a fixed OP, at $\alpha = \alpha_{min}$.

Firstly, a small α_{ref}step command was given, at t=0 sec, with initial value of $\alpha_{min} = \frac{\pi}{16}$ radians (11.2500°) and final value in the vicinity of the OP, at $\alpha_{ref} = 1.001\alpha_{min}$(11.2613°), $\Delta\alpha_{ref} = +0.001\alpha_{min}$

Secondly, a big α_{ref}step command was given, at t=0 sec, with the same initial value as in the previous simulation, and final value far from the designed OP, at $\alpha_{ref} = 3\alpha_{min}$(33.7500°), $\Delta\alpha_{ref} = +2\alpha_{min}$.

Both step responses, together with the reference and signal statistics are illustrated in Figure 32. As it was expected, for positive phase displacements (i.e. toward misalignment) in the vicinity of OP=α_{min} , the actual response (Figure 32, upper graph) is very similar to the predicted response from our design (Figure 30, upper graph). But for higher positive displacements, such as three times the initial value, actual and predicted response change drastically (Figure 32, lower graph). Particularly, the actual response has a much-reduced overshoot.

To see the effect of negative angular phase displacements (i.e. toward alignment) on the step response, another set of simulations were carried out, first for $\Delta\alpha_{ref} = -0.001\alpha_{min}$ and second for $\Delta\alpha_{ref} = -2\alpha_{min}$, with initial phase displacement of $\alpha_{max} = \frac{\pi}{2}$ radians (90°). The responses are illustrated in Figure 33, together with the respective references and signal statistics. It can be easily visualized that the actual responses are different from

the designed response of Figure 30, upper graph. Not only this, but in contrast with the case of positive phase displacements, the overshoot increases with greater negative phase displacement.

This phenomenon could be explained by looking at the closed loop transfer function, particularly at the characteristic polynomial:

$$s^2 - A_0 k_d s - A_0 k_p = s^2 + 2\zeta\omega_n s + \omega_n^2$$

$$2\zeta\omega_n = -A_0 k_d$$

$$\omega_n = \sqrt{-A_0 k_p}$$

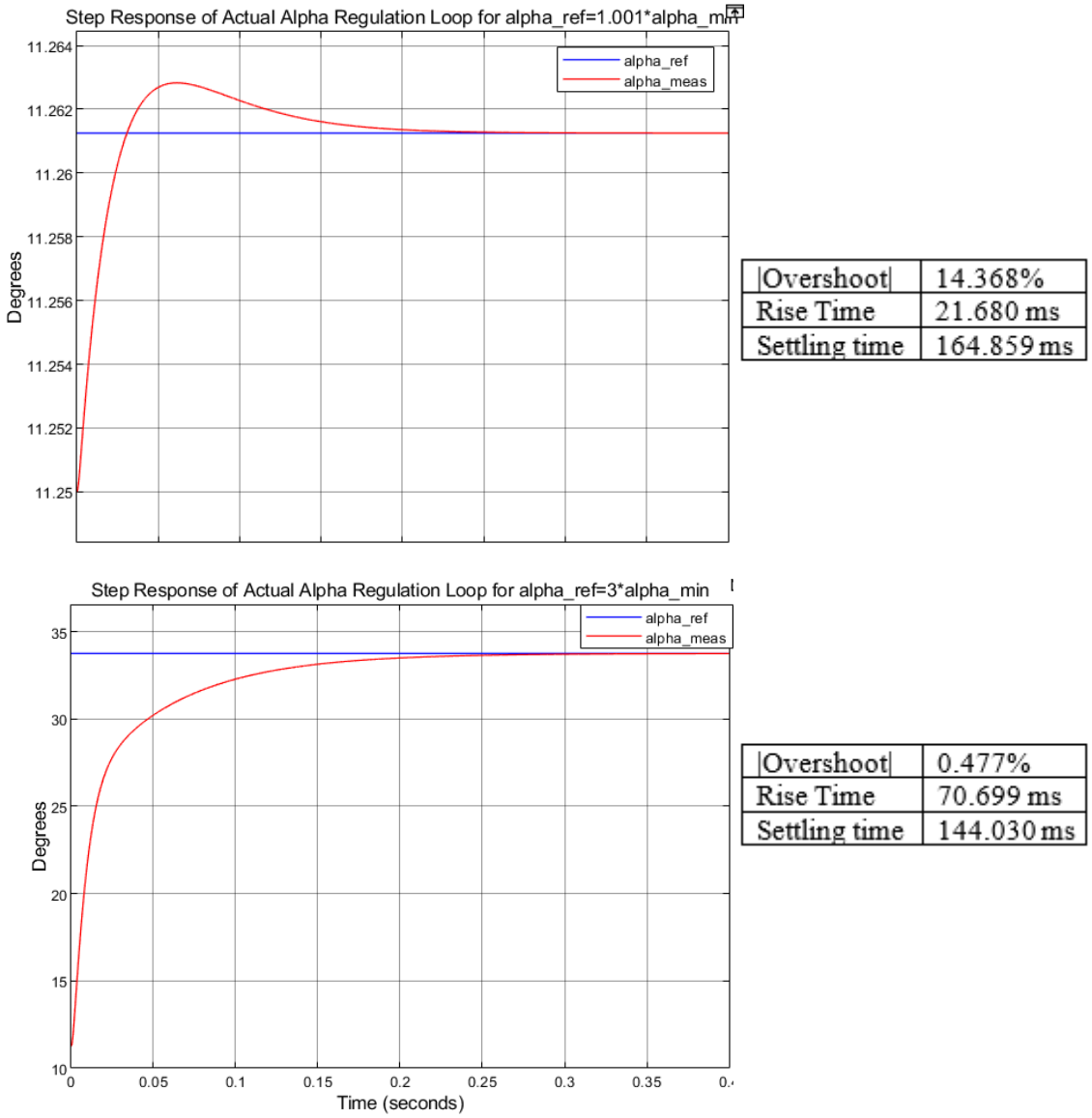

Overshoot	14.368%
Rise Time	21.680 ms
Settling time	164.859 ms

Overshoot	0.477%
Rise Time	70.699 ms
Settling time	144.030 ms

*Figure 32: Step response of actual angular phase displacement loop, for Δalpha_ref=+0.001*alpha_min (upper graph) and for Δalpha_ref=+2*alpha_min (lower graph). Note: initial value = alpha_min*

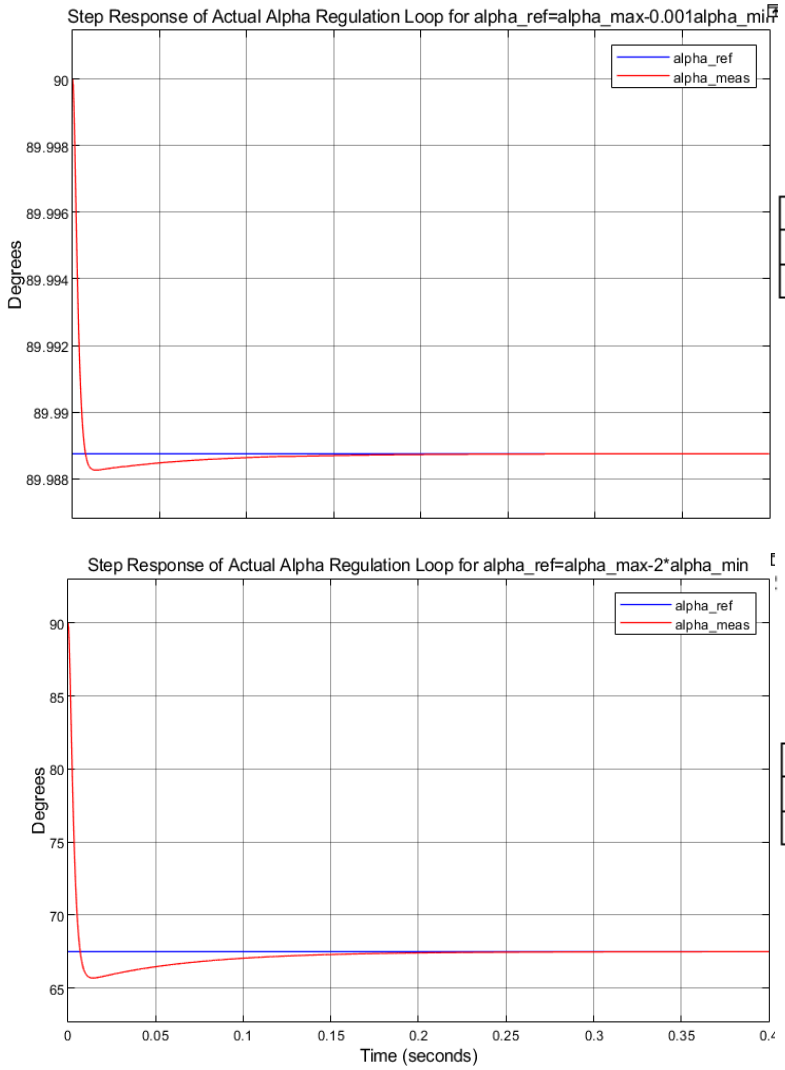

|Overshoot|	4.737%
Rise Time	4.450 ms
Settling time	70.086 ms

|Overshoot|	8.152%
Rise Time	4.391 ms
Settling time	100.176 ms

*Figure 33: Step response of actual angular phase displacement loop, for Δalpha_ref=-0.001*alpha_min (upper graph) and for Δalpha_ref=-2*alpha_min (lower graph). Note: initial value = alpha_max*

According to the characteristic polynomial, zeta (i.e. damping factor) is proportional to the gain A_0 of the plant transfer function, where A_0 changes with operating point:

$$\zeta = \frac{-A_0 k_d}{2\omega_n} = \frac{-A_0 k_d}{2\sqrt{-A_0 k_p}} = \sqrt{-A_0}\frac{k_d}{2\sqrt{k_p}} = \sqrt{-A_0}c^{te}$$

$$G_{ai_d}(s) = -\frac{A_0}{s^2}$$

$$A_0 = \frac{3}{4}\frac{P^2}{J_{shift}}\Lambda_{PM}\, sin(\alpha_0)$$

Our designed k_p and k_d for the PD controller are fixed values, calculated based on a fixed OP at $\alpha_0 = \alpha_{min}$. However, in the actual plant (AFPM machine SIMULINK model), the gain A_0 changes when the angular phase displacement α changes. Therefore, the actual

closed loop transfer function changes as well, with OP. In particular, an increase in α produces an increase in $sin(\alpha\ )$ and consequently a higher gain A. Since the damping factor ζ is proportional to A_0, this translates to a reduced overshoot, explaining the response of Figure 32, lower graph, for higher positive phase displacements. The opposite is also true, explaining the increase in overshoot with higher negative phase displacements (i.e. decreasing α).

The respective data, for the four plotted step responses of the actual angular phase displacement loop, together with the predicted step response of the design loop, are collected in the table below:

Table 2: Peak overshoot magnitude comparison, with changing OP and simple PD controller

Table of Peak Overshoot Magnitude Comparison |**PO**| [%]	Design Alpha Closed Loop	Actual Alpha Closed Loop with PD at OP=α_{min}			
$\Delta\alpha_{ref}$	-	$+0.001*\alpha_{min}$	$+2*\alpha_{min}$	$-0.001*\alpha_{min}$	$-2*\alpha_{min}$
$\alpha_{initial}$	-	α_{min}	α_{min}	α_{max}	α_{max}
|Overshoot|	14.0 %	14.4 %	0.5 %	4.7 %	8.2 %

The increased damping that our controlled system manifests with positive angular phase displacement, is not particularly a bad effect, considering that our design aims for a well damped response.

In contrast, the negatively increasing overshoot with greater negative phase displacements, might pose undesirable effects. This overshoot pushes the rotors towards a smaller angular phase displacement α than the reference, before settling to the final value. This translates to a proportional positive overshoot in flux linkage, and consequently an undesired transient increase in voltage, according to the formula:

$$E = \omega_e \Lambda_{PM} \cos(\alpha)$$

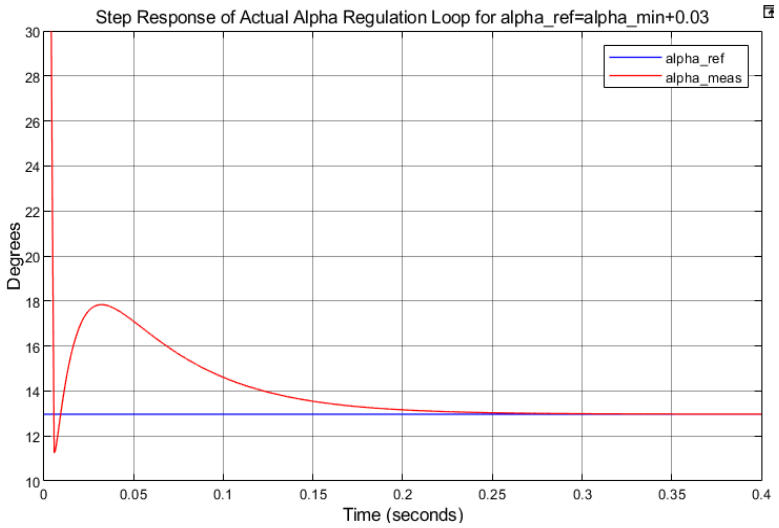

Figure 34: Alteration of the step response when hitting the minimum mechanical stop

A particular case of response to a step reference from α_{max} to $(\alpha_{min} + 0.03)$ is illustrated in Figure 34. Since the reference is very close to the minimum mechanical stop, the negative overshoot pushes the response to hit the stop. This alters unexpectedly the dynamics, causing the rotors to move back towards greater phase displacement, until they finally settle to the desired reference.

In both cases, the voltage regulation is compromised. As it was explained previously, the unpredicted negative effects come because the actual plant transfer function changes with operating point, while the PD controller gains are designed for a specific OP, making the regulation only valid for operation in the vicinity of that OP. Naturally comes to mind that a solution would be a controller with OP-variant k_p and k_d. This type of controller was investigated next.

2.3.2.4 Operating Point Variant, Proportional Derivative controller (VPD)

Transfer function of a VPD controller is of the following form:

$$G_{VPD}(s) = k_{vp} + k_{vd}s$$

Our OP-variant plant transfer function is recalled again:

$$G_{ai_{d_0}}(s) = -\frac{A_0}{s^2} = -\frac{\frac{3}{4}\frac{P^2}{J_{shift}}\Lambda_{PM}\,sin(\alpha_0)}{s^2}$$

Based on it, OP-dependency of the gain A_0, comes only from the term $sin(\alpha_0)$. Thus the plant transfer function can be re-configured as:

$$G_{ai_{d_0}}(s) = -\frac{A\,sin(\alpha_0)}{s^2}$$

where A is c[te], and is equal to:

$$A = \frac{3}{4}\frac{P^2}{J_{shift}}\Lambda_{PM}$$

Then, open loop transfer function is equal to:

$$G_{OL_{VPD}}(s) = G_{VPD}(s) * G_{ai_{d_0}}(s)$$

$$= (k_{vp} + k_{vd}s)\left(-\frac{A\,sin(\alpha_0)}{s^2}\right)$$

If controller's gains k_{vp} and k_{vd} have the OP-variant term $sin(\alpha_0)$ in the denominator, it would cancel the same term in the plant, yielding an invariant open loop transfer function:

$$G_{OL_{VPD}}(s) = \left(\frac{k_p}{sin(\alpha_0)} + \frac{k_d}{sin(\alpha_0)}s\right)\left(-\frac{A\,sin(\alpha_0)}{s^2}\right)$$

$$= (k_p + k_d s)\left(-\frac{A}{s^2}\right) = -k_d\left(s + \frac{k_p}{k_d}\right)\frac{A}{s^2}$$

$$G_{OL_{VPD}}(s) = -\frac{Ak_d\left(s + \frac{k_p}{k_d}\right)}{s^2}$$

This modification in controller's gains, in practice, is easily implemented, since, for the purpose of field weakening control, we are measuring the angular phase displacement α anyway. Then, getting the *sine* of it for the calculation of the gains k_{vp} and $k_{vd}$is just a simple function in the control algorithm. Of course, to reach a high level of OP-independency, a high-resolution encoder is required so that $\alpha_{meas} = \alpha_{real}$.

Assuming this is the case, the design for $k_p$and k_d follows in the same way as for the simple PD controller, which was analyzed previously. Closed loop transfer function of alpha regulation becomes:

$$G_{CL_{VPD}}(s) = \frac{\alpha_{meas}}{\alpha_{ref}} = \frac{G_{OL_{VPD}}(s)}{1 + G_{OL_{VPD}}(s)}$$

$$= \frac{-A\,k_d\left(s + \frac{k_p}{k_d}\right)}{s^2 - Ak_d s - Ak_p}$$

Therefore, the fixed gains $k_p$and k_d are calculated according to our specifications for bandwidth frequency $\omega_{BW} \approx \omega_n$ and damping ζ, as:

$$\omega_n^2 = -A\,k_p$$

$$k_p = -\frac{\omega_n^2}{A}$$

$$2\zeta\omega_n = -A\,k_d$$

$$k_d = -\frac{2\zeta\omega_n}{A}$$

The final OP-variant gains and resulting VPD controller transfer function are:

$$k_{vp} = \frac{k_p}{sin(\alpha_{meas})}$$

$$k_{vd} = \frac{k_d}{sin(\alpha_{meas})}$$

$$VPD(s) = \frac{k_p + k_d s}{sin(\alpha_{meas})}$$

As in the previous case of a simple PD controller, the calculation of the fixed gains $k_p$and k_d for our AFPM machine prototype was done in the MATLAB script, with the only modification that A_0 is substituted by A in the plant transfer function:

```
% Control alpha:
A=3/4*P^2/J_shift_est*LambdaPM;
alpha_vs_id=-A/s^2;
f_BW_alpha=5;
zeta_alpha=1;
kp_alpha=-(2*pi*f_BW_alpha)^2/A;
kd_alpha=-2*zeta_alpha*2*pi*f_BW_alpha/A;
alpha_open=alpha_vs_id*(kp_alpha+kd_alpha*s)*current_loop;
alpha_loop=feedback(alpha_open,1);
```

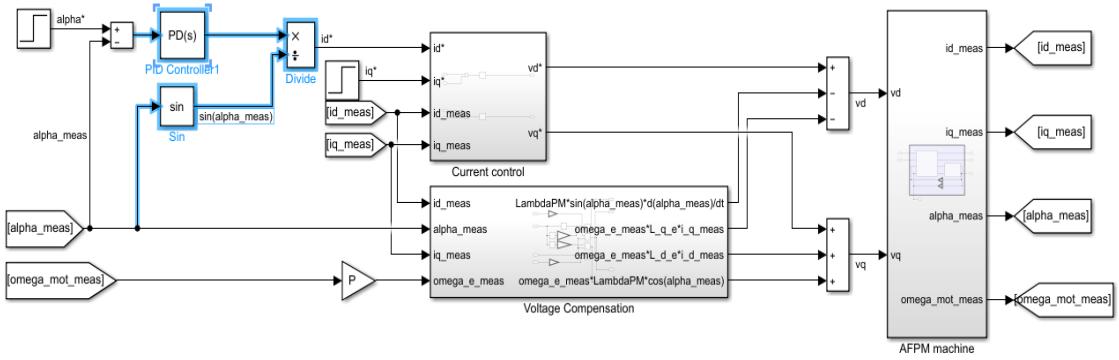

Figure 35: Operating Point Variant PD controller

SIMULINK model of Figure 31 was modified slightly to incorporate the new VPD controller block, illustrated in Figure 35.

Numerous step commands were given to α_{ref}, of the same amplitudes like in the previous case of a simple PD controller, i.e. $+0.001\alpha_{min}$; $+2\alpha_{min}$; $-0.001\alpha_{min}$; $-2\alpha_{min}$. The respective responses of α_{meas}, together with signal statistics, are illustrated in Figure 36. As expected, the shape of the response is almost identical in the four cases, proving that the VPD controller makes the angular phase displacement regulation system have a great deal of independence from the change in operating point. A final table of peak overshoot |PO| comparison between the predicted response, PD response and VPD response, is presented below:

Table 3: Peak Overshoot Magnitude Comparison, between a system with PD and a system with VPD

Table of Peak Overshoot Magnitude Comparison **|PO|** [%]	$\Delta\alpha_{ref}$			
	$+0.001*\alpha_{min}$ $\alpha_{initial}=\alpha_{min}$	$+2*\alpha_{min}$ $\alpha_{initial}=\alpha_{min}$	$-0.001*\alpha_{min}$ $\alpha_{initial}=\alpha_{max}$	$-2*\alpha_{min}$ $\alpha_{initial}=\alpha_{max}$
Alpha Closed Loop with PD at OP= α_{min}	14.4 %	0.5 %	4.7 %	8.2 %
Alpha Closed Loop with VPD	14.4%	15.7%	14.4%	14.4%
Design Alpha Closed Loop	14.4%			

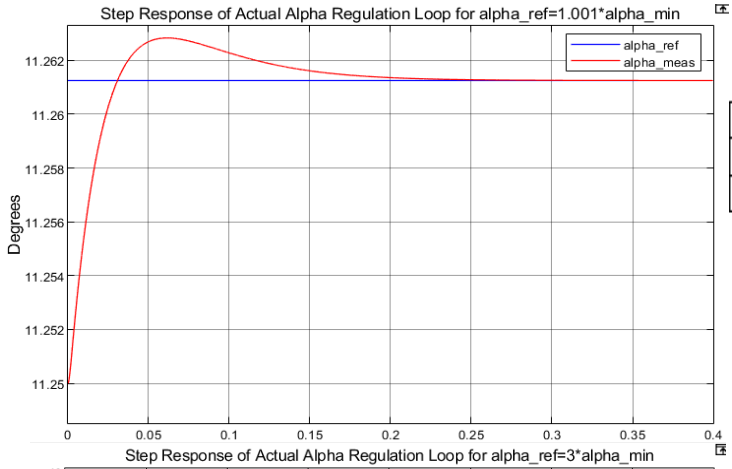

|Overshoot|	14.368%
Rise Time	21.690 ms
Settling time	164.106 ms

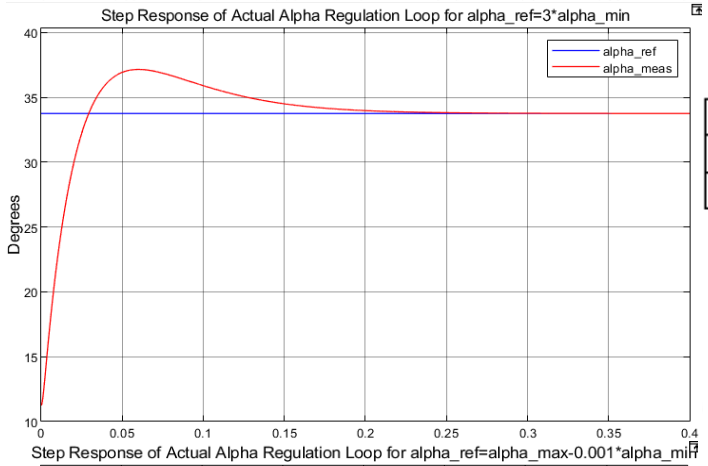

|Overshoot|	15.698%
Rise Time	20.637 ms
Settling time	172.168 ms

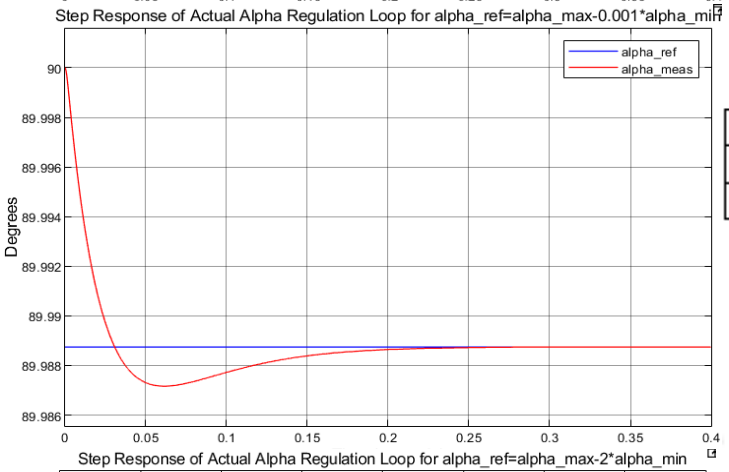

|Overshoot|	14.368%
Rise Time	21.691 ms
Settling time	164.093 ms

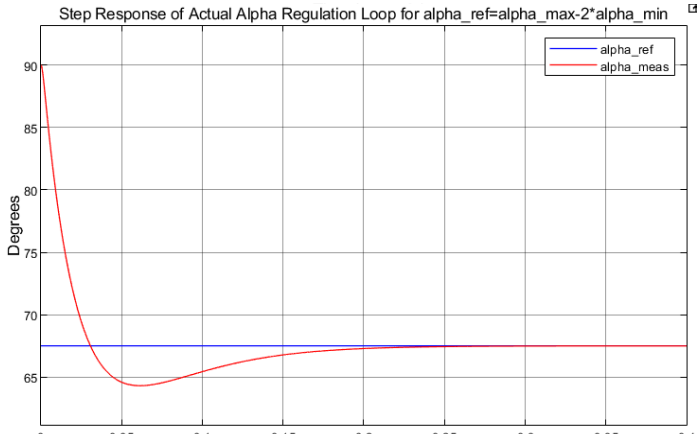

|Overshoot|	14.368%
Rise Time	21.707 ms
Settling time	162.014 ms

Figure 36: Step response of angular phase displacement loop, for Δalpha_ref=+0.001alpha_min (first graph), for Δalpha_ref=+2alpha_min (second graph), for Δalpha_ref=-0.001alpha_min (third graph) and for Δalpha_ref=-2alpha_min (bottom graph)

Once more, the four requirements that the controller of the angular phase displacement regulation needs to fulfill, are:

1. Guarantee stability of controlled system
2. Achieve zero steady state error
3. Produce the desired reasonable dynamics
4. Reject common disturbances

The preceding analysis demonstrated that the VPD controller satisfies three first requirements. However, the simulations were done with the assumption that there aren't any disturbances in the angular phase displacement system. In practice, mechanical disturbances are common, since the AFPM machine protype aims at working both as a starter and alternator. In starting mode, a high amount of motoring torque is expected to be delivered in order to rotate the engine, which represents a big load torque. It is likely that, during starting, the engine might impose a torque that tends to displace the rotors from one another. Thus, in the lack of angular phase displacement control, it is not possible to keep the rotors at the position of minimum displacement mechanical stops. This yields a lower motoring torque capability, according to the formula:

$$T_{mot} = \frac{3}{2} P \Lambda_{PM} \mathbf{cos}(\boldsymbol{\alpha})\, i_q$$

To evaluate the capability of VPD controller in rejecting this kind of disturbance, a load torque block, that tends to displace the rotors, was attached to the mechanical system model. For the purpose of demonstration, the value of the load torque was chosen randomly, to be $\frac{T_n}{10}$. A simulation was carried out, for a constant $\alpha_{ref} = \alpha_{min}$. The response in α and $i_d$current is shown in Figure 37. The VPD controller attains stability of the system, by commanding enough $i_d$current to balance the load torque. However, it cannot achieve zero steady state error. This because the derivative term inside the controller, only reacts to a change in error, so when $\varepsilon_a = c^{te}$, it stops trying to reduce it. In this case, an integral term must be added in the controller, which continuously integrates the error, only stopping when the error is actually zero.

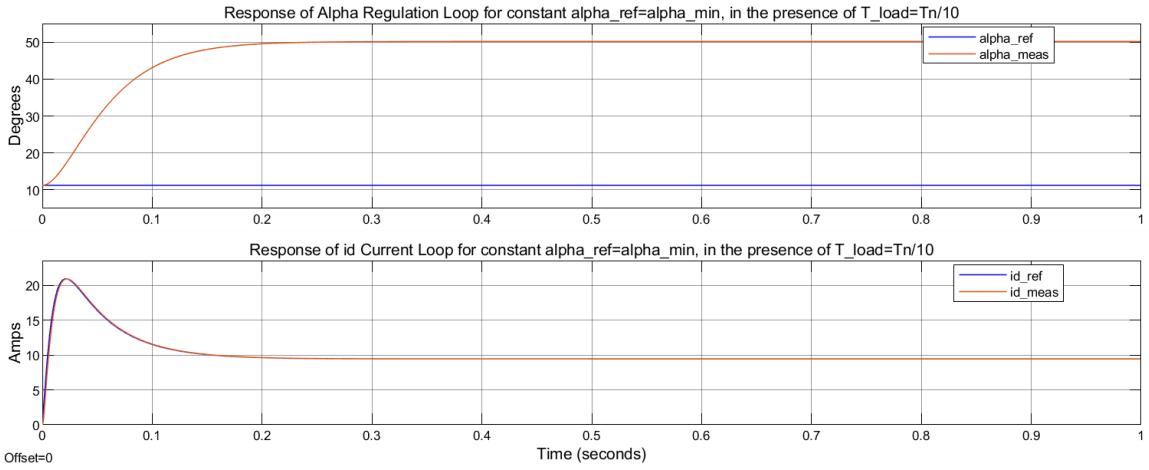

Figure 37: Response of alpha loop and id current loop, with VPD controller, for constant alpha_ref, in the presence of load torque

2.3.2.5 Operating Point Variant, Proportional Integral Derivative Controller (VPID)

By adding an integral term, the transfer function of the OP-variant controller becomes:

$$VPID(s) = \frac{k_p + k_d s + \frac{k_i}{s}}{sin(\alpha_{meas})}$$

The integral guarantees zero steady state error, in the presence of constant disturbances. This because unlike a derivative, which only reacts to a change in error, the integral continuously integrates a constant error, only giving zero action when $\varepsilon_a = 0$.

The closed loop transfer function is now of third order, making the design much more complex. For the purpose of demonstration, the choice for the gain k_i was made by some trials, to be $k_i = 50$.

Another simulation was carried out, under the same conditions like in the previous case of VPD controller (i.e. $\alpha_{ref} = c^{te} = \alpha_{min}; T_{load} = \frac{T_n}{10}$). The responses in α_{meas} and $i_{d_{meas}}$ are plotted in Figure 38. As expected, VPID attains zero steady state error, eventually keeping the rotors aligned at the minimum angular displacement $\alpha_{ref} = \alpha_{min}$, regardless the presence of a constant load disturbance. The dynamics of the response can be modified by further tuning k_i, however, there are no clear specification regarding the eventual load torque magnitude and desired rejection profile, therefore this is not investigated further.

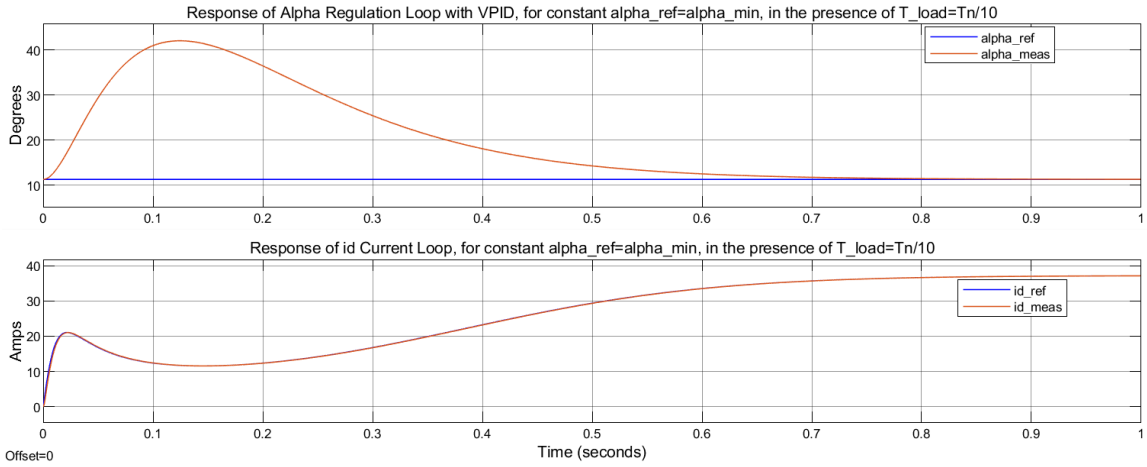

Figure 38: Response of alpha loop and id current loop, with VPID controller, for constant alpha_ref, in the presence of load torque

What should be noted is that, opposing a constant load torque 10 times lower than the nominal in the Constant Torque Speed Region, requires a steady state d-axis current which is approximately ½ of the rated current (see Figure 38, bottom graph). If we consider that the rated current is the maximum current allowed to circulate, this leaves only $\sqrt{1^2 - \left(\frac{1}{2}\right)^2} \approx 86\%$ available q-axis current. Looking again at equation:

$$T_{mot} = \frac{3}{2} P \Lambda_{PM} \cos(\alpha)\, i_q$$

it is clear that motoring torque capability drops to 86% of rated torque. That can be problematic during the phase of engine starting, where the maximum possible torque is needed.

A possible solution to this problem, is a mechanical spring configuration that acts with a force on the rotors, tending to keep them aligned. This removes the "responsibility" of producing load-opposing current, from the VPID controller. This configuration is analyzed in the next chapter.

Chapter 3

AFPM Machine with Spring Configurations

3.1 AFPM Machine with Alignment Spring

An alignment spring configuration acts with a torque on the rotors, tending to keep them at the position of minimum angular phase displacement, even under the influence of a load torque. This removes the "responsibility" of producing load-opposing current, from the VPID controller.

3.1.1 Mechanical Model of AFPM machine with Alignment Spring

An elastic spring counteracts its displacement (stretching or compression), by a force that is proportional to the magnitude of the displacement. Mathematically, this is expressed as:

$$F_{spring} = k * x$$

where k is the spring constant representing its stiffness, and x is the magnitude of displacement.

An alignment spring tends to keep the rotors at the position of minimum angular phase displacement α_{min}. Hence, the reacting force must increase with bigger angular phase displacements. Equation (6), that describes the angular displacement mechanical behavior of the AFPM machine, is modified to incorporate the addition of the alignment spring:

$$T_{shift} - T_{algn_{spring}} = J_{shift} \frac{d^2(2\alpha_{shift})}{dt^2} + B_{shift} \frac{d\,(2\alpha_{shift})}{dt}$$

$$T_{algn_{spring}} = k_{algn_{spring}}(2\alpha_{shift})$$

In the SIMULINK model of the AFPM machine, the mechanical subsystem was modified to account for the presence of an alignment spring, like it is illustrated in Figure 39.

For the purpose of mechanical disturbance rejection during operation in CTSR, the designed alignment spring is required to produce a minimal torque which is opposite and

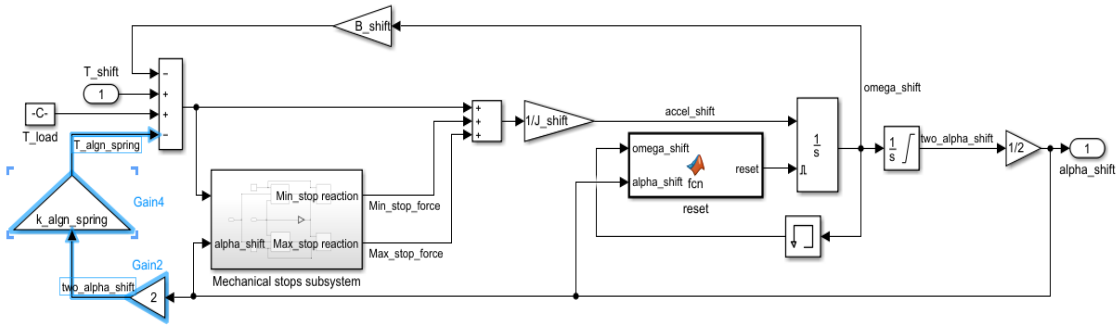

Figure 39: Angular phase displacement mechanical subsystem, with the addition of alignment spring

equal to the maximum displacing load torque. This is achieved by choosing a spring constant according to:

$$T_{algn_{spring\_min}} = k_{algn_{spring}} 2\alpha_{shift_{\min}} = T_{load_{max}}$$

$$k_{algn_{spring}} = \frac{T_{load_{max}}}{2\alpha_{min}/P}$$

3.1.2 Closed Loop Control of the Angular Phase Displacement, with Alignment Spring Configuration

The design for the controller in the preceding analysis was made based on equation (8) that relates d-axis current and the mechanical angular phase displacement, considering $B_{shift} = 0$:

$$J_{shift} \frac{d^2\left(\frac{2\alpha}{P}\right)}{dt^2} + \frac{3}{2} P \Lambda_{PM} \, sin(\alpha) \, i_d = 0$$

However, the incorporation of an alignment spring is reflected in this equation by the addition of one term, as:

$$J_{shift} \frac{d^2\left(\frac{2\alpha}{P}\right)}{dt^2} + \frac{3}{2} P \Lambda_{PM} \, sin(\alpha) \, i_d + \boldsymbol{k_{algn_{spring}}} \left(\frac{\boldsymbol{2\alpha}}{\boldsymbol{P}}\right) = 0$$

The modified equation was re-linearized around an OP, to get the new plant transfer function $G_{algn_{ai_{d_0}}}(s)$. The left-hand side remains a function of three variables $f(\ddot{\alpha}, \alpha, i_d)$. Therefore, the modified equation can be linearly approximated in the vicinity of an OP $(\ddot{\alpha_0}, \alpha_0, i_{d_0})$, using the same linearization formula, as:

$$f(\ddot{\alpha}, \alpha, i_d) \approx f\left(\ddot{\alpha_0}, \alpha_0, i_{d_0}\right) + \frac{\partial f(\ddot{\alpha}, \alpha, i_d)}{\partial \ddot{\alpha}}|_{\ddot{\alpha_0}, \alpha_0, i_{d_0}} (\ddot{\alpha} - \ddot{\alpha_0}) + \frac{\partial f(\ddot{\alpha}, \alpha, i_d)}{\partial \alpha}|_{\ddot{\alpha_0}, \alpha_0, i_{d_0}} (\alpha - \alpha_0) + \frac{\partial f(\ddot{\alpha}, \alpha, i_d)}{\partial i_d}|_{\ddot{\alpha_0}, \alpha_0, i_{d_0}} \left(i_d - i_{d_0}\right) = 0$$

Partial derivatives are equal to:

$$\frac{\partial f(\ddot{\alpha}, \alpha, i_d)}{\partial \ddot{\alpha}}|_{\ddot{\alpha_0}, \alpha_0, i_{d_0}} = 2\frac{J_{shift}}{P}$$

$$\frac{\partial f(\ddot{\alpha}, \alpha, i_d)}{\partial \alpha}|_{\ddot{\alpha_0}, \alpha_0, i_{d_0}} = \frac{3}{2} P \Lambda_{PM} \cos(\alpha_0)\, i_{d_0} + \frac{\boldsymbol{2k_{algn_{spring}}}}{\boldsymbol{P}}$$

$$\frac{\partial f(\ddot{\alpha}, \alpha, i_d)}{\partial i_d}|_{\ddot{\alpha_0}, \alpha_0, i_{d_0}} = \frac{3}{2} P \Lambda_{PM}\, sin(\alpha_0)$$

Meanwhile, $f\left(\ddot{\alpha_0}, \alpha_0, i_{d_0}\right)$ is equal to zero, at any OP. Consequently, our linearized equation is:

$$2\frac{J_{shift}}{P}(\Delta\ddot{\alpha_0}) + \left(\frac{3}{2} P \Lambda_{PM} \cos(\alpha_0)\, i_{d_0} + \frac{\boldsymbol{2k_{algn_{spring}}}}{\boldsymbol{P}}\right)(\Delta\alpha_0) + \frac{3}{2} P \Lambda_{PM}\, sin(\alpha_0)\left(\Delta i_{d_0}\right) = 0$$

After linearizing, Laplace transformation is applied, and the resulting equation in "s" domain is:

$$2\frac{J_{shift}}{P} s^2 \Delta\alpha(s)_0 + \left(\frac{3}{2} P \Lambda_{PM} \cos(\alpha_0)\, i_{d_0} + \frac{\boldsymbol{2k_{algn_{spring}}}}{\boldsymbol{P}}\right)\Delta\alpha(s)_0 + \frac{3}{2} P \Lambda_{PM}\, sin(\alpha_0)\, \Delta i_d(s)_0 = 0$$

Therefore, the new OP-variant plant transfer function is:

$$\frac{\Delta\alpha(s)}{\Delta i_d(s)}_{algn_0} = -\frac{\frac{3}{4}\frac{P^2}{J_{shift}} \Lambda_{PM}\, sin(\alpha_0)}{s^2 + \frac{\frac{3}{4} P^2 \Lambda_{PM} \cos(\alpha_0)\, i_{d_0} + \boldsymbol{k_{algn_{spring}}}}{J_{shift}}}$$

As it was explained in the first case, second order derivative of alpha is equal to zero at any steady state OP: $\ddot{\alpha_0} = 0$. Therefore, for the following equation to stand true:

$$f\left(\ddot{\alpha_0}, \alpha_0, i_{d_0}\right) = 2\frac{J_{shift}}{P}\ddot{\alpha_0} + \frac{3}{2} P \Lambda_{PM}\, sin(\alpha_0)\, i_{d_0} + \frac{\boldsymbol{2k_{algn_{spring}}}}{\boldsymbol{P}}\boldsymbol{\alpha_0} = 0$$

d-axis current at a specific OP, must be equal to:

$$i_{d_0} = -\frac{\frac{2k_{algn_{spring}}}{P}\alpha_0}{\frac{3}{2}P\Lambda_{PM}\,sin(\alpha_0)} = -\frac{4k_{algn_{spring}}\alpha_0}{3P^2\Lambda_{PM}\,sin(\alpha_0)}$$

Substituting the expression found for i_{d_0} in the plant transfer function, we get the final expression for $G_{algn_{ai_{d_0}}}(s)$:

$$G_{algn_{ai_{d_0}}}(s) = -\frac{\frac{3}{4}\frac{P^2}{J_{shift}}\Lambda_{PM}\,sin(\alpha_0)}{s^2 + \frac{\boldsymbol{k_{algn_{spring}}}\left(1 - \frac{\alpha_0\cos(\alpha_0)}{sin(\alpha_0)}\right)}{J_{shift}}}$$

$$= -\frac{A\,sin(\alpha_0)}{s^2 + C_0}$$

Compared with the previous plant transfer function, $G_{algn_{ai_{d_0}}}(s)$ has one additional OP-variant term in the denominator, named C_0. Depending on the sign of C_0, a step command on the d-axis current would produce an oscillating response ($C_0 > 0$), or an unstable response ($C_0 < 0$), in the angular phase displacement. In comparison, the previous plant $G_{ai_{d_0}}(s)$, being a pure double integrator, could only produce an oscillatory response for the same reference. Therefore, the prior observations regarding the unsuitability of P, PI, PD and VPD controllers for the system w/o spring, are also valid in this case, since the plant with alignment spring is only tougher to control. Consequently, it was concluded that the final VPID controller should be employed in a system with alignment spring as well. The design for the three gains of the controller followed the same logic as for the system w/o spring: due to the complexity of a third order system, the design for k_p and k_d was done supposing the use of a VPD instead, and finally k_i is chosen by trial:

Open loop transfer function is equal to:

$$G_{OL_{VPD_{algn}}}(s) = G_{VPD_{algn}}(s) * G_{algn_{ai_{d_0}}}(s)$$

$$= (k_{vp} + k_{vd}s)\left(-\frac{A\,sin(\alpha_0)}{s^2 + C_0}\right)$$

Same as for a system w/o spring, controller's gains k_{vp} and k_{vd} have the OP-variant term $sin(\alpha_0)$ in the denominator, cancelling the same term in the plant. However, in this case the open loop is still OP-variant, because of C_0:

$$G_{OL_{VPD_{algn}}}(s) = (k_p + k_d s)\left(-\frac{A}{s^2 + C_0}\right)$$

Consequently, closed loop transfer function is:

$$G_{CL_{VPD_{algn}}}(s) = -\frac{Ak_d\left(s + \frac{k_p}{k_d}\right)}{s^2 - Ak_d s - Ak_p + C_0}$$

Compared to the closed loop transfer function for a system w/o spring, the only difference is the addition of OP-variant term C_0 in the denominator. Based on the canonical form of the characteristic polynomial:

$$s^2 + 2\zeta\omega_n s + \omega_n^2$$

gains k_p and k_d are calculated as:

$$\omega_n^2 = -A\,k_p + C_0$$

$$k_p = -\frac{\omega_n^2}{A} - \frac{C_0}{A}$$

$$2\zeta\omega_n = -A\,k_d$$

$$k_d = -\frac{2\zeta\omega_n}{A}$$

Compared to the VPD gains in the system w/o spring, for the same requirements in ζ and ω_n, k_d would be exactly the same, while k_p has a first term which would be the same, and an additional term that needs to variate with OP to suppress the change in dynamics.

Therefore, the SIMULINK VPD controller block of Figure 35 for a system w/o spring, was modified to account for the dependence of k_p in C_0. The expression for this last, is recalled once again:

$$C_0 = \frac{\boldsymbol{k_{algn_{spring}}}\left(1 - \frac{\alpha_0\cos(\alpha_0)}{sin(\alpha_0)}\right)}{J_{shift}}$$

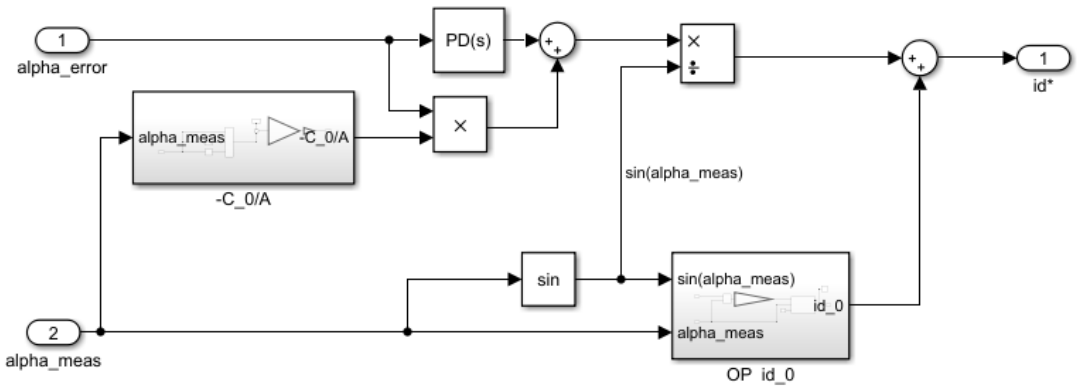

Figure 40: VPD controller of angular phase displacement regulation, in the system with alignment spring

In SIMULINK, it is calculated as:

$$C_0 = \frac{\boldsymbol{k_{algn_{spring}}}\left(1 - \frac{\alpha_{meas}\cos(\alpha_{meas})}{sin(\alpha_{meas})}\right)}{J_{shift}}$$

Still, the VPD controller only commands enough $i_{d_{ref}}$ to support the transient change in α. The change in OP, on the other hand, requires a respective change in steady state d-axis current, according to the earlier formula:

$$i_{d_0} = -\frac{4k_{algn_{spring}}\alpha_0}{3P^2\Lambda_{PM}\,sin(\alpha_0)}$$

In SIMULINK, this steady state reference is calculated as:

$$i_{d_{0_{ref}}} = -\frac{4k_{algn_{spring}}\alpha_{meas}}{3P^2\Lambda_{PM}\,sin(\alpha_{meas})}$$

and is fed forward to the output from the VPD controller.

The final VPD controller block, of the present system with alignment spring, is illustrated in Figure 40.

The response of the present system was compared to the response of the system w/o spring, using the same step reference of $\Delta\alpha_{ref} = +2\alpha_{min}$ and $\Delta\alpha_{ref} = -2\alpha_{min}$. The choice for the spring constant was done, in the continuation of previous analysis of Figure 38 for a maximum load torque of $T_{load_{max}} = \frac{T_n}{10}$. The respective responses are illustrated in Figure 41. As conclusion, we can say that the system with alignment spring shows a greater dependency on the OP, even with the implementation of an OP-variant PD controller.

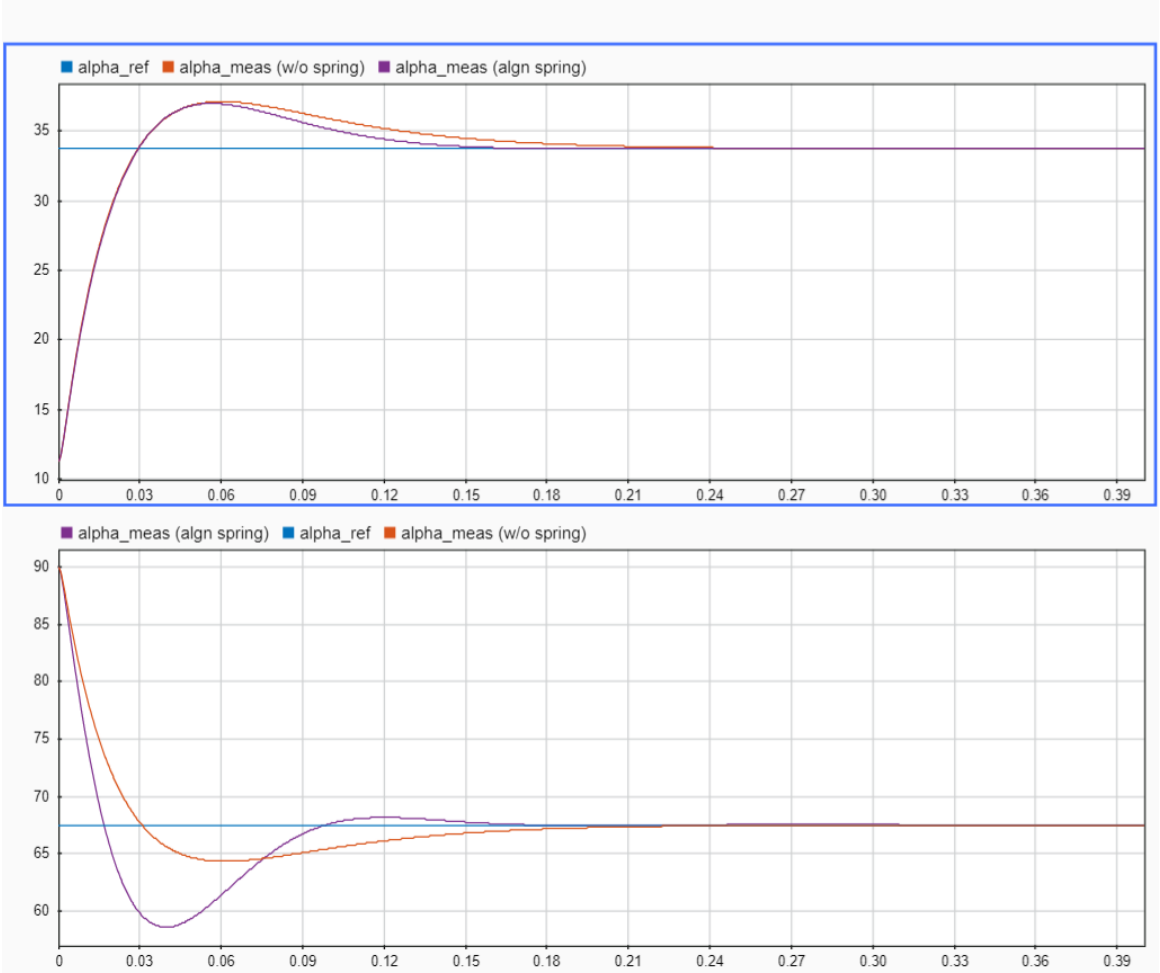

Figure 41: Comparison of step response between a system w/o spring and a system with alignment spring, using a VPD controller, for step reference of Δαref=+2αmin (upper graph) and Δαref=-2αmin (lower graph)

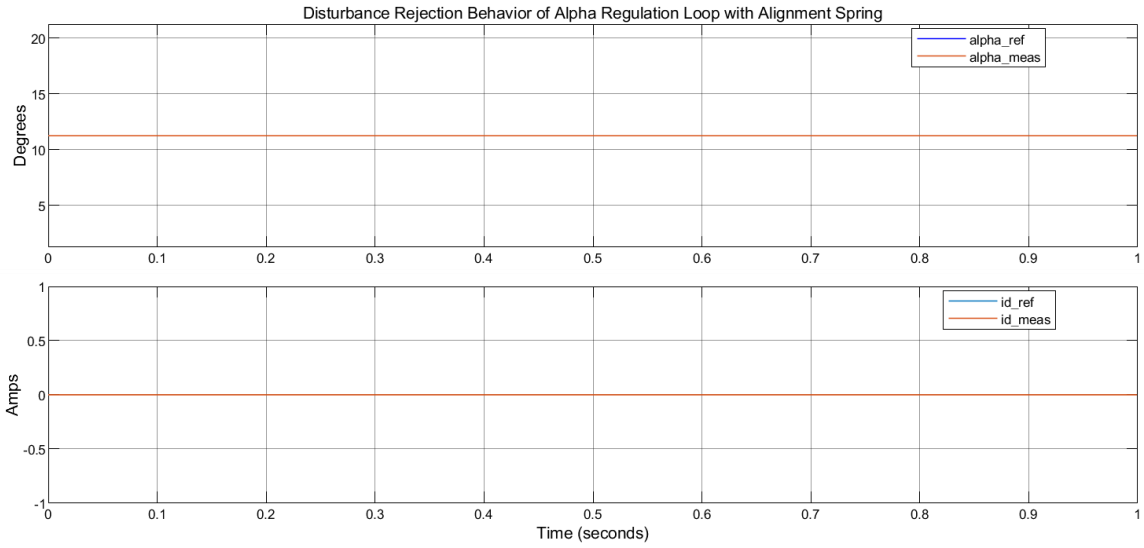

Figure 42: Response of alpha loop and id-current loop, for a system with alignment spring and VPID controller, for constant alpha_ref=alpha_min, in the presence of T_load=Tn/10

Like in the system w/o spring, the final angular phase displacement controller requires also the integral term, whose gain is chosen by trial to be $k_i = -50$.

In the continuation of analysis of Figure 38 the disturbance rejection behavior during CTSR, of the configuration with alignment spring, is illustrated through the graphs of Figure 42. Based on the first graph, the alignment spring produces enough reactive torque to keep the rotors in the position of minimum displacement, even when a load torque is applied. This means that no d-axis current is required to balance the load torque during CTSR, reflected in the second graph. Therefore, unlike in a system w/o spring, the motoring torque capability during operation in CTSR is 100%.

3.2 AFPM Machine with Displacing Spring

Field weakening should not depend only on electric measures. A sudden loss of control on d-axis current during high-speed operation wouldn't enable the angular displacement between the rotors to increase, consequently raising the voltage at the terminals to unacceptable values. Therefore, an alternative way of displacing the rotors should be made available. This thesis investigates the option of a displacing spring configuration.

3.2.1 Mechanical Model of AFPM machine with Displacing Spring

In contrast with the previously analyzed alignment spring, a displacing spring tends to send the rotors at the position of maximum angular phase displacement α_{max}, where ideally is zero flux linkage. Hence, the reacting force must increase with smaller angular phase displacements. Equation (6) of the AFPM machine mathematical model, is modified to incorporate the addition of the displacing spring:

$$T_{shift} + T_{disp_{spring}} = J_{shift}\frac{d^2(2\alpha_{shift})}{dt^2} + B_{shift}\frac{d\,(2\alpha_{shift})}{dt}$$

$$T_{disp_{spring}} = k_{disp_{spring}} * x$$

To find the relation between x and the mechanical angular displacement between the rotors $2\alpha_{shift}$ the following logic was used:

$$\begin{cases} for\ \ 2\alpha_{shift} = \ 2\alpha_{shift_{min}} \quad : \quad x = \ 2\alpha_{shift_{max}} \\ for\ \ 2\alpha_{shift} = \ 2\alpha_{shift_{max}} \quad : \quad x = \ 2\alpha_{shift_{min}} \end{cases}$$

This relation is the equation of a line: $x = k(\ 2\alpha_{shift}) + b$

$$k = \frac{2\alpha_{shift_{min}} - \ 2\alpha_{shift_{max}}}{2\alpha_{shift_{max}} - \ 2\alpha_{shift_{min}}} = -1$$

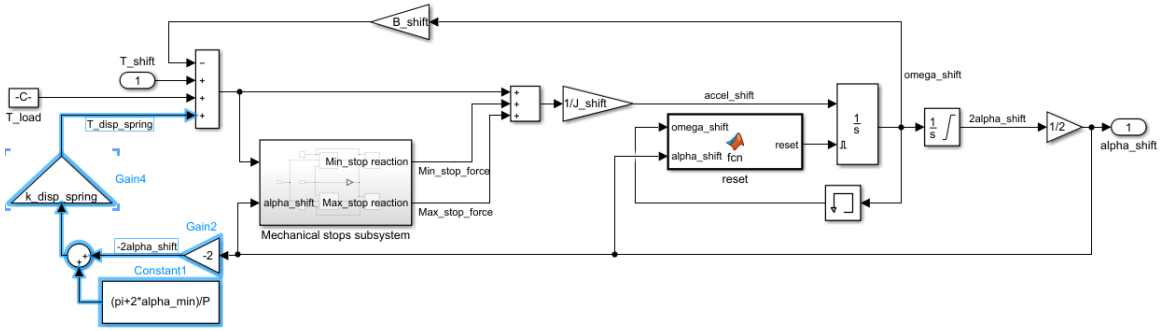

Figure 43: Angular phase displacement mechanical subsystem, with the addition of the displacing spring

$$b = 2\alpha_{shift_{max}} + 2\alpha_{shift_{min}} = \frac{\pi + 2\alpha_{min}}{P}$$

Therefore, the torque exerted from the displacing spring is equal to:

$$T_{disp_{spring}} = k_{disp_{spring}} \left(-2\alpha_{shift} + \frac{\pi + 2\alpha_{min}}{P} \right)$$

In the SIMULINK model of the AFPM machine, the mechanical subsystem was modified to account for the presence of a displacing spring, like it is illustrated in Figure 43.

3.2.2 Closed Loop Control of the Angular Phase Displacement, with Displacing Spring Configuration

To find the plant transfer function for the configuration with displacing spring, the same base equation relating d-axis current and the mechanical angular phase displacement is effective, only adding the terms for spring torque (bolded):

$$J_{shift} \frac{d^2\left(\frac{2\alpha}{P}\right)}{dt^2} + \frac{3}{2} P \Lambda_{PM} \sin(\alpha)\, i_d - \boldsymbol{k_{disp_{spring}} \left(-\frac{2\alpha}{P} + \frac{\pi + 2\alpha_{min}}{P} \right)} = 0$$

The modified equation was re-linearized around an OP, to get the new plant transfer function $G_{disp_{ai_{d_0}}}(s)$. The left-hand side remains a function of three variables $f(\ddot{\alpha}, \alpha, i_d)$. The formula for linearization in the vicinity of an OP $(\ddot{\alpha_0}, \alpha_0, i_{d_0})$ is recalled again below:

$$f(\ddot{\alpha}, \alpha, i_d) \approx f(\ddot{\alpha_0}, \alpha_0, i_{d_0}) + \frac{\partial f(\ddot{\alpha}, \alpha, i_d)}{\partial \ddot{\alpha}}\Big|_{\ddot{\alpha_0}, \alpha_0, i_{d_0}} (\ddot{\alpha} - \ddot{\alpha_0})$$
$$+ \frac{\partial f(\ddot{\alpha}, \alpha, i_d)}{\partial \alpha}\Big|_{\ddot{\alpha_0}, \alpha_0, i_{d_0}} (\alpha - \alpha_0) + \frac{\partial f(\ddot{\alpha}, \alpha, i_d)}{\partial i_d}\Big|_{\ddot{\alpha_0}, \alpha_0, i_{d_0}} (i_d - i_{d_0}) = 0$$

For this configuration, partial derivatives are equal to:

$$\frac{\partial f(\ddot{\alpha}, \alpha, i_d)}{\partial \ddot{\alpha}}|_{\ddot{\alpha_0}, \alpha_0, i_{d_0}} = 2\frac{J_{shift}}{P}$$

$$\frac{\partial f(\ddot{\alpha}, \alpha, i_d)}{\partial \alpha}|_{\ddot{\alpha_0}, \alpha_0, i_{d_0}} = \frac{3}{2}P\Lambda_{PM}\cos(\alpha_0)\, i_{d_0} + \frac{\boldsymbol{2k_{disp_{spring}}}}{\boldsymbol{P}}$$

$$\frac{\partial f(\ddot{\alpha}, \alpha, i_d)}{\partial i_d}|_{\ddot{\alpha_0}, \alpha_0, i_{d_0}} = \frac{3}{2}P\Lambda_{PM}\, sin(\alpha_0)$$

Meanwhile, $f(\ddot{\alpha_0}, \alpha_0, i_{d_0})$ is equal to zero, at any OP. Consequently, our linearized equation is:

$$2\frac{J_{shift}}{P}(\Delta\ddot{\alpha_0}) + \left(\frac{3}{2}P\Lambda_{PM}\cos(\alpha_0)\, i_{d_0} + \frac{\boldsymbol{2k_{disp_{spring}}}}{\boldsymbol{P}}\right)(\Delta\alpha_0) + \frac{3}{2}P\Lambda_{PM}\, sin(\alpha_0)\,(\Delta i_{d_0}) = 0$$

After linearizing, Laplace transformation is applied, and the resulting equation in "s" domain is:

$$2\frac{J_{shift}}{P}s^2\Delta\alpha(s)_0 + \left(\frac{3}{2}P\Lambda_{PM}\cos(\alpha_0)\, i_{d_0} + \frac{\boldsymbol{2k_{disp_{spring}}}}{\boldsymbol{P}}\right)\Delta\alpha(s)_0 + \frac{3}{2}P\Lambda_{PM}\, sin(\alpha_0)\,\Delta i_d(s)_0 = 0$$

Therefore, the OP-variant plant transfer function for the configuration with displacing spring is:

$$\frac{\Delta\alpha(s)}{\Delta i_d(s)}_{disp_0} = -\frac{\frac{3}{4}\frac{P^2}{J_{shift}}\Lambda_{PM}\, sin(\alpha_0)}{s^2 + \frac{\frac{3}{4}P^2\Lambda_{PM}\cos(\alpha_0)\, i_{d_0} + \boldsymbol{k_{disp_{spring}}}}{J_{shift}}}$$

It is interesting to note that the transfer function has the same form as that for the configuration with alignment spring. The difference between them, is hidden in the steady state values for the d-axis current, which are calculated as follows:

At any steady OP: $\ddot{\alpha_0} = 0$. Therefore, for the following equation to stand true:

$$f(\ddot{\alpha_0}, \alpha_0, i_{d_0}) = 2\frac{J_{shift}}{P}\ddot{\alpha_0} + \frac{3}{2}P\Lambda_{PM}\, sin(\alpha_0)\, i_{d_0} + \frac{\boldsymbol{2k_{disp_{spring}}}}{\boldsymbol{P}}\boldsymbol{\alpha_0} - \boldsymbol{k_{disp_{spr}}}\frac{\boldsymbol{\pi + 2\alpha_{min}}}{\boldsymbol{P}} = 0$$

d-axis current at a specific OP, must be equal to:

$$i_{d_0} = -\frac{\frac{2k_{disp_{spring}}}{P}\alpha_0 - k_{disp_{spr}}\frac{\pi + 2\alpha_{min}}{P}}{\frac{3}{2}P\Lambda_{PM}\,sin(\alpha_0)} = -\frac{4k_{disp_{spring}}(\alpha_0 - \frac{\pi}{2} - \alpha_{min})}{3P^2\Lambda_{PM}\,sin(\alpha_0)}$$

Substituting the expression found for i_{d_0} in the plant transfer function, we get the final expression for $G_{disp_{ai_{d_0}}}(s)$:

$$G_{disp_{ai_{d_0}}}(s) = -\frac{\frac{3}{4}\frac{P^2}{J_{shift}}\Lambda_{PM}\,sin(\alpha_0)}{s^2 + \frac{k_{disp_{spring}}\left(1 - \frac{(\alpha_0 - \frac{\pi}{2} - \alpha_{min})\cos(\alpha_0)}{sin(\alpha_0)}\right)}{J_{shift}}}$$

$$= -\frac{A\,sin(\alpha_0)}{s^2 + D_0}$$

As expected, OP-variant transfer functions $G_{disp_{ai_{d_0}}}(s)$ and $G_{algn_{ai_{d_0}}}(s)$ have the same form. They change only by the value of OP-variant pair of poles. Consequently, the design for the controller gains followed the logic used in the prior configuration with alignment spring: the design for k_p and k_d was done supposing the use of a VPD, and finally k_i is chosen by trial.

Compared to the closed loop transfer function for a system with alignment spring, the only difference is the substitution of OP-variant term C_0 in the denominator by D_0. Based on the canonical form of the characteristic polynomial:

$$s^2 + 2\zeta\omega_n s + \omega_n^2$$

gains k_p and k_d are calculated as:

$$\omega_n^2 = -A\,k_p + D_0$$

$$k_p = -\frac{\omega_n^2}{A} - \frac{D_0}{A}$$

$$2 * \zeta * \omega_n = -A\,k_d$$

$$k_d = -\frac{2\zeta\omega_n}{A}$$

Therefore, the SIMULINK VPD controller block of Figure 40, for a system with alignment spring, was modified to account for the dependence of k_p in D_0, instead of C_0. The expression for D_0, is recalled once again:

$$D_0 = \frac{k_{disp_{spring}} \left(1 - \frac{(\alpha_0 - \frac{\pi}{2} - \alpha_{min}) \cos(\alpha_0)}{sin(\alpha_0)} \right)}{J_{shift}}$$

In SIMULINK, it is calculated as:

$$D_0 = \frac{k_{disp_{spring}} \left(1 - \frac{(\alpha_{meas} - \frac{\pi}{2} - \alpha_{min}) \cos(\alpha_{meas})}{sin(\alpha_{meas})} \right)}{J_{shift}}$$

The change in OP requires a respective change in steady state d-axis current, according to the earlier formula:

$$i_{d_0} = -\frac{4k_{disp_{spring}}(\alpha_0 - \frac{\pi}{2} - \alpha_{min})}{3P^2 \Lambda_{PM} \, sin(\alpha_0)}$$

In SIMULINK, this steady state reference is calculated as:

$$i_{d_{0_{ref}}} = -\frac{4k_{disp_{spring}}(\alpha_{meas} - \frac{\pi}{2} - \alpha_{min})}{3P^2 \Lambda_{PM} \, sin(\alpha_{meas})}$$

and is fed forward to the output from the VPD controller.

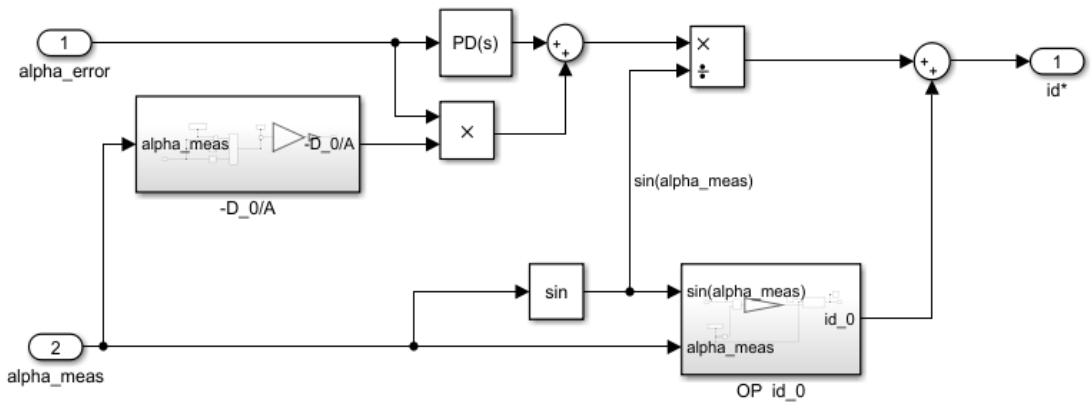

Figure 44: VPD controller of angular phase displacement regulation, in the system with displacing spring

The final VPD controller block, of the present system with displacing spring, is illustrated in Figure 44.

The step response of the present system was compared to the responses of the system w/o spring and with alignment spring in Figure 41, using the same step reference of $\Delta\alpha_{\text{ref}} = +2\alpha_{\min}$ and $\Delta\alpha_{\text{ref}} = -2\alpha_{\min}$. The choice for the spring constant $k_{disp_{spring}}$ was done, for the purpose of comparison, to be equal to that of alignment spring:

$$k_{disp_{spring}} = k_{algn_{spring}}$$

The respective responses are illustrated in Figure 45. As a conclusion, we can say that the system with displacing spring exhibits the greatest dependency on the OP, even with the implementation of an OP-variant PD controller. On the other hand, in the system w/o spring, this controller manages to achieve a very good cancellation of the OP-variant term in the plant transfer function. In all the simulations, random values were used for the spring constants. In practice, these constants would require careful tuning, because their value greatly influences the behavior of the angular phase displacement system, reflected in the OP-variant terms in the denominator of $G_{algn_{ai_{d_0}}}(s)$ and $G_{disp_{ai_{d_0}}}(s)$, C_0 and D_0, respectively. It is intuitive to think that lower values for the spring constants would make the responses more similar to those of the no-spring configuration.

To verify this, displacing spring constant $k_{disp_{spring}}$ was made 100 times smaller in the MATLAB script, and two other simulations were carried, for the same references as prior.

The response of the systems w/o spring and with displacing spring are illustrated in Figure 46. As expected, having a spring which is less stiff makes the angular phase displacement regulation much less dependent on the OP, and the response almost equal to that of no spring configuration.

Of course, in the end the integral term of the controller should also be added, to guarantee zero steady state error, even in the presence of eventual disturbances.

The final block diagrams for the purpose of angular phase displacement regulation, for use in the system without spring and for the configurations with springs, are illustrated in Figure 47.

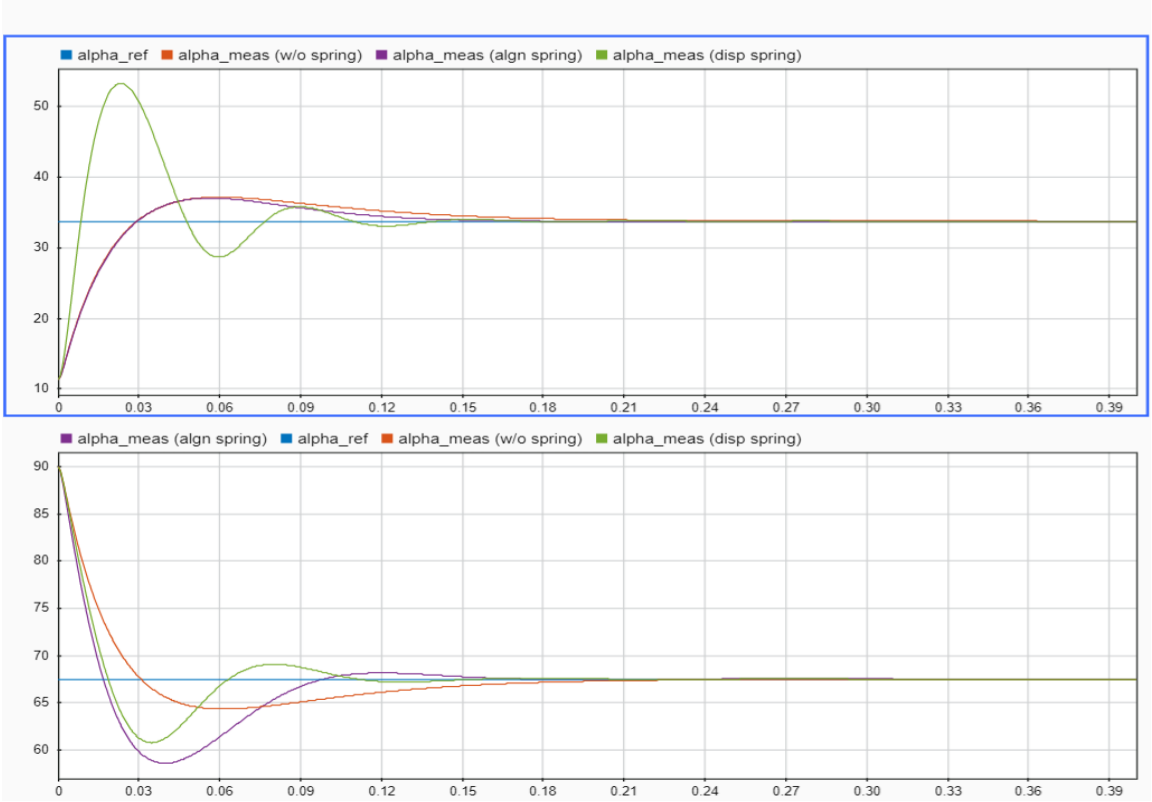

Figure 45: Comparison of step response between a system w/o spring, a system with alignment spring and a system with displacing spring, using a VPD controller, for step reference of Δαref=+2αmin (upper graph) and Δαref=-2αmin (lower graph)

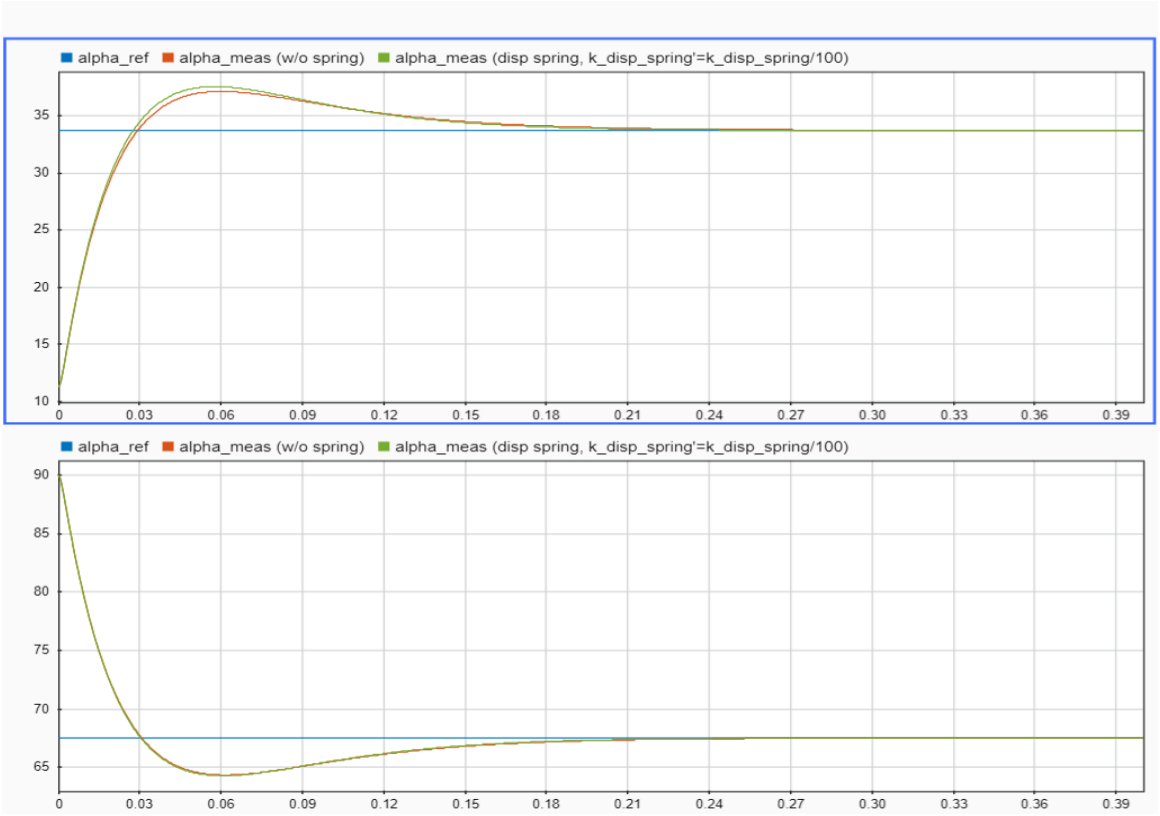

Figure 46: Comparison of step response between a system w/o spring and a system with displacing spring with smaller spring constant, using a VPD controller, for step reference of Δαref=+2αmin (upper graph) and Δαref=-2αmin (lower graph)

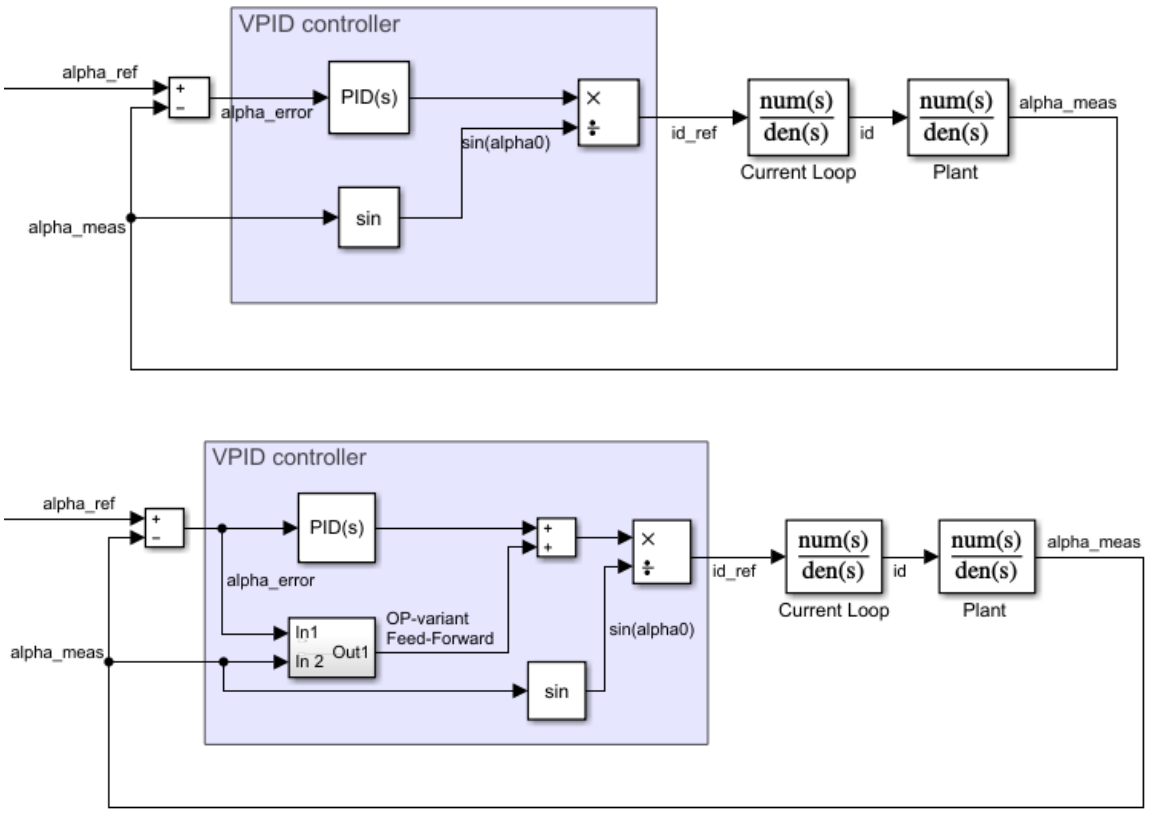

Figure 47: Control block diagrams for the angular phase displacement regulation, for a system w/o spring (up) and a system with either spring (bottom)

Chapter 4

Effectiveness of the AFPM Machine with Mechanical Flux Weakening in CTSR and CPSR operation

4.1 Problem Stating

For the purpose of working both as a starter and an alternator with a wide constant power speed region (10:1 CPSR), our AFPM machine would have to reproduce the torque vs speed characteristic illustrated in Figure 48.

Before base speed $n_{pu} = 1$, it's the Constant Torque Speed Range (CTSR). During this speed range, based on equation (3) of the mathematical model:

$$T_{mot} = \frac{3}{2} P \Lambda_{PM} \cos(\alpha)\, i_q$$

maximum flux linkage should be available, for the AFPM machine to provide full motoring torque capability. This translates to a requirement for the smallest possible value for the angular phase displacement. Ideally, $\alpha_{min} = 0$ would be the most efficient value during CTSR. However, in that condition a shifting torque cannot be produced,

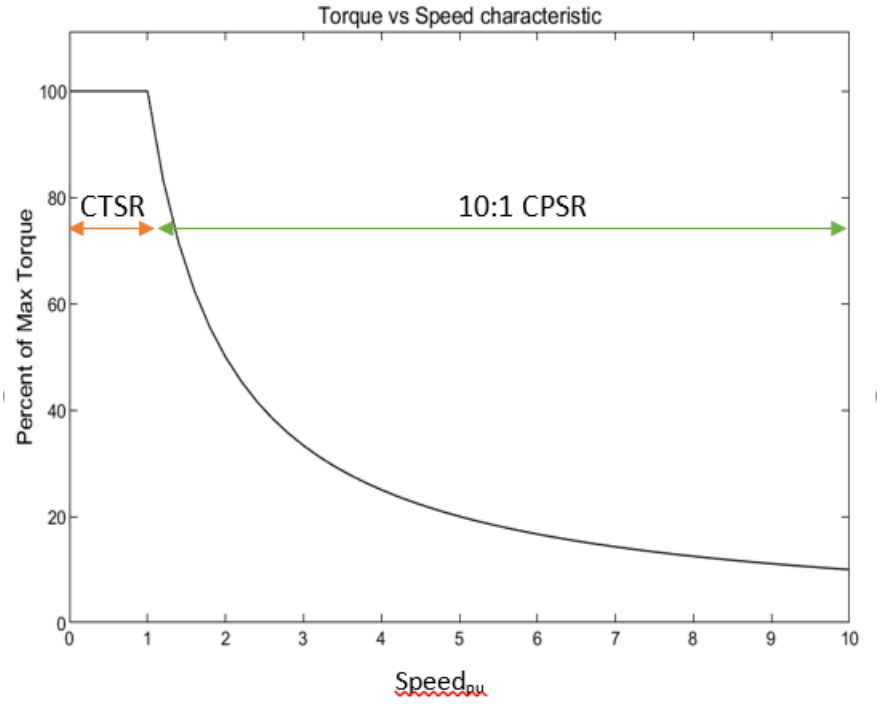

Figure 48: Torque vs Speed Characteristic of the AFPM machine employed as a starter/alternator

because the term $sin(\alpha)$ in equation (4) of the AFPM machine mathematical model would be equal to zero:

$$T_{shift} = T_1 - T_2 = -\frac{3}{2} P \Lambda_{PM} \, sin(0) \, i_d = 0 \qquad (4)$$

Shifting torque production is crucial for the mechanical field weakening, investigated in this thesis.

After base speed (CPSR), for the induced voltage to remain constant and equal to E_{base}, flux linkage must be weakened. This is realized using a transient shifting torque to increase the angular phase displacement between the rotors, based on equation (4) above. And, in order to produce a big T_{shift} with as small as possible transient i_d (since we have limitations on the max current amplitude), the initial angular phase displacement should be large.

Therefore, there are conflicting tendencies among the CTSR and CPSR, regarding the choice for the initial angular phase displacement α_{min}.

Furthermore, the introduction of alignment/displacing spring configuration presents additional requirements on the steady state levels of d-axis current, which might influence the reachable CPSR.

4.2 Motoring Torque Capability in CTSR operation

4.2.1 Motoring Torque Capability vs minimum angular phase displacement α_{min}

Based on equation (3) of the AFPM machine model, if all the parameters remain constant except for α_{min}, Motoring Torque Capability is related to the minimum angular phase displacement, in the following way:

$$\frac{T_{mot}}{T_{mot_{max}}} = \frac{\frac{3}{2} P \Lambda_{PM} \cos(\alpha_{min}) \, i_{q_{rat}}}{\frac{3}{2} P \Lambda_{PM} \cos(0) \, i_{q_{rat}}}$$

$$T_{mot\_CAPABILITY}[\%] = 100 * \cos(\alpha_{min}) \qquad \text{where } 0 < \alpha_{min} \leq \frac{\pi}{2}$$

This relation is plotted in Figure 49.

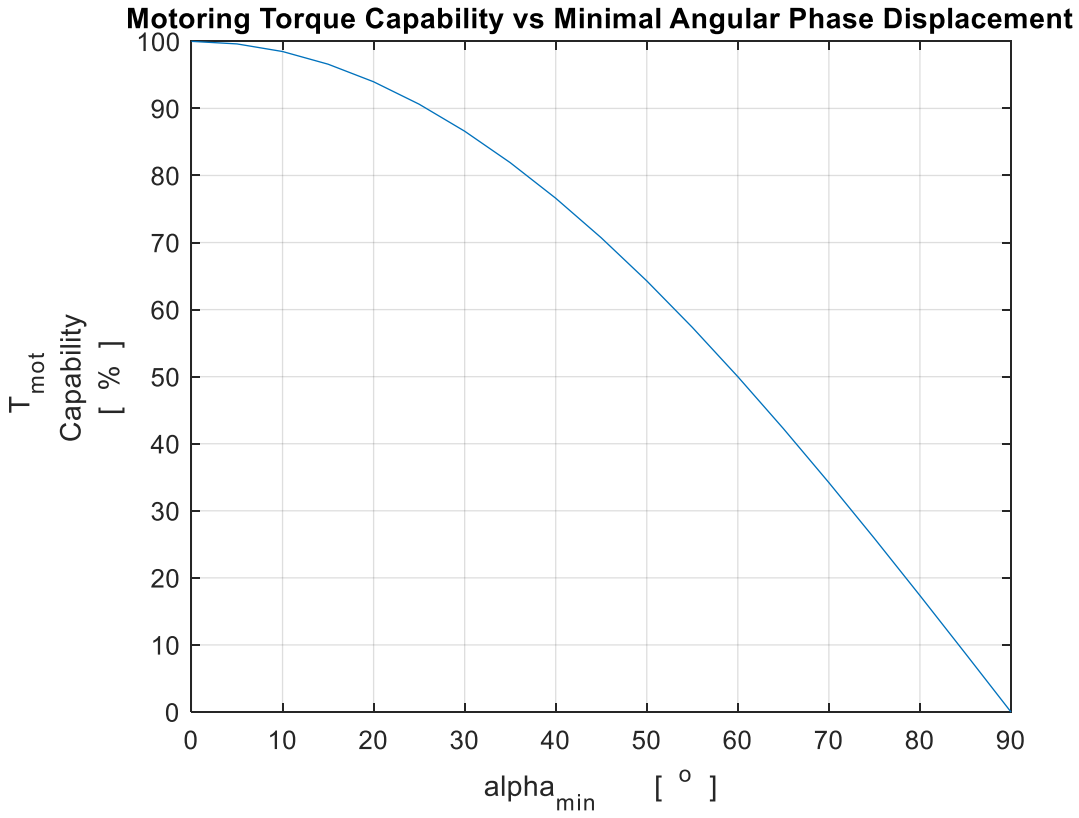

Figure 49: Motoring torque capability vs minimal angular phase displacement

A general guideline would be a motoring torque capability not lower than 90%. Then, based on Figure 49, the minimal angular phase displacement should be under 25º.

4.2.2 Motoring Torque Capability vs Spring Configuration

The effect of different configurations, namely system w/o spring, with alignment spring and with displacing spring, on the Motoring Torque Capability was analyzed through simulations. These were carried out for operating conditions under the influence of a constant load torque, that tends to displace the rotors from one another, and is equal to:

$$T_{load} = \frac{Tn}{10}$$

In these conditions, the three configurations would have to produce a steady counter-balancing torque, to keep the rotors at the position of minimum angular phase displacement. This last, was kept constant throughout all the simulations and equal to:

$$\alpha_{min} = 10^{o}$$

Therefore, the motoring torque capability is only dependent on the available steady state q-axis current, and can be calculated as:

$$T_{mot\_CAPABILITY}[\%] = 100\cos(10^o)\, i_{q_{available_{pu}}}$$

where the available per-unit q-axis current is equal to:

$$i_{q_{available\_pu}} = \sqrt{1 - \frac{i_{d_{ref}}}{i_{q_{max}}}}$$

$i_{q_{max}}$ is also the nominal d-axis current, which was calculated in the MATLAB script as: $i_{q_{max}} = \sqrt{2} I_{nom_{rms}}$.

The required steady state d-axis current $i_{d_{ref}}$ was determined from the simulations.

Three sets of simulations were carried out, for the following spring constants:

1. $k_{algn_{spring}} = k_{base}$
2. $k_{algn_{spring}} = \frac{k_{base}}{10}$
3. $k_{algn_{spring}} = \frac{k_{base}}{100}$,

where k_{base} is the minimal alignment spring constant, that is sufficiently stiff to counterbalance a load torque as above, $T_{load} = \frac{T_n}{10}$, at the position of $\alpha_{min} = 10^o$.

For comparison $k_{disp_{spring}} = k_{algn_{spring}}$, even though in practice they wouldn't normally be equal.

Simulation results are collected in the charts of Figure 50. Based on the data of the upper chart, a comparison of steady state d-axis current requirements during CTSR, between the three spring configurations, can be made. The resulting Motoring Torque Capability for every configuration, is presented in the bottom chart. As expected, in the case of $k_{algn_{spring}} = k_{base}$, the reactive torque from the alignment spring fully balances the load torque. Therefore, there is zero steady state d-axis current expenditure in CTSR, translating to maximum q-axis current availability and consequently the highest (nearly 100%) Motoring Torque Capability. For a system w/o spring, this capability drops to 80%. For a displacing spring, this high value for the spring constant translates to a large displacing force exerted during CTSR. Therefore, a very big d-axis current (>5 p.u.) is required to keep the rotors from displacing. Consequently, there is no q-axis current availability, i.e. zero Motoring Torque Capability.

Figure 50: Per-unit d-axis current requirements (up) and Motoring torque capability (bottom) vs different spring configurations, under T_load=Tn/10

On the other hand, for $k_{algn_{spring}} = \frac{k_{base}}{10}$, the alignment spring reactive torque is not enough to fully counterbalance the load torque. A big part of the balancing force must be produced electrically, using a constant d-axis current. Therefore, the Motoring Torque Capability drops substantially, for a system with alignment spring.

Following the same trend, for $k_{algn_{spring}} = k_{disp_{spring}} = \frac{k_{base}}{100}$, in an alignment spring configuration the Motoring Torque Capability decrements a bit more. Meanwhile, for a displacing spring configuration, this smaller value for the spring constant permits enough q-axis current availability to have a Motoring Torque Capability of nearly 80%.

4.3 Peak transient d-axis current amplitude vs minimum angular phase displacement α_{min} and vs spring constant

As it was mentioned earlier, after base speed $n_{pu} = 1$ a transient shifting torque must be produced, in order to start the mechanical field weakening. The peak transient $id_{ref_{peak}}$, required to produce enough shifting torque, depends greatly on the initial angular phase displacement α_{min}. Since we have current limits, the choice for α_{min} is largely based in this peak value. The maximum transient $id_{ref_{peak}}$ would be commanded when the highest angular acceleration is required, i.e. the fastest displacement between the rotors, according to equation (6):

$$T_{shift} = -\frac{3}{2} * P * \Lambda_{PM} * sin(\alpha_{min}) * i_d = J_{shift} * \frac{d\omega_{shift}}{dt}$$

During changing of the gears, the engine can change its speed of rotation by up to 6000 rpm in half a second. To keep a constant induced voltage, the angular phase displacement would have to change with the same rate (assuming the shaft is directly coupled to the engine). This maximum acceleration requirement is used to evaluate the peak transient i_d for different α_{min}, being the slope of the 3:1 speed profile in Figure 51 (upper graph). This last provides the reference for the signal α_{ref} in Figure 47, according to equation (7) for mechanical flux weakening:

$$\alpha_{ref} = \alpha_{min} \qquad \text{for: } n_{pu} \leq n_{base_{pu}}$$

$$\alpha_{ref} = arcos\left(\frac{n_{base_{pu}}}{n_{pu}} * \cos(\alpha_{min})\right) \qquad \text{for: } n_{pu} > n_{base_{pu}}$$

In Figure 51 middle graph shows the reference angular phase displacement α_{ref}, according to this speed profile, for a choice of $\alpha_{min} = 10^o$. The tracking signal α_{meas} of the system w/o spring is also plotted in the same graph and demonstrates perfect tracking. Lastly, bottom graph presents the response in d-axis current, for both the reference and tracking signals. As expected, a high peak transient is observed initially, and then the current settles to steady state zero value (the simulation is carried out with $T_{load} = 0$.

The same simulation was repeated for different values of α_{min}, and for each spring configuration. Results are presented on the chart of Figure 52. As expected, with smaller

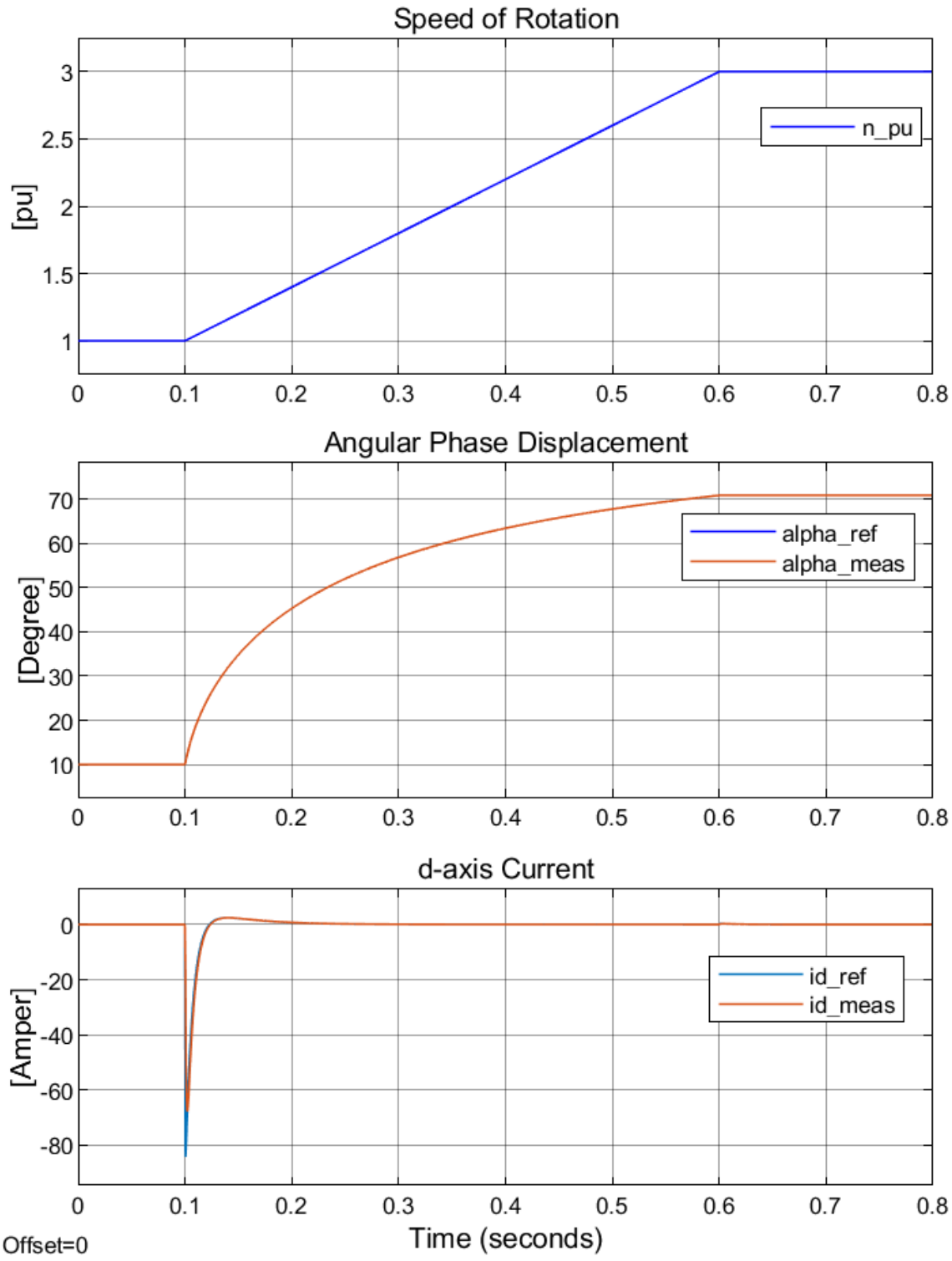

Figure 51: Speed profile for the evaluation of peak id_ref vs alpha_min (up), angular phase displacement response to this speed profile (middle), d-axis current response (bottom)

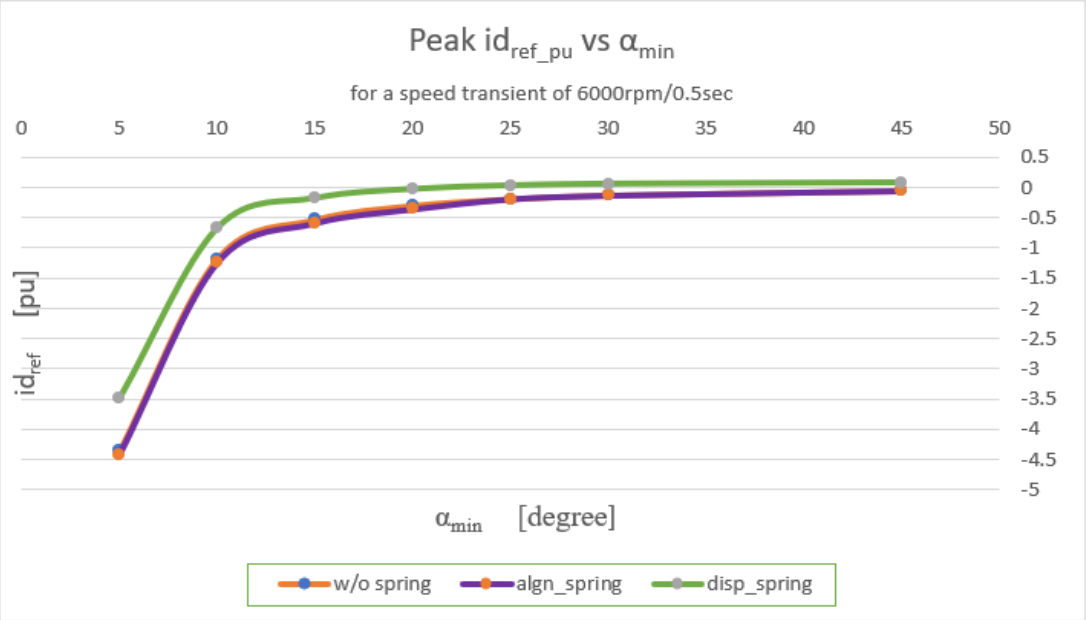

Figure 52: Peak transient id reference [p.u] vs minimum angular phase displacement, vs different spring configuration

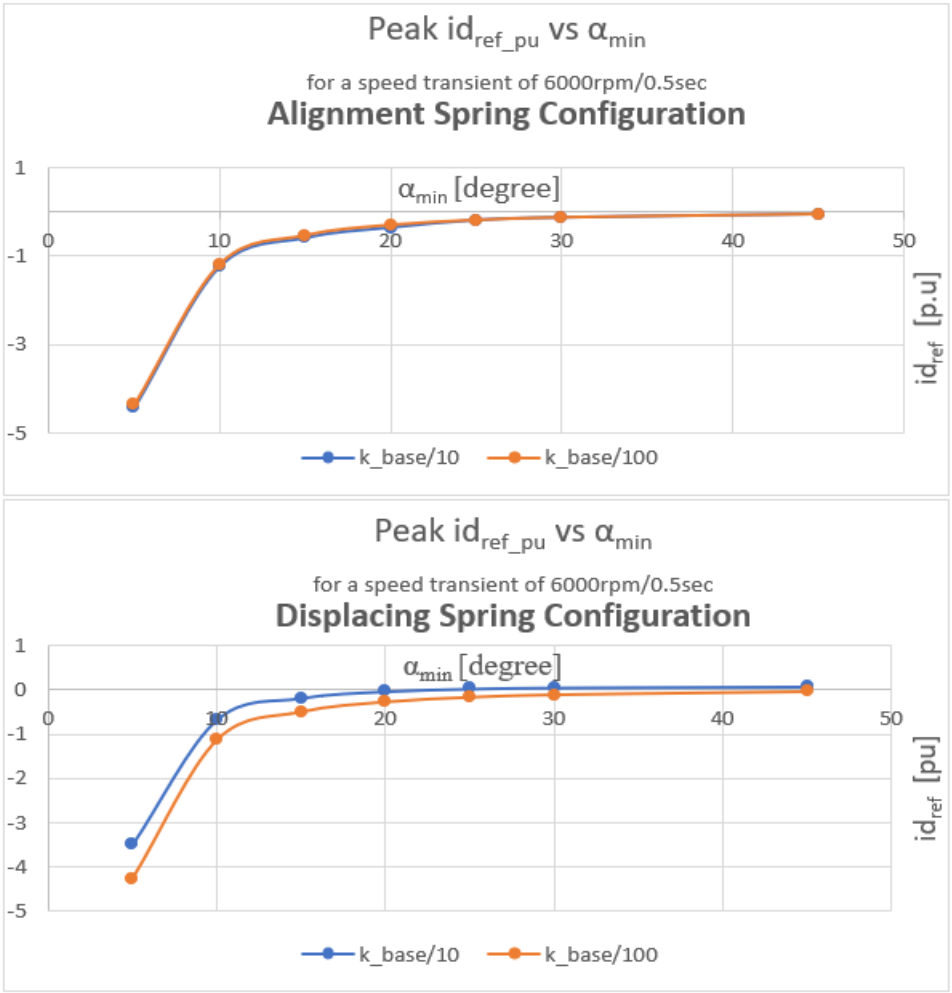

Figure 53: Peak transient id reference [p.u] vs minimum angular phase displacement, vs different value of spring constant, for alignment spring configuration (up), and for displacing spring configuration (bottom)

minimum angular phase displacement comes greater peak value of transient d-axis

current. This relation preserves the same shape between different spring configuration, only for a displacing spring the relation is offset in the positive direction, because of the bigger steady state value for the d-axis current in this type of configuration. In conclusion, assuming as maximum current limitation the rated value (i.e. 1 p.u), the minimum angular phase displacement should be greater than 10^o,

Furthermore, the effect of different spring constant value in the peak transient d-axis current was also investigated. Particularly, the previous relation $i_{d\_ref_{peak\_pu}} = f(a_{min})$ for $k_{algn_{spring}} = k_{disp_{spring}} = \frac{k_{base}}{10}$, is compared to a new relation for $k_{algn_{spring}} = k_{disp_{spring}} = \frac{k_{base}}{100}$, as it is illustrated in Figure 53. The shape of the relation remains the same, however, it is noticed that a lower value for the spring constant translates to a lower peak transient current for the alignment spring configuration, but to a higher peak for the configuration with displacing spring. This is expected, since an alignment spring tends to prevent the displacement, representing therefore a barrier to the transient $i_{d_{ref}}$. It is clear that for a displacing spring it is the opposite.

4.4 Attainable CPSR vs type of spring configuration

The effect on the attainable CPSR, of steady state (SS) current requirements after base speed was investigated. For that, two sets of simulations were carried out, for the alignment spring configuration, and for the displacing spring configuration. Since the analysis was carried out with the assumption of zero load disturbance, there wouldn't be any SS d-axis current requirement for the configuration w/o spring, therefore this last is exempted from the comparison. Each set of simulation consists of four runs:

1. $i_{d_{SS\_pu}}$ @ $n_{pu} = 1.5n_{base}$
2. $i_{d_{SS\_pu}}$ @ $n_{pu} = 3n_{base}$
3. $i_{d_{SS\_pu}}$ @ $n_{pu} = 6n_{base}$
4. $i_{d_{SS\_pu}}$ @ $n_{pu} = 10n_{base}$

Simulation results are presented in Figure 54, for two values of spring constants: k_{base}(up), and $k_{base}/10$ (bottom). First observance is that increasing the spring constant 10 times, leads to 10 times higher d-axis current at steady state (SS). Secondly, for the alignment spring configuration, more and more d-axis current is required at SS with increasing speed, which limits the attainable CPSR eventually, depending on our

specifications regarding efficiency. Opposite for displacing spring configuration, on which the level of necessary d-axis current decreases while speed increases. This, of course happens because the torque exerted from the alignment spring increases with bigger angular phase displacement (i.e. bigger speed of rotation), while the force exerted by the displacing spring decreases.

The formula for the instantaneous active power in a constant amplitude two-phase (dq) reference frame is:

$$P = \frac{3}{2}(v_q * i_q + v_d * i_d)$$

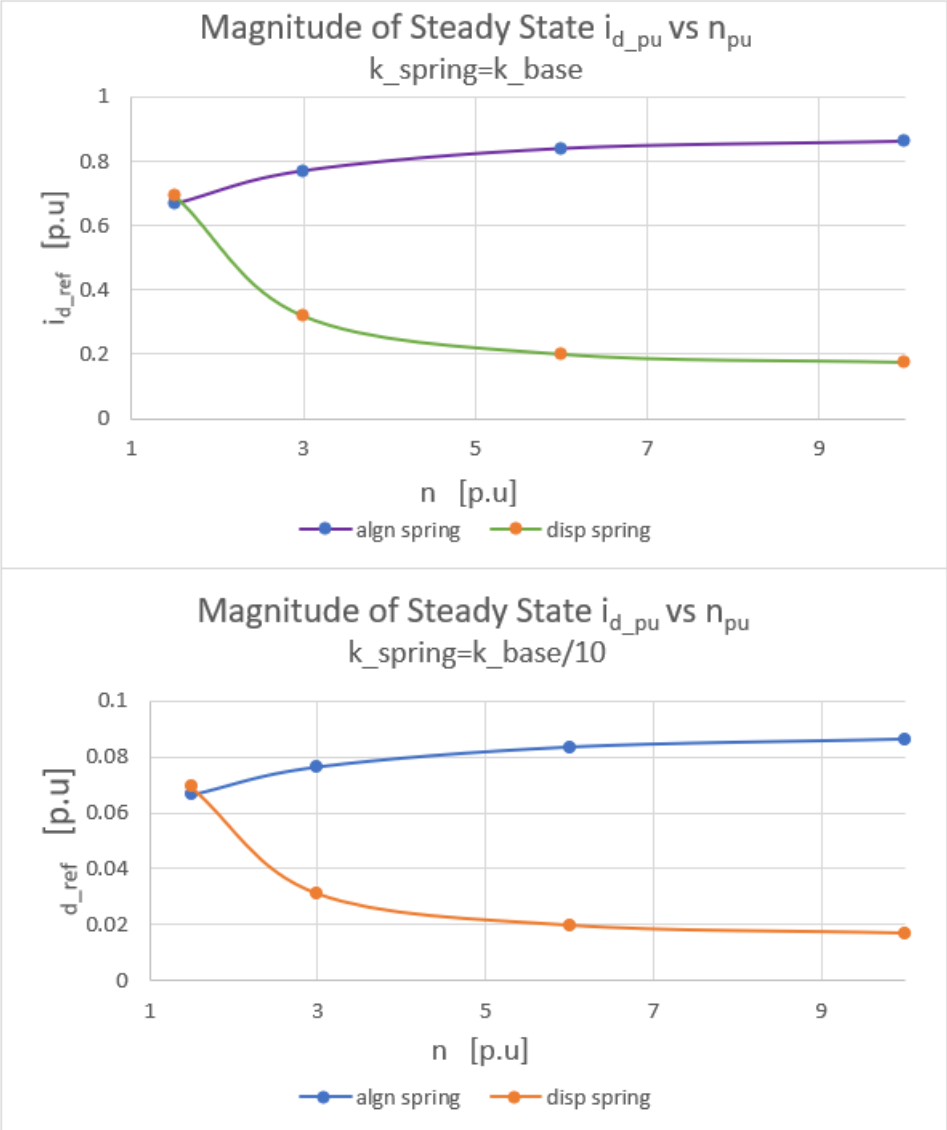

Figure 54: Steady state d-axis current [p.u] requirement versus speed of rotation [p.u], for k_spring=k_base (up) and k_spring=k_base/10 (bottom)

Applied to our AFPM machine, in steady state CPSR operation, the formula is expressed as:

$$P = \frac{3}{2}\left[\left(E_{base_{PM}} + \omega_e * L_d * i_d\right) * i_q - \omega_e * L_q * i_q * i_d\right] \quad (9)$$

Since our machine is considered isotropic, $L_d = L_q$ and the formula for the maximum base power becomes:

$$P_{max} = \frac{3}{2} E_{base_{PM}} iq_{rat}$$

Consequently, the maximum available active power in percent of the maximum power, at a specific SS d-axis current amplitude, can be calculated as:

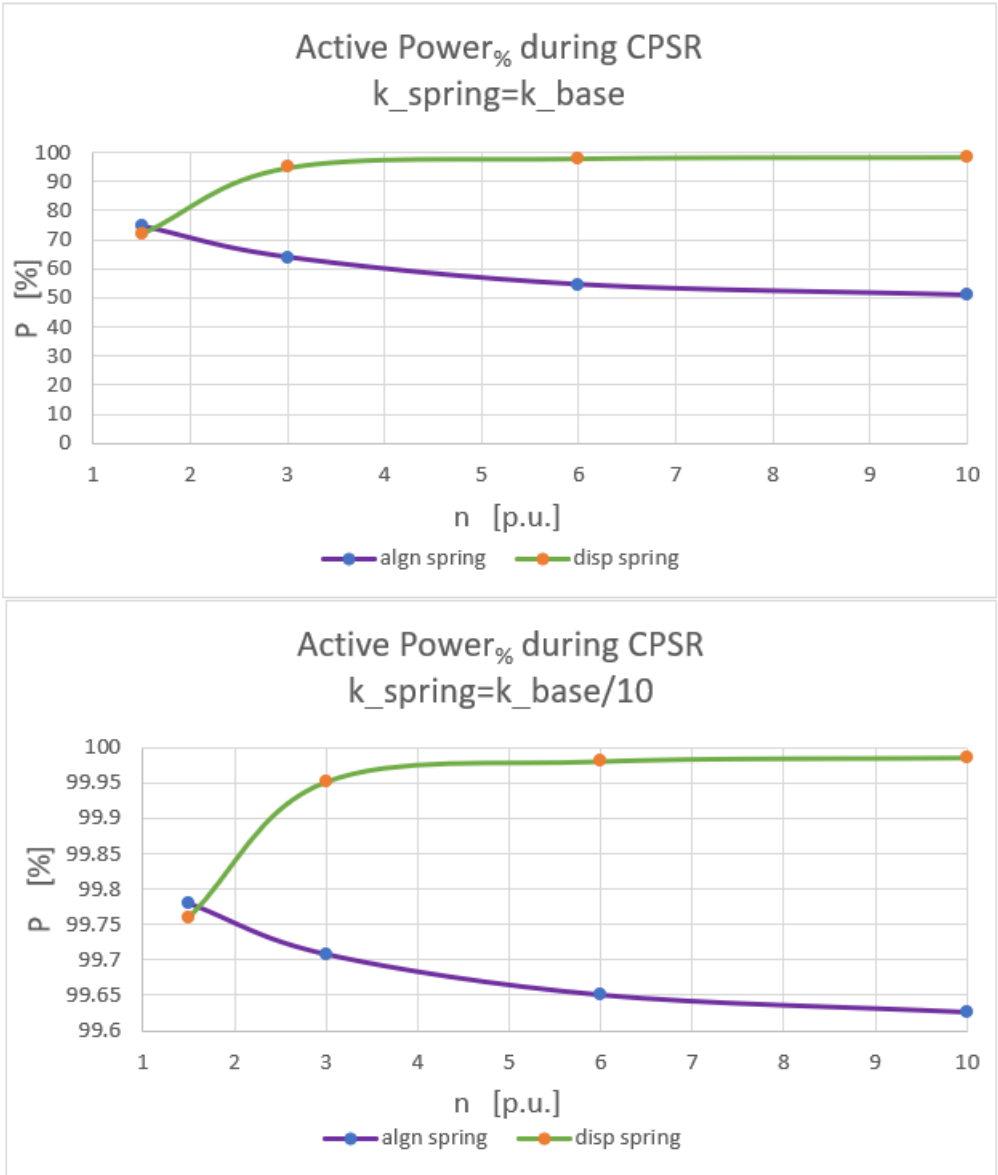

Figure 55: Active Power Profile [%] during CPSR operation, for the configuration with alignment and displacing spring, for k_spring=k_base (up) and k_spring=k_base/10 (bottom)

$$P_{\%} = 100\sqrt{1 - id_{ref_{pu}}^2}$$

Therefore, using the data from the graphs in Figure 54, the resulting Active Power Profiles during CPSR operation, are plotted in Figure 55. Based on these profiles it is concluded that:

1. The amount of deviance from the maximum power profile (a straight line at $P_{\%} = 100\%$), depends greatly on the spring constant, increasing with higher values of it.
2. For the alignment spring configuration there is a limit on the maximum attainable CPSR, depending on our efficiency constraints.
3. For the configurations w/o spring and with displacing spring, in ideal no load conditions CPSR can be extended indefinitely, with the first having also 100% efficiency through the whole CPSR.

4.5 AFPM Machine with Mechanical Flux Weakening, for the alternator function

Figure 56 illustrates the vector diagram of AFPM machine, for operation at base speed $\mathrm{n} = 1\mathrm{p.u.}$ and for operation in FW at $\mathrm{n} = 3\mathrm{p.u.}$ Also, it is assumed that $i_q = i_{q_{rat}}$ and $i_d = 0$. At both speeds, induced q-axis voltage is kept constant through the employment

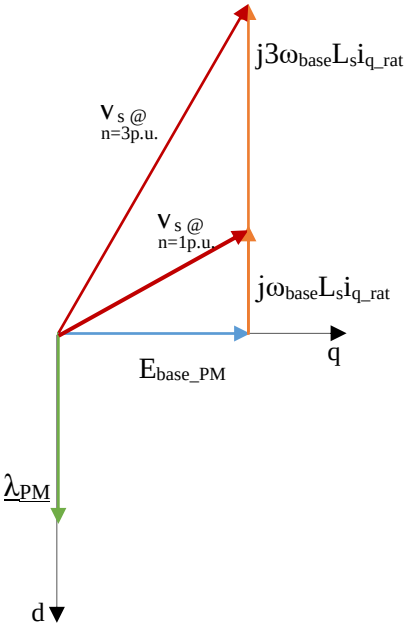

Figure 56: Vector Diagram for n=1pu, n=3pu, iq=iq_rat

of mechanical flux weakening at $v_{q_{pu}} = E_{base_{PM_{p.u.}}} = 1$. Meanwhile, d-axis voltage keeps increasing with speed:

$$@\, n = 1p.u. \qquad v_{d_{pu}} = \omega_{base_{pu}} L_{s_{pu}} iq_{rat_{pu}} = 1 * 0.57 * 1 = 0.57\, p.u.$$

$$@\, n = 3p.u. \qquad v_{d_{pu}} = \omega_{pu} L_{s_{pu}} iq_{rat_{pu}} = 3 * 0.57 * 1 = 1.71\, p.u.$$

Consequently, per-unit stator voltage, at both speeds is:

$$@\, n = 1p.u. \qquad v_s = \sqrt{1^2 + 0.57^2} = 1.15\, p.u.$$

$$@\, n = 3p.u. \qquad v_{d_{pu}} = \sqrt{1^2 + 1.71^2} = 1.98\, p.u.$$

And at $n = 10p.u.$ the stator voltage would be:

$$\sqrt{1^2 + 5.7^2} = 5.79\, p.u.$$

Our machine prototype has a rated phase voltage of 102 V. For operation at $n = 10\, p.u.$ voltage at the terminals would be $5.79 * 102 = 590\, V$. For alternator operation at constant voltage, a buck stage would be required to lower the voltage, which increases the costs. Furthermore, these voltage levels present danger to humans. Solutions would be lowering the stator inductance or otherwise working at de-rated conditions. This last alternative is appropriate for the alternator purpose since, usually, the voltage levels inside the car are at the range of 12-24 Volts. De-rated operation would require mechanical coupling through gears, between the engine and the rotors shaft.

4.6 Comparison with Traditional Field Weakening

In traditional field weakening, the q-axis voltage is kept constant employing the armature reaction flux $L_d * i_d$ to limit the induced voltage from the PMs, according to the following equation:

$$v_q = \omega_e \Lambda_{PM} + \omega_e L_d i_d = \omega_{base} \Lambda_{PM} = E_{base_{PM}} \qquad @\, \omega_e > \omega_{base}$$

Therefore, the amount of negative d-axis current that must be fed after base speed, is calculated as:

$$i_{d_{ref}} = \frac{\Lambda_{PM}(1 - n_{pu})}{n_{pu} L_d}$$

Figure 57 illustrates the required d-axis current [p.u.] with increasing per-unit speed greater than base speed, to maintain a constant base voltage using the traditional flux weakening, in our AFPM machine protype.

Considering $i_{q_{rat}} = \sqrt{2} * I_{ph_{rms}}$ as the maximum current limitation, then the available per-unit q-axis current in Field Weakening Region can be calculated as:

$$i_{q_{\text{avail\_}pu}} = \sqrt{1 - id^2_{ref_{pu}}}$$

Meanwhile, the per-unit q-axis current required for constant power operation, based on equation (9) is:

$$i_{q_{CPSR_{pu}}} = \frac{\frac{P_{max}}{\frac{3}{2}\omega_e \Lambda_{PM}}}{i_{q_{rat}}} = \frac{\frac{P_{max}}{\frac{3}{2}n_{pu}\omega_{base}\Lambda_{PM}}}{i_{q_{rat}}} = \frac{\frac{P_{max}}{\frac{3}{2}n_{pu}E_{base_{PM}}}}{i_{q_{rat}}} = \frac{P_{max}}{\frac{3}{2}E_{base_{PM}}i_{q_{rat}}}\frac{1}{n_{pu}}$$

$$= \frac{1}{n_{pu}}$$

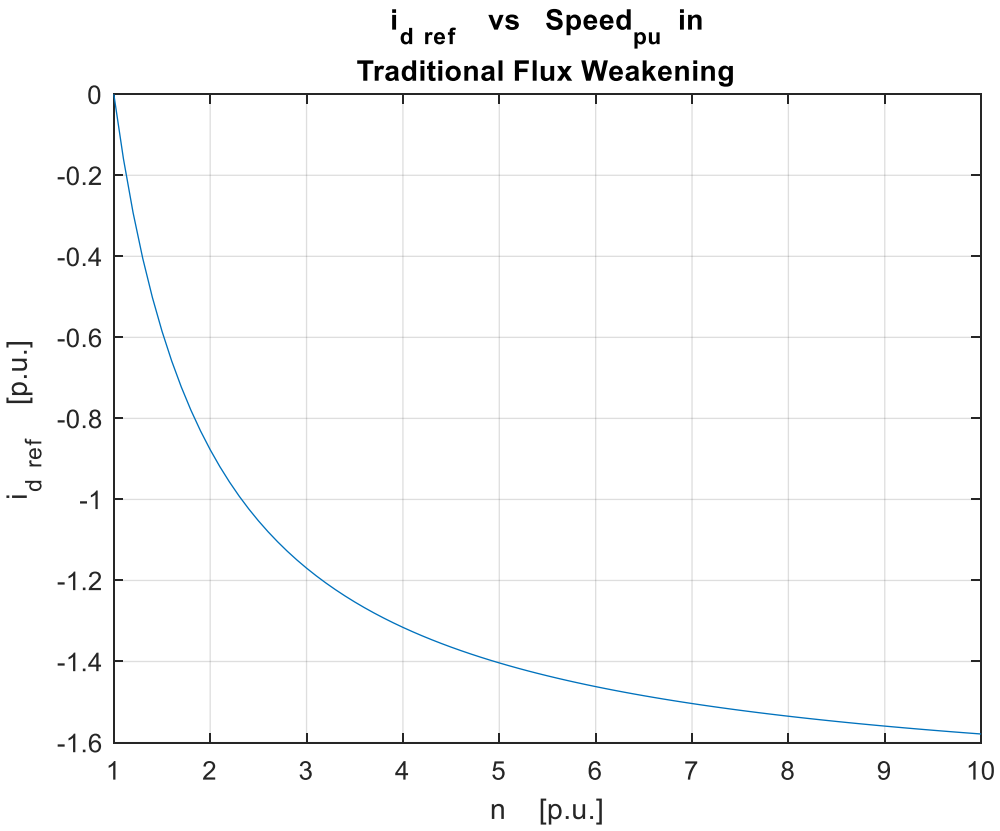

Figure 57: d-axis current requirement for Traditional Flux Weakening

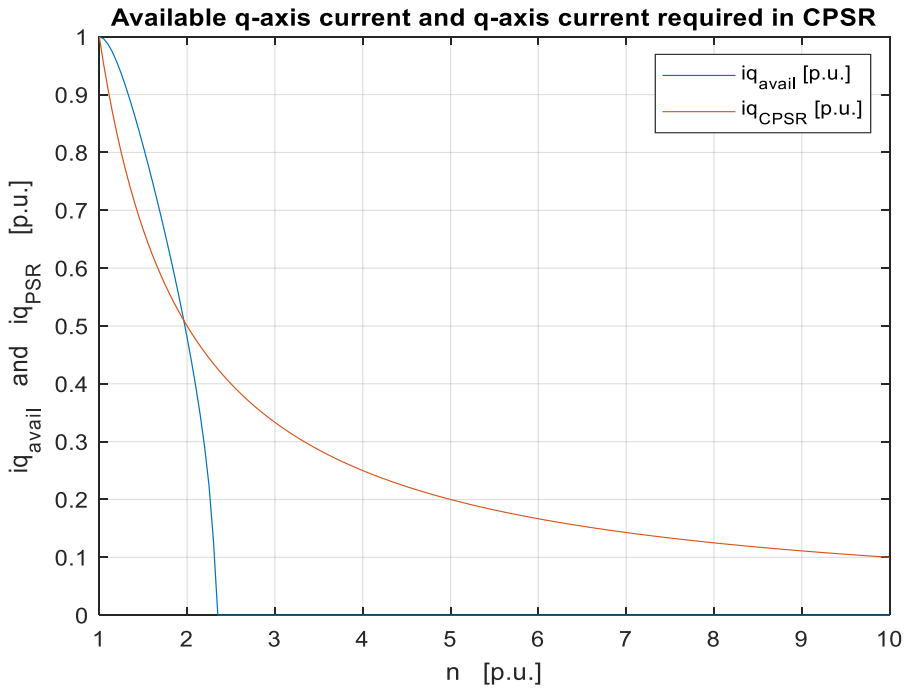

Figure 58: Available q-axis current and required q-axis current for Constant Power Operation

These last two relations are plotted in Figure 58. The q-axis current profile follows the red line, maintaining a constant maximum power, until $n \approx 2\ [p.u.]$. From this point on, there is no available q-axis current left to maintain P_{max}, thus the current profile follows the blue line instead, providing reduced power. Regardless, FW continues, maintaining constant voltage until $n \approx 2.4.\ [p.u.]$, when the maximum current limit is surpassed, and machine cannot increase the speed further.

Therefore, the Active Power Profile can be mathematically expressed as:

$$P = P_{max} = \frac{3}{2} E_{base_{PM}} i_{q_{rat}} \qquad for \quad 1 < n \approx 2\ [p.u.]$$

$$P = P_{FW} = \frac{3}{2} \omega_e \Lambda_{PM} i_{q_{avail}} = \frac{3}{2} n_{pu} E_{base\_PM} i_{q_{avail}} \qquad for \quad 2 < n \approx 2.4\ [p.u.]$$

Figure 59 illustrates the Active Power Profile achievable with Traditional Flux Weakening (upper graph). For comparison, the previous CPSR Profile of Figure 55 for Mechanical Flux Weakening in a configuration with springs, is shown at the bottom. Based on the respective profiles we can conclude that:

Traditional Flux Weakening cannot attain a wide CPSR. Particularly, for our AFPM machine protype with $L_d = L_q = 0.57\ p.u.$ only a 2:1 CPSR is attainable.

Mechanical Flux Weakening can achieve a 10:1 CPSR with proper choice of the spring constant. The constant power attainable can never be the maximum one, but fine tuning of the spring constant can produce a Power Profile that stays within 99-100% of the maximum power, for a 10:1 speed range.

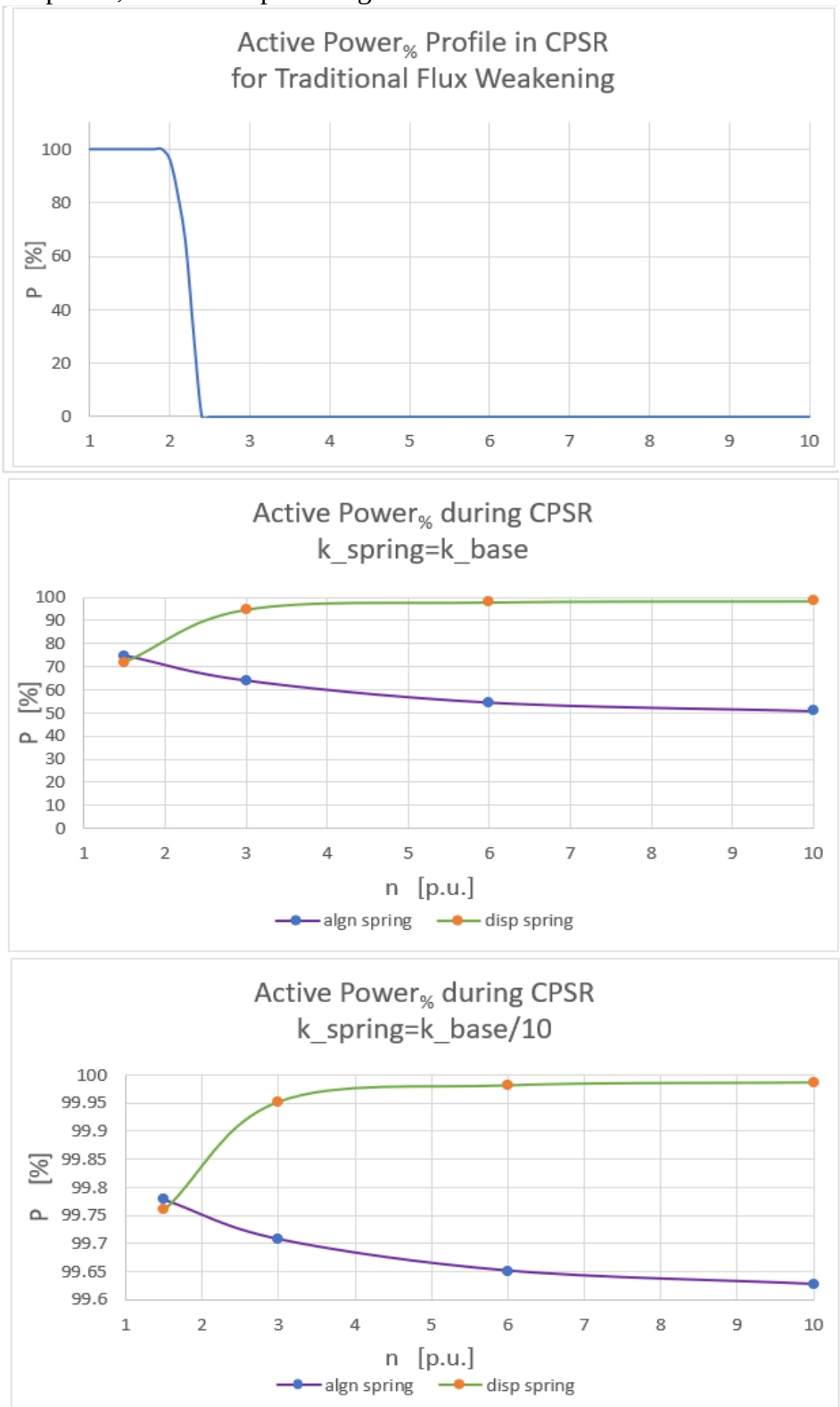

Figure 59: Active Power Profile in CPSR, for Traditional Flux Weakening (up), and for Mechanical Flux Weakening with spring configurations (middle/bottom)

Conclusions and Recommendations

- Mechanical Flux Weakening demonstrated the capability of extending the CPSR to five times more of what is achievable with Traditional Flux Weakening, when employed on the same AFPM machine.
- The configuration w/o spring can maintain a rated constant power for a theoretically infinite CPSR, if there aren't any load disturbances present.
- The configuration with displacing spring has an increased safety factor against overvoltage but cannot attain the rated constant power in CPSR. However, with a small enough value for the spring constant, it can manage to keep the active power profile in CPSR within a very efficient range, such as >95% of Max Power
- For maximum Motoring Torque Capability during CTSR, the best configuration is that with alignment spring. On the other hand, that is also the worst configuration for constant power operation.
- Employing a Variable-OP, PID (VPID) controller makes the angular phase displacement regulation demonstrate great independency from the operating point, in a configuration w/o spring.
- In contrast, for a system with alignment/displacing spring configuration, the same VPID controller cannot achieve the same level of independency from the OP. In these cases, OP-dependency increases with the increase in the value of the spring constant.
- The choice for the minimum angular phase displacement, mostly influences the Motoring Torque Capability in CTSR operation. Its selection should follow this guideline:
    i. First, the chosen value must guarantee respect of the peak transient d-axis current limitation, therefore must be greater than a borderline value.
    ii. Then, the smallest value is chosen among those that comply with (i), to achieve the highest possible Motoring Torque Capability
- The choice for the spring constant influences both Motoring Torque Capability and attainable CPSR. Its selection requires a more involved analysis. The spring constant should be big enough to achieve:
    i. Counterbalancing of the eventual load torque during CTSR, for an alignment spring;

ii. Fast overvoltage prevention response in case of loss of FW control, for a displacing spring

However, with greater values for the spring constant come higher OP-dependency of the angular phase displacement regulation, and lower CPSR attainability.

Thus, the value of the spring constant requires careful tuning.

- For the specific use of the analyzed AFPM machine prototype, as an alternator, it is recommended to employ a machine with a lower armature inductance. This way, the voltage at the terminals can be limited to be $c^{te} \pm \Delta v_{tol}$ throughout a 10:1 CPSR, without the increased costs of an intermediate buck stage.

REFERENCES

[1] CSANYI E. 2016, “Every car has it- The Lundell generator with claw pole rotor”, CSANYI E, viewed June 2019, <https://electrical-engineering-portal.com/lundell-generator-claw-pole-rotor/>.

[2] L. Del Ferraro, F. Caricchi, F. Giulii Capponi, G. De Donato, *“Axial-Flux PM Starter/Alternator Machine with a Novel Mechanical Device for Extended Flux Weakening Capabilities,”* Proc. of 39th Annual Meeting of IEEE-IAS Industry Applications Society, IAS 2004, Seattle, Washington (USA), 3-7 ottobre 2004.

[3] F. Caricchi, F. Crescimbini, F. Giulii Capponi, L. Solero, *“Permanent-Magnet, Direct-Drive, Starter/Alternator Machine with Weakened Flux Linkage for Constant-Power Operation Over Extremely Wide Speed Range,”* Proc. of 36th Annual Meeting of IEEE-IAS Industry Application Society, IAS 2001, Chicago, Illinois (USA), 30 settembre-4 ottobre 2001.